Development and Protein Composition of the Striated Organelle and Spectrin Localization in the Inner Ear

BY

ROBSTEIN L. CHIDAVAENZI
B.Sc. Hons., University of Zimbabwe, 1995

THESIS

Submitted in partial fulfillment of the requirements for the degree of Doctor of Philosophy in Anatomy and Cell Biology in the Graduate College of the University of Illinois at Chicago, 2014.

Chicago, Illinois

Defense Committee:
Jonathan Art, Chair
James R. Bartles, Northwestern University
Scott Brady
Ronald R. Dubreuil
Anna Lysakowski, Advisor

This thesis is dedicated to three of the most important people in my life: Ashleigh Chiedza, Anotidaishe Seth, and Tayana Chanel.

ACKNOWLEDGEMENTS

This work is the culmination of an amazing but long journey in which so many people have contributed immensely in different capacities. I am deeply indebted to so many people that inevitably most will not be mentioned by name this acknowledgement. Words cannot adequately capture how grateful I am to my advisor and mentor, Dr Anna Lysakowski, for her patience and invaluable scientific guidance and encouragement through the years. I acknowledge and value contributions from past and present laboratory members (viz. Steven Price, Florin Vranceanu, Irina Calin-Jageman, Marcin Klapczynski, Christine Politis, Paulina Struk, Tess Requena, Kavish Thakkar, Aashutos Patel, and Reggie Vlahodimos). I'm deeply indebted to the chairman of my thesis committee, Dr Jonathan Art for making this possible, for steering my progress and selflessly guiding me through some treacherous waters. Besides my chair and advisor, I was also extremely fortunate in having very dynamic and knowledgeable, and capable committee members: Drs Scott Brady, Gerardo Morfini, Ronald Dubreuil, and James Bartles who accorded me excellent scientific supervision. There are no words that can fully articulate the blessings that flowed from coming into the UIC Anatomy and Cell Biology family, the life-long friendships and collaborations formed – they represent some of my most treasured memories of Chicago. This journey began in Zimbabwe, a tiny southern African country, with a family who believed in me and encouraged me to go for what I wanted in life; and this journey brought me to the shores of this great nation, and for this I want to acknowledge funding through the Fulbright Fellowship award, it represented the catalyst that lowered the barriers and made all this possible.

TABLE OF CONTENTS

TABLE OF CONTENTS (continued)

TABLE OF CONTENTS (continued)

LIST OF TABLES

LIST OF FIGURES

LIST OF COMMON ABBREVIATIONS

BSA	Bovine serum albumin
CP	Cuticular plate
DTT	Dithiothreitol
EDTA	Ethylenediamine-tetraacetic Acid
EM	Electron microscopy
F-actin	Filamentous actin
HCl	Hydrochloric acid
HCs	Hair cells
HPLC	High-perfomance liquid chromatography
hr	hour
IACUC	Institutional Animal Care and use Committee
IHC	Inner hair cell
IP	immunoprecipitation
LC-MS	Liquid chromatography mass spectrometry
min	minute
MS-MS	Tandem mass spectrometry
NaCl	Sodium chloride
NaBH	Sodium borohydride
OHC	Outer hair cell
P0, P1…	Postnatal day 0, 1…
PB	Phosphate buffer

LIST OF COMMON ABBREVIATIONS (continued)

PBS	Phosphate buffered saline
PPM	Parts per million
PVDF	Polyvinylidene difluoride
RIPA	Radioimmunoprecipitation assay
SC	Supporting cell
SDS	Sodium dodecyl sulfate
SO	Striated organelle
VHC	Vestibular hair cell

SUMMARY

The striated organelle (SO) is an intriguing cytoskeletal structure that has consistently been observed to occur in the subcuticular region of inner ear vestibular type I and type II hair cells, and cochlear inner (but not outer) hair cells, in most vertebrates. Its function is still unknown, and what little has been reported of its protein composition indicates that it consists largely of multifunctional, common, everyday proteins (such as α-II-spectrin and F-actin) whose presence proffers no obvious clues from which one can infer function. What is known from previous studies, however, is that the SO has been observed to occur in both normal and diseased hair cells; is intricately linked to microtubules, stereociliar rootlets and 'giant' apical mitochondria; and is composed of alternating bands of filaments 10nm and 35nm thick that lie 65nm apart. Based on this, the primary objectives of this work were to: 1) Determine some of the major proteins making up the organelle by identifying those interacting with alpha-II-spectrin; 2. Determine the timeline of the SO appearance in hair cells by tracking the developmental expression of αII spectrin and any other associated proteins; and 3) Map all the beta spectrins to identify their inner ear localization and expression patterns and thereby identify the β-spectrin partner for αII-spectrin in the SO.

To accomplish these aims, I primarily relied on and performed immunohistochemistry (confocal and electron microscopy), western blots, immunoprecipitations, and liquid chromatography-mass spectroscopy for data acquisition. From my results it appears that βII-spectrin is the pairing partner to αII-spectrin in the cuticular plate, striated organelle and lateral membranes of all vestibular cell types except type I hair cells; striated organelle biogenesis is postnatal, with the organelle appearing between postnatal days 3 and 4 (P3-P4), and is preceded by maturation of

the cuticular plate as defined by spectrin incorporation; and there is evidence to suggest that nebulin, γ-actin, and ankyrin G likely also localize to the striated organelle, contributing to the assembly of this complex cytoskeletal structure in hair cells.

In addition to the two identified SO-spectrins, evidence suggests that all the seven mammalian spectrin subunits occur in the inner ear sensory epithelium where they are differentially expressed and localized and likely play different functional roles. Noteworthy is that antibodies raised against the previously reported erythrocyte-restricted αI- and βI-spectrin forms, show immunoreactivity in hair cell lateral membranes, occurring in vestibular type I hair cells and cochlear inner hair cells; and αI- and αII- do not coincide anywhere in the inner ear, just as βI- and βIII-spectrin, raising the specter of complementarity between these pairs.

However, having largely devoted my research to the molecular and structural characterization of the SO, including its association with spectrins, the function of this hair cell organelle still remains unresolved.

1. INTRODUCTION

1.1. General Introduction

Sensory perception is the primary mode via which organisms communicate among themselves within their environment. The ability to perceive external and internal cues and respond appropriately is one of the fundamental characteristics used to define life itself. Such interactions occur at many different strata, from immobile flora to mobile fauna, from single-celled prokaryotes to multi-cellular eukaryotic organisms, etc., and become more elaborate as the cellular and/or organism's evolutionary level of complexity increases. One can thus argue that, at a primal level, survival is merely a reflection of how adept an organism has become at communicating, i.e., how well it 'senses' its surroundings and adapts accordingly. Any disruption or breakdown thereof of the sensory machinery is likely to negatively impact the organism's ability to sustain an optimal quality of existence or maintain life itself.

Defined as that part of the nervous system primarily assembled and organized for the reception, processing and interpretation of sensory data, sensory systems are named for the predominant cues being transmitted. Some of the commonly recognized systems are those for olfaction, vision, gustation, somatosensation, audition and balance. The last two are responsible for detecting auditory and gravito-inertial stimuli, respectively. They have their 'seat' in the inner ear, and attempting to understand and decipher an organelle found within their receptor cells is the primary focus of this study.

It is undeniable that the painful economic and social impact of inner ear maladies is significantly underestimated (Neuhauser et al., 2008). For instance, permanent hearing loss is one of the most common birth defects known, affecting approximately 3 in 1,000 babies born annually in the United States (Eiserman et al., 2008; Ross et al., 2008). Diagnosing vestibular disorders in infants is a more challenging undertaking, and the lack of pediatric studies is offset by the larger burden that vestibular insults place on our aging population. Agrawal and coworkers (2009) estimate that 35% of American adults 40 years and above, representing some 69 million people, have suffered some form of vestibular defect; this proportion climbs to over 80% for the over 65 age group. Hence, quenching our scientific curiosity is not the only reason to dissect out the inner ear, but it goes without saying that a better basic understanding of the sensory machinery, and how it all comes together, would lead to an amelioration of the associated social cost, usher in better management regimes and treatment protocols for the otherwise costly and debilitating vestibular and auditory afflictions.

1.2. **I**nner Ear Sensory Epithelia

Named for its location in the petrous portion of the temporal bone, deep in the vertebrate ear, the 'inner ear' is a hollow labyrinthine cavity. Bony on the outside, membranous on the inside, this cavity is fluid-filled and has both auditory and vestibular sensory epithelia containing receptor cells that sense sound and balance, respectively. The snail-shell shaped cochlea houses the hearing apparatus, whereas the morphologically and functionally distinct semicircular canals and otolith organs contain the vestibular sensory machinery responsible for balance. Innervation of the inner ear sensory epithelia is via the 8th cranial nerve, also called the vestibulo-cochlear

nerve; and the morphology of the afferent nerve fiber terminals at their points of contact with the sensory epithelia is a useful criterion used in classifying hair cells (HCs) into different types.

Hair cells are the most conspicuous feature of vertebrate inner ear sensory epithelia. They get their name from the prominent and distinctive apical finger-like projections — the so-called hair bundles. Each individual specialization is referred to as a 'stereocilium'; and each bundle is composed of rows of stereocilia that increase in height stepwise toward the kinocilium. These are not true "cilia", but rather stereocilia, elongated microvilli-like or plasma membrane projections enclosing bundles of actin filaments. Structurally similar projections can be encountered in the epithelium of intestinal brush border cells of the gastro-intestinal tract. Both epithelial cell types possess apical projections and it has been postulated that HC stereocilia might even have evolved from similar microvilli (DeRosier & Tilney, 2000). Notable differences are that intestinal microvilli are shorter (1-2μm vs 40μm in cochlea) and thinner, of uniform length versus the staircase pattern of HCs, and each microvillus is made up of fewer actin filaments (20 vs 1200 in a single cochlear stereocilium) (DeRosier & Tilney, 2000; Mogensen et al., 2007). Fortuitously, these hair bundles, each with 100-300 stereocilia, do contain one true cilium in which nine peripheral microtubule doublets surround a singlet pair (9+2 axoneme structure), the kinocilium, positioned just behind the tallest stereocilia (Spoon and Grant, 2011). The direction of the staircase and kinocilial position define the polarity of the hair bundles. Whereas they persist throughout life in VHCs, in the cochlea, kinocilia are present only in developing hair cells, but are resorbed and thus absent from the mature cells, in which only rudimentary basal bodies remain (Engstrom and Engstrom, 1978; Hirokawa, 1978).

As previously mentioned, the bony labyrinth is a fluid filled environment, with two entirely different fluid types occupying either side of the membranous labyrinth, both immersing different parts of hair and supporting cells. Between the inside wall of the bony labyrinth and outer wall of the membranous labyrinth is perilymph, which, although not identical, is similar to other extracellular fluids in the body in that it is rich in sodium (Na^+) ions and poor in potassium (K^+) ions. Within the membranous labyrinth is endolymph, unique among extracellular fluids in that it has a K^+concentration that is higher than its Na^+ concentration. These two fluid types are not continuous, but are spatially separated, with the endolymph bathing the exposed sensory epithelial apical surfaces, and the perilymph surrounding the basolateral membranes. This means the inner ear sensory cells are sitting between a K^+ rich (Na^+ poor) top, and a Na^+ rich (K^+ poor) base. The prevailing ionic gradients drive the observed cationic conductances at the two poles, which in turn shapes the inner ear microenvironment. These gradients are utilized in both the driving and design of the transduction and synaptic current profiles.

In this environment, inner ear hair cells, further separated from directly contacting each other by intervening supporting cells, are thus able to detect sound and gravito-inertial acceleration through mechanotransduction, convert these mechanical forces and deformations into biochemical signals, propagate these in turn to the synaptic zones, and ultimately (via the afferent nerve fibers) to the brain for interpretation. The brain 'talks' back to the inner ear cells via the efferent system, which in the cochlea culminates in the electromotility phenomenon of OHCs. Even though an efferent feedback loop is also present in the vestibular system, there has been no verifiable evidence of electromotility, defined as a fast, force-generating, length change in OHCs that occurs in response to an electrical stimulus (Dallos et al., 1993). Hence, one must

remain cognizant of the fact that for all this to come about, the precise temporal and spatial assembly of the ion channels, organelles, and proteins in the right places is paramount.

From the anatomy we know that the petrous portion of the temporal bone housing these senses is densest bony structure in the human skeleton (Shipman et al., 1985; Schwartz and Tattersall, 1996). Therefore the inner ear sensory epithelia are relatively inaccessible to all but the most invasive approaches, which is partly why they lag somewhat behind other senses in terms of what is known about them. Consequently they still hold some functional and structural mysteries, some of which are the function of the calyx endings on vestibular type I hair cells, the identity and nature of the mechanotransduction channels, and the nature, composition and function of associated organelles, a good example being the apically-placed cytoskeletal structure known as the striated organelle.

1.2.1. Auditory System

Clearly, hearing is an important sense for communication in animals. Whereas loss or failure of hearing negatively impacts most animal species' chances of survival in the wild, humans have devised means of ameliorating this handicap. However, this entails prosthetic devices, thereby exerting more pressure on the need to fully understand the basic biology of the auditory system to be incorporated into the engineering design of these devices.

The cochlea represents the auditory part of the inner ear. Morphologically, it is a hollow fluid-filled spirally-coiled tube with an inner membranous lining that divides it into three 'spaces'

(scalae). This lining gives rise to two outer spaces, the perilymph-containing scala vestibuli and scala tympani, sandwiching the inner scala media (or cochlear duct), containing endolymph.

The cochlear duct is bounded on three sides by the stria vascularis laterally, Reissner's membrane superiorly, and basilar membrane inferiorly. The stria vascularis, rich in blood vessels, provides active ion transport crucial for maintenance of the unique endolymphic ion composition. Reissner's membrane is the principal structural element separating endolymph from perilymph, forming the border between scala vestibuli and scala media. The basilar membrane, while separating the scala media from scala tympani, acts also primarily as the mechanical base for the sensory epithelia where its tautness is important for frequency selectivity and sensitivity of the overlying sensory epithelium. Maintenance of the permeability barriers ensures separation of the two fluid types and is essential for the proper physiologic function of the inner ear (Kobayashi et al., 1999).

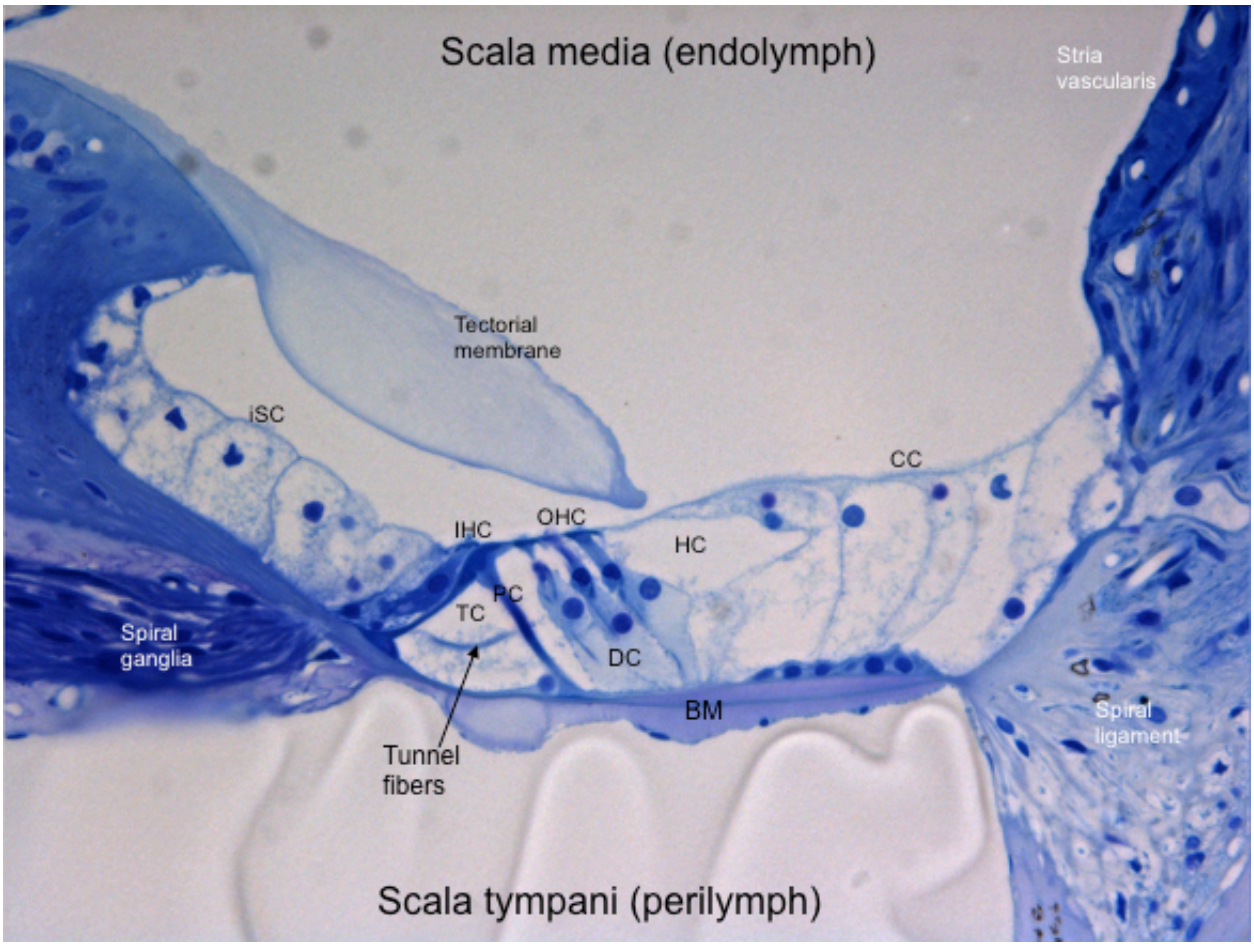

Figure 1.1. A cross-section image of a rodent cochlea showing some of the important structures. Scala media is the cochlear duct or superior chamber containing endolymph and communicates with the apical surfaces of the inner hair cells (IHC) and outer hair cells (OHC), whereas the inferior scala tympani chamber contains perilymph and bathes the basolateral membranes of the hair cells. The hair cells sit on the basilar membrane (BM), with the pillar cells (PC), and tunnel of Corti (TC) containing the tunnel fibers lying between the IHCs and OHCs. Inferior to the OHCs are the Deiter's cells (DC). Flanking the organ of Corti are the inner sulcus cells (iSC) medially and laterally the Hensen cells (HC) proximally and the cells of Claudius (CC) distally. On the lateral wall of the cochlear duct is the stria vascularis, rich in blood vessels and the source of the endolymph. The scala vestibule chamber is not shown in this section but would lie superior to the cochlear duct, separated from the latter by Reissner's membrane.

The mammalian cochlear sensory epithelium, also called the organ of Corti, sits on the basilar membrane with its hair cells lining up along the entire length of the cochlear coil. It is tonotopically organized, with high frequency sounds detected at its base and low frequency ones at the apex. It is important to highlight that the resultant gradient is due to the properties of the basilar membrane rather than the hair cells. The organ of Corti characteristically contains two types of hair cells, a single row of inner hair cells (IHCs) near the modiolus and three rows of outer hair cells (OHCs). Within the body of the duct itself are two named spaces containing perilymph: the tunnel of Corti sitting between the inner hair and outer hair cells and the spaces of Nuel between the OHCs. Morphologically the OHCs tend to be cylindrically shaped and their stereocilia contact the underside of the overlying tectorial membrane, while the IHCs are flask-shaped and their stereocilia exhibit no tectorial membrane attachments. OHCs also have lateral cisternae and other structural adaptations consistent with their role as contractile cells.

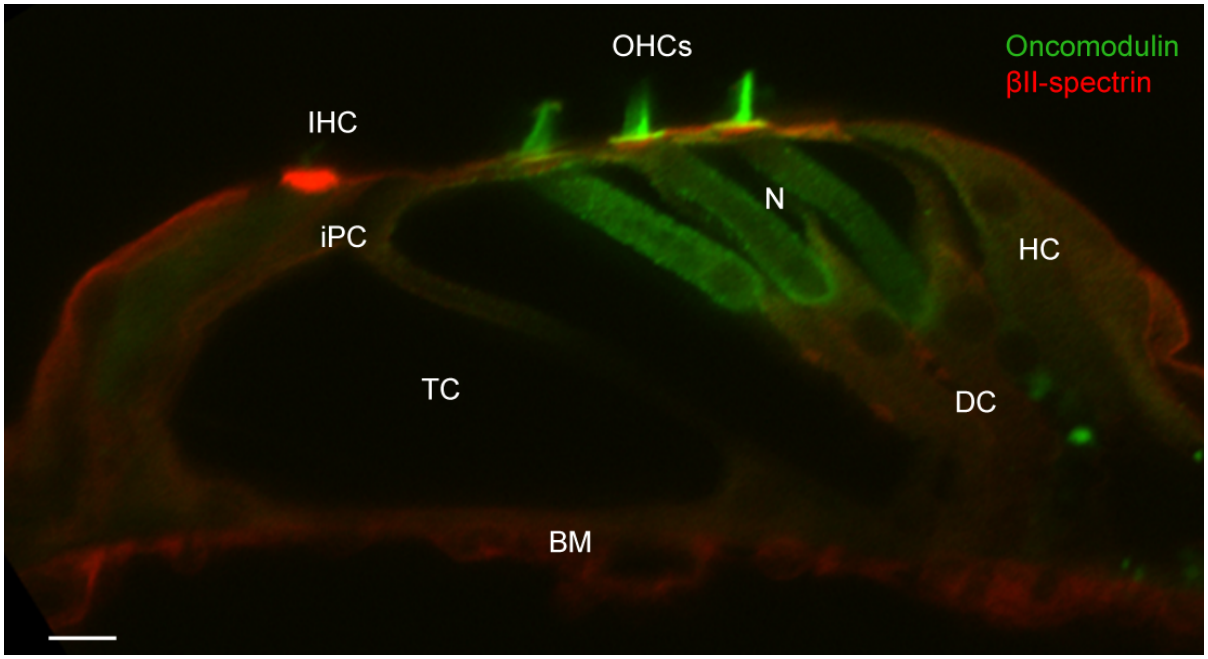

Figure 1.2. The organ of Corti in the adult rat cochlear duct has one row of inner hair cells (*IC*) separated by the tunnel of Corti (*TC*) from three rows of outer hair cells (*OHC*). These cells sit atop the basilar membrane (*BM*), which is crucial for frequency selectivity. Prominent supporting cells in the image are the inner Pillar cells (*iPC*), Deiter cells (*DC*) and Hensen's cells (*HC*). Between the OHCs are the spaces of Nuel (*N*). Scale bar: 5μm.

There are about 15000 HCs in a mature adult human cochlea, of which 3000 are IHCs and the rest OHCs. Afferents making contact with these hair cells are from either type I or II fibers. These fibers are named for the spiral ganglion neurons from which they arise, with the myelinated type I fibers making up 95% of these fibers and all of them innervating the IHCs (Santos-Sacchi, 1993). The remaining 5% are the unmyelinated type II fibers, which contact OHCs. The efferent system, on the other hand, has 80% of the fibers terminating on the OHCs, while the remaining 20% that go to the IHCs terminate, not on the hair cells proper but onto the afferent nerves (Forge and Wright, 2002). Hence IHCs provide the main neural output from the cochlea to the brain, whereas efferent input goes predominantly to the OHCs where it mediates their function as cochlear amplifiers.

1.2.2. Vestibular System

The vestibular system derives its name from having been classically considered merely as a 'vestibule' or opening into the cochlea. Later on, of course, it was realized that it is much more complicated than initially envisioned, forming a three-dimensional orthogonal structure made up of three semi-circular canals that are oriented in the three different planes: viz. the horizontal, superior, and posterior canals. Three balance-based functions can be assigned to it: 1) it is central to detecting angular and linear motion, as well as spatial orientation of the head, 2) it plays a role in the establishment of muscular tone and postural maintenance, and 3) it participates

in spatial gaze stabilization. Because the vestibular apparatus provides this information only with respect to the head, it cannot accomplish postural adjustments on its own, and is thus multimodal- recruiting other systems for the overall effect. Clearly the biology of this portion of the inner ear stems directly from the type of cells involved, the unique fluid environment, and molecular architecture inherent in this compartment.

Just like the auditory system, the vestibular system has an endolymph-filled membranous labyrinth within a perilymph-containing bony one. Besides the three semi-circular canals, it also has two sac-like structures: the oval-shaped utricule, and flattened and irregularly-shaped saccule. These two are referred to as 'otolith organs' as they contain calcium carbonate crystals. They appear as dilatations within the vestibule of the bony labyrinth between the cochlea and canals, and contain sensory epithelia referred to as 'maculae'. In an upright head, the utricular maculae is oriented parallel to the ground, and the saccular macular is vertical.

Opening into the utricle are the lumens from each of the three semi-circular canals. One canal, the horizontal, is tilted 30° up from horizontal plane; whereas the other two (posterior and superior) are vertical. There are two sets of canals in an individual organism, one for the right inner ear and another for the left. The horizontal canals lie in the same plane, but the posterior canal on one side of the head, lies in a plane parallel to that containing the superior canal on the other side. Each canal has two ends/junctions that open into the utricle, the superior and posterior canals join in a common crus before entering the utricle, meaning there are only 5 such openings per utricle in total - two from the horizontal canal, one exclusively from the superior canal, another exclusively from the posterior canal, and a joint one from the posterior and

superior canals together. Towards one end of each smooth canal is a dilatation referred to as an ampulla. Running perpendicular to the plane of the canal inside each ampulla, is where one finds the sensory epithelium of the semi-circular canals: the crista ampullaris.

Just as in the auditory system, vestibular receptor cells are called hair cells. The hair cells of the vestibular system are somewhat different from those found in the auditory system, and hence bear different names. Vestibular hair cells are of two types: type I and type II. The primary physical determinant of hair cell type is the afferent terminal that contacts it. Type II hair cells have dimorphic and bouton-only afferents innervating them, whereas type Is are innervated by dimorphic and calyx-only afferents. Typically the type I vestibular hair cells (VHCs) are goblet- or amphora-shaped while the type II cells are cylindrical or dumbbell-shaped. They also have different electrical current signatures. Both types of VHCs occur in the ampullares and maculae where one striking difference between the organs is the bundle polarity of their resident hair cells. In the crista ampullares, hair cells have hair bundles all polarized in the same direction. The same is not true in the utricular and saccular maculae where two populations can be recognized based on hair bundle polarity. In the utricule, hair bundles are oriented with the kinocilia facing each other at the reversal line on the lateral edge of the striolar region (Li et al., 2008; Schweizer et al., 2009), whereas the saccular hair bundles are polarized with the kinocilia facing away from each other at the reversal line.

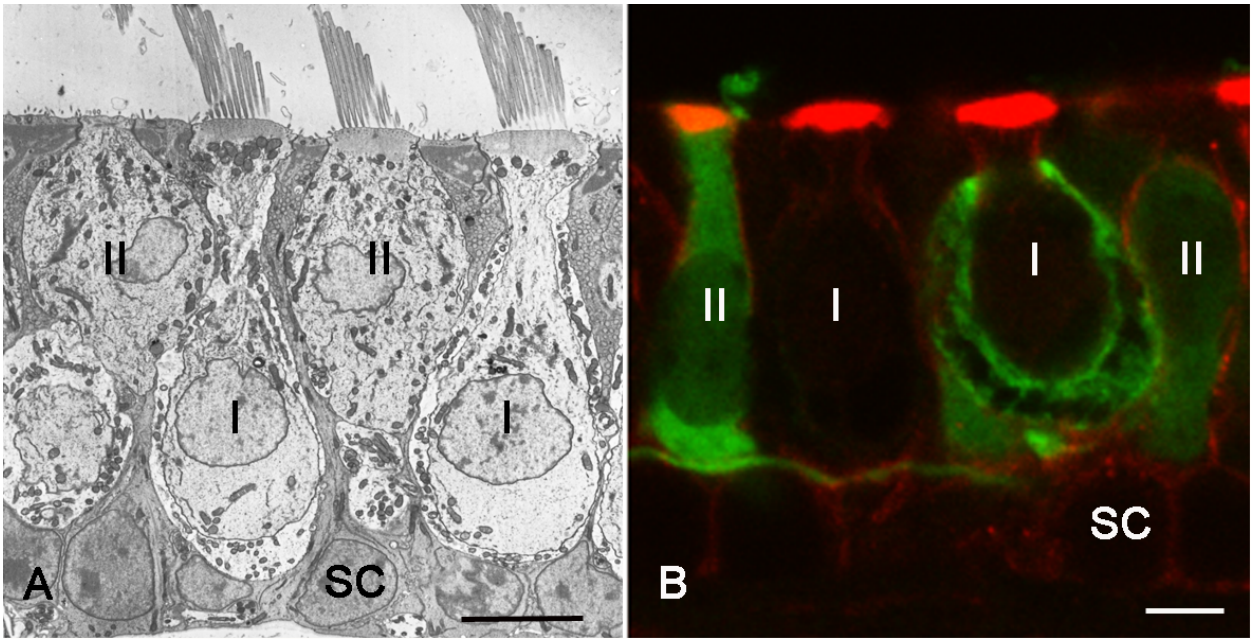

Figure 1.3. A) An electron micrograph of a chinchilla utricule showing the two types of hair cells found in the vestibular system: type I (*I*) and type II (*II*). The supporting cells (*SC*) arise from the basement membrane below the hair cells with the nuclei lying inferior to the hair cells but projecting all the way to the apical surface of the epithelium, at the same time wedging themselves between neighboring hair cells to ensure that no two hair cells are in contact. **B)** Hair cells from an adult rat's utricula macula double-stained with calretinin (green), a 29kDa calcium binding protein, and αII-spectrin (red), a 285kDa cytoskeletal protein. Type II hair cells (II) label with both calretinin and αII-spectrin, whereas all type Is are immunoreactive for αII-spectrin but not for calretinin. Only the (the centrally located) pure calyx afferents that surround type I hair cells are positive for calretinin, while the calyx terminals that arise from (the mostly peripheral) mixed afferents, i.e., dimorphic fibers with both calyceal and bouton endings, are calretinin negative. Scale bars: 5μm.

Adjacent to the sensory epithelia, there are other non-sensory supporting cells whose main role is the maintenance of an environment necessary for optimal function of the inner ear. The dark cells, just like the marginal cells of the stria vascularis in the cochlea, are the active ion transporting epithelia of the vestibular system. The permeability barrier maintenance function of keeping endolymph and perilymph apart is taken over by the epithelium of the roof of the utricular and saccular maculae, crista ampullares and semicircular canals (Forge and Wright, 2002).

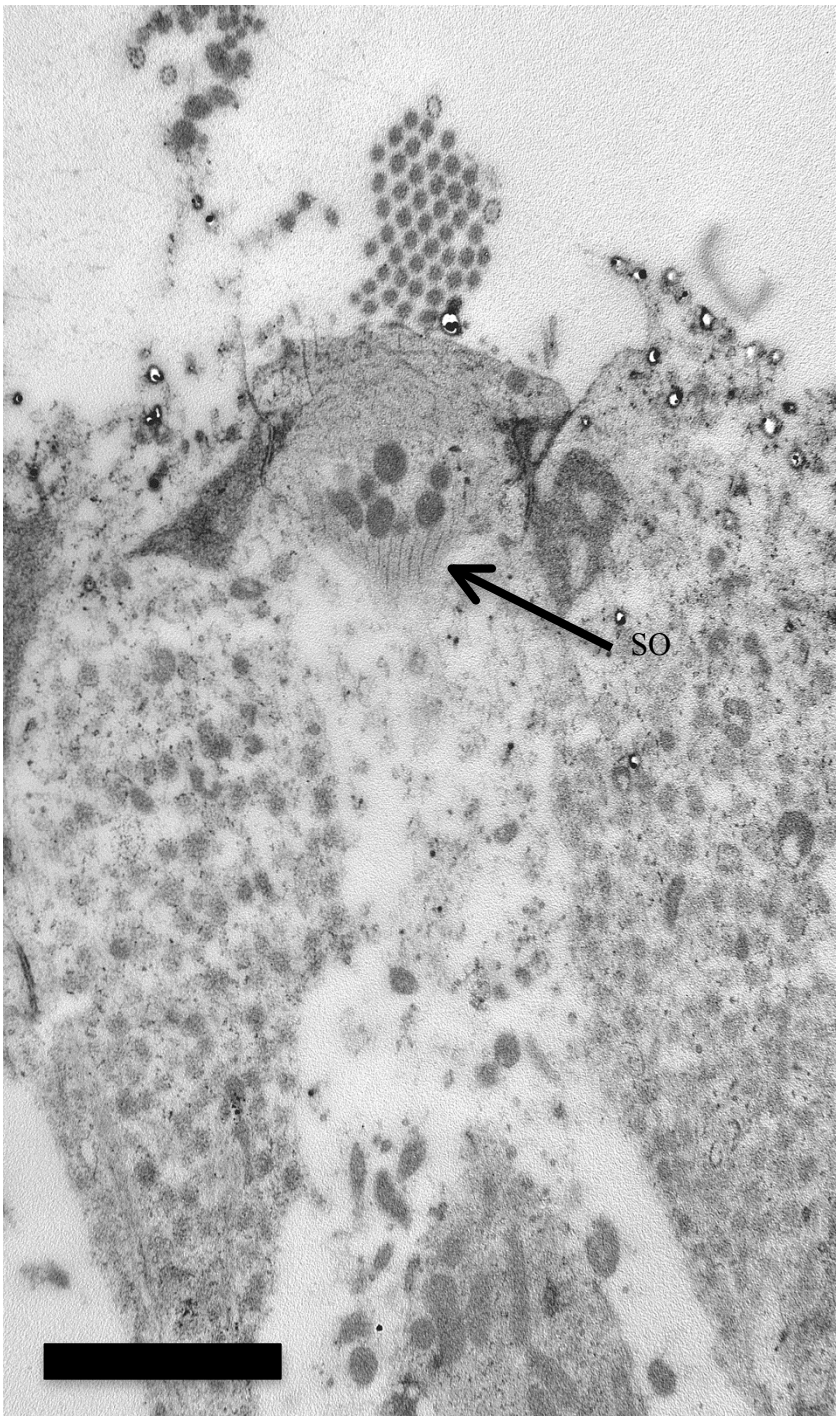

Figure 1.4. Normal transmission electron microscopy image of the apical half of an adult female rat type I utricular hair cell depicting a striated organelle (*SO*) just underneath the cuticular plate. Just superior to the SO, very distinct mitochondria can be seen. Scale bar: 2μm.

1.3. The Striated Organelle

1.3.1. What is the Striated Organelle?

Inner ear hair cells contain a cytoskeletal structure referred to as the striated organelle (SO), or alternatively the "Friedman's body" or "laminated cytoplasmic inclusion body". This is an intriguing structure in vestibulocochlear hair cell architecture that requires serial electron microscopy to systematically observe, and not surprisingly only a handful of researchers have reported seeing it. As the name would suggest, the SO consists of alternating thick (32nm) and thin (10nm) bands (striations) of electron-opaque filaments with small cross-linking filaments in between (Friedmann et al., 1963; Slepecky et al., 1980). The distance between any two adjacent thick (or thin) bands is approximately 130nm (Ross and Bourne, 1983; Vranceanu et al., 2012).

The organelle sits in the subcuticular region of cochlear IHC and VHC, and at times extends to the infracuticular region for various distances. However, it is consistently located in the apical part of hair cells, and specifically in type I's it localizes to the constricted neck portion of the cell, whereas in other hair cell types it is much longer and more extensive (Ross, 1982; Ross and Bourne, 1983). The SO forms an inverted open-ended cone-shaped cage-like structure that attaches to the cell membrane along its upper circumference and is separated from the cuticular plate by a dense cluster of large mitochondria (Vranceanu et al., 2012).

These subcuticular mitochondria in type I VHCs are roughly ten times larger in volume and have twice as much surface area as mitochondria found in other HCs (Vranceanu et al., 2012). In this

study, the SO was also found in close association with microtubules and smooth endoplasmic reticulum, and has been shown to be directly connected to some of the stereociliar rootlets. In electron microscopy tomography reconstructions, stereocilia rootlets closest to the kinocilium exhibited a 110º bend inside the cuticular plate, crossed the entire cuticular plate, passed the large mitochondria underneath, before inserting into the opposite cell membrane near the SO, completing the apparatus (Vranceanu et al., 2012). It is not clear what the significance of such an angle would be, but it is likely that once all the proteins making up the SO are known then some of these physical attributes can be explained in terms of protein interactions.

1.3.2. History of the Striated Organelle

First observed in degenerating utricular hair cells in Meinere's disease (Friedmann et al., 1963), its initial association with inner ear pathology meant researchers working on normal animals rarely paid any attention to the SO nor did they do any functional research involving them, believing them to be artifacts of disease. This is evidenced by the fact that early literature identifies striated organelles in such varied pathological conditions like eighth nerve tumors (Hilding and House, 1964), Conn's syndrome (Friedmann et al., 1965), drug toxicity (Friedmann et al., 1966; Jahnke, 1969), and senescence (Rosenhall and Engstrom, 1974).

The SO has a ubiquitous distribution in vertebrates. Striated organelles are a feature in the inner ears of normal lamprey (Lowenstein and Osborne, 1964; Hoshino, 1975), snake (Jorgensen, 1982), chinchilla (Slepecky et al., 1980), rat (Jorgensen, 1982; Ross and Bourne, 1983), cat (Kimura, 1966; Spoendlin, 1966), deaf white mink (Hilding et al., 1967), squirrel-monkey (Engstrom et al., 1972), and humans (Sans, 1989). By 1980 Slepecky and others, citing this

accumulating evidence, were no longer subscribing to the idea that SOs were present only in 'abnormal' or 'diseased' animals but had begun to view them as a normal constituent of cochlear inner hair cells and vestibular type I and II hair cells in most vertebrates. Very few workers since then have attempted to shed light on these organelles, specifically asking questions about what they are, how common they are, what they do, or even whether they differ in diseased versus normal animals. The exact nature and function of the SO thus remains largely unknown, and although several suggestions have been put forward, none have been experimentally tested, verified or substantiated.

1.3.3. Protein Composition of the Striated Organelle

Although there is a dearth of information on the striated organelle, a little is known about its protein composition. Slepecky and Chamberlain (1982) demonstrated that the SO dense bands are made up of actin which can be decorated with the myosin subfragment 1 (S1). No such decoration was observed for the intervening thinner fibrils, but basing his argument on morphometric similarities, Sans (1989) hypothesized that these were also likely made up of actin filaments. The S1 myosin fragment has been shown to cross-link actin filaments running in doublet or triplet networks, in addition to its role in delaying actin depolymerization (Grazi et al., 1989). This could account for the occurrence of the 'dense bands', and their dimensions could be the result of stacking owing to delayed depolmerization. It has been reported that each dense band is made up of multiple thinner filaments, with at least four such fibrils having been observed in the chinchilla (Vranceanu et al., 2012).

αII-spectrin (also called α Fodrin) has been shown to be present in the SO of vestibular hair cells (Demêmes and Scarfone 1992; Vranceanu et al., 2012). Known to cross-link actin filaments in the cuticular plate, terminal web of the interstitial brush border cells, and gastric parietal cells (Glenney et al., 1983; Mizuno et al., 1989), a similar role for αII-spectrin has been suggested in the SO (Scarfone et al., 1988; Sans 1989).

The two well-documented SO-proteins, αII-spectrin and F-actin, are not unique to the organelle itself, but have a general distribution in the apical portion of the hair cell that includes the cuticular plate and stereocilia rootlets. Subsequently other cytoskeletal proteins whose distribution patterns place them in the same general apical area as αII-spectrin appear to be good candidate constituents of the SO. Proteins making up the stereocilia, their rootlets and cuticular plate are largely known. Stereocilia have been shown to be composed of various forms of actin (Tilney et al., 1980; Furness et al., 2008). Slepecky and Chamberlin (1985) and Sans (1989) also found actin, myosin, tropomyosin, and fimbrin in the cuticular plate at the light microscopy level. In an EM immunogold study, Drenckhahn et al. (1991) found tropomyosin in the stereociliar rootlets, but not in the stereocilia themselves. Actin-binding proteins, such as fimbrin and espin, play an important role in linking actin filaments within the stereocilia to each other and to the cuticular plate (Flock et al., 1982; Zheng et al., 2000).

1.3.4. Function of the Striated Organelle

In previous attempts to assign function to the SO, several theories have been proposed by various researchers based on three indirect lines of evidence: 1) its protein composition; 2) structures observed to associate with it; and 3) similarities to other cytoskeletal elements and/or structures.

1.3.4.1 What does protein composition tells us?

Actin and spectrin are two proteins that have been localized to the SO. They are both structural, so the question has been whether they are active and dynamic, or passive and rigid.

1.3.4.2 What do the associated structures tell us?

Furness and coworkers (2008) postulated that structures that associate intimately with stereociliar rootlets could conceivably contribute not only to the former's sensitivity, but also to the passive and active properties of the mechanotransduction apparatus. It has since been demonstrated that some striated organelle fibers are continuous with these rootlets (Vranceanu et al., 2012), hence roles in stereocilia anchoring and flexibility are plausible.

The striated organelle also has a very close association with microtubules (Vranceanu et al., 2012). It has been documented that hair cells contain microtubules that are dominated by tyrosinated tubulins, whereas the tubulin forms in supporting cells have undergone post-translational modifications and are thus detyrosinated, acetylated or polyglutamylated (Slepecky et al., 1995). Cells with the tyrosinated forms tend to be those undergoing rapid cycles of polymerization and depolymerization, as one would expect to see in sensory cells in which active processes are occurring. Supporting cells, with their carboxy-terminal tyrosine residues removed, by contrast, would be more quiescent and stable. This could suggest that the SO has some direct role in active processes, which would tie in neatly with the observation that the location is rich in large mitochondria (Vranceanu et al., 2012).

The classical approach is to think of mitochondria as energy reservoirs for the cell, but they also known to modulate cytosolic calcium ion (Ca^{2+}) levels, an important consideration given the high concentration of calcium channels on the apical hair cell membrane. Mitochondria are also involved in HC programmed cell death where they release cytochrome c, which together with the cytoplasmic apoptotic protease activating factor, dATP, and procaspase-9, activates caspase-9. This leads directly to the activation of caspase-3, which carries out the apoptotic program by cleaving the survival proteins, including Bcl-2, thereby sealing the cell's fate. This mitochondrial association with the SO could lead to one to suspect its involvement in the following activities: 1) mitochondria supply the SO with huge amounts of energy which the latter would use to regulate the sensitivity of the stereocilia and with them the mechanotransduction channels through active contraction; 2) the SO could participating in calcium buffering by providing a barrier that localizes mitochondria to the apical HC for just that purpose; and 3) the SO could be participating in the HC apoptosis by allowing the pinching off the lower HC portion from the apical part, thereby ensuring that the apical endolymph rich scala media is always plugged off from the perilymph underneath. The presence of the SO could thus explain the oft-observed apical extrusion that occurs when HCs die off, accompanied by the retention of the inferior hair cell portion.

1.3.4.5. Comparable Cytoskeletal Organelles

Stereocilia bearing hair cells of the inner ear structurally resemble microvilli-containing epithelia of the intestinal brush border cells, kidney brush border cells, and retinal pigment cells (Hirokawa and Heuser, 1981; Rodman et al., 1986; Philp and Nachmias, 1985). They are all designed around an actin-based apical protrusion framework, which terminates in rootlets that

anchor into a filamentous terminal web structure underneath. This terminal web, in turn reminds one of the striated organelle, and could possibly provide clues as to the latter's nature and function in inner ear hair cells. A minor complication could be that such terminal webs are not restricted to the microvilli bearing brush border cells, but have also been observed in the non-brush border epithelial cells from a variety of tissues, such as the prostate, parotid gland, pancreas, and liver (Rodriguez et al., 1994; Salas et al., 1997). In all the above instances, the terminal webs are apically placed and have been suggested to participate in the organization of the epithelial apical pole (Salas et al., 1997).

The terminal web of the intestinal brush border epithelium is known to contain actin, spectrin, myosin, and intermediate filaments (Hirokawa et al., 1982). These same molecular constituents have also been recorded in the terminal webs of nonbrush border epithelial cells (Rodman et al, 1986). Evidence exists that actin and spectrin also occur within the striated organelles. These proteins, however, are notorious for being so widely distributed and having so many functions that that knowledge is of limited use. All the same it raises the specter that the body is deliberately and constantly fashioning and placing these actin and spectrin rich assemblages in polarized epithelial cells, where they must play some important role.

1.4. **I**nner Ear Spectrins

Spectrins were first identified in erythrocytes where they play a pivotal role in determining the cells' characteristic binconcave shape (Hulsmeier et al, 2007). Predictably when these red blood cells lack spectrins they not only lose their biconcavity and integrity, but in humans a severe form of anemia has also been documented (Tse and Lux, 1999). It is now generally accepted that

spectrins are ubiquitously expressed in most cells where they tend to form an extended protein meshwork linking actin filaments and other cytoskeletal proteins just below the plasma membrane.

This restricted localization to the plasma membrane seems to be generally maintained in post mitotic metazoan cells where they associate, primarily via ankyrins, with a plethora of different players including among them ion channels, ion pumps, adaptor proteins, and adhesion receptors (Fowler and Adam, 1992). Thus a purely passive structural function although possible seems unlikely, hence spectrin involvement and roles in mitosis (Fowler and Adam, 1992), axonal pathfinding (Hulsmeier et al, 2007), synaptogenesis (Stankewich et al, 2010), neurodenerative disease progression (Yan and Jeromin, 2012), nodal assembly (Lacas-Gervais et al, 2004), cell signaling (Machnicka et al, 2012), neural and cardiac cell development, organization and growth (Stankewich et al, 2011) having been intimated.

1.5. **S**ummary of the Study

With all the technological advances made and the new technique developed, it is simply amazing that we are still encountering new organelles in the inner ear sensory epithelia. Primarily we wonder what the exact function of the striated organelle is. Given that the SO has not been fully characterized, its development, protein composition, and function are still largely unknown (Vranceanu et al., 2012). Until we find answers to the first two, it is likely that apportioning function will remain elusive.

We embarked on this study endeavoring to determine the molecular composition of the striated organelle and how this can point us towards some function. The three-pronged approach was to look at development, protein composition and function. This work intends to build upon the morphological work already done by carrying out microscopic, biochemical, proteomic and physiological investigations that would allow us to clarify exactly when the SO appears, what it is made up of, and what it does. In order to answer these questions, the following specific aims based on research questions were pursued and investigated:

1.5.1. Aims and Objectives

Aim 1: To determine a timeline for the appearance of the striated organelle during development of the rat inner ear hair cells, with initial emphasis on, the vestibular type I hair cell, and then type II and cochlear inner hair cells in rat pups.

Objectives:

a) Is the assembly/appearance of the SO pre- or post-natal during development?

The objective was to trace the development of the SO using a biological marker (αII-spectrin) in confocal microscopy and EM experiments.

b) Can the time of development be instructive as to probable function?

To endeavor to interpret development in light of the available body of literature on events occurring at the same time.

Aim 2: To identify the major proteins that constitute the SO

Objectives

a) To identify the β-spectrin moiety that interacts with αII-spectrin in the SO.

b) To identify other proteins making up the SO.

c) To validate putative interaction partners identified as localizing to the SO using electron microscopy.

Aim 3: To map the topographical distribution of spectrin subunits in the inner ear.

Objective

How do the distribution and localization patterns of spectrins in the inner contribute to the larger body of knowledge about their roles and function?

1.5.2. Limitations

Approaches that were attempted in this study would not enable us to validate or confirm physiological relevance. Ascertaining such relevance is crucial before assigning ultimate function.

Co-immunoprecipitation experiments come with the caveat that the lysis process might lead to retention of nonspecific binding partners not encountered *in vivo*. Equally worrying is the possibility we would lose specific but low affinity partners. Ideally a trade off must be reached between employing high stringency purification methods that preserve the high abundant and high affinity specific interactions and low stringency methods that preserve all interactions including those of low abundance and low affinity specific partners. The strategy attempted here was to preserve as many specific interaction events as possible, inevitably hoping this would result in a large number of nonspecific proteins also co-purifying. We added a layer of verification in order to give ourselves confidence about the identity of partners by using, where possible, imaging methods.

1.5.3 Model Animals

Long-Evans rats (*Rattus norvegicus*) were used. Procedures involving animals were approved by the Institutional Animal Care and Use Committee (IACUC) at Univ. of Illinois at Chicago. Rats were selected because they are frequently used in otological research and they also have ears similar to those of humans (Albuquerque et. al., 2009). In the absence of data to the contrary, the outbred, pigmented Long Evans rats were preferred over inbred and albino strains that might be otherwise genetically, developmentally and functionally compromised. Except for the developmental series, adult female animals were employed for the imaging experiments. Stemming from experience that adult female rats are easier to work with, this accorded us the advantage of having a level of consistency in our data. Animals ranged in age from a few hours after birth, designated postnatal day 0 (P0), until after the first observed 24-hour period, to P133 (the oldest animal used).

A total of 109 animals were used in the confocal microscopy experiments, 80 of which were for development, as 3 replicates were done per assigned age up to P28. In the ultrastructural studies 35 animals were employed (28 for development), while the western blot and proteomic experiments utilized 11 animals.

2. POSTNATAL DEVELOPMENT OF THE VESTUBULOCOCHLEAR STRIATED ORGANELLE IN THE RAT INNER EAR

2.1. Abstract

Situated just below the cuticular plate in auditory inner and vestibular type I and II hair cells of most vertebrate species is a cytoskeletal structure composed of alternating light (~10nm) and dense (~35nm) bands of filaments 65nm apart, called the striated organelle (SO). The function of this organelle is as yet unresolved. However, the SO has a precise three-dimensional morphological assembly, and occurs in close association with microtubules and a population of relatively large apically-restricted mitochondria. Because of the consistency of this deliberate and elaborate assembly, location, design, occurrence, and associations, we have previously postulated that this organelle modulates the mechanotransduction apparatus. Initially known to be composed of actin and αII-spectrin, we report that using electron microscopy (EM) immunogold and confocal microscopy, we have accumulated evidence suggesting that βII-spectrin is also a component of the striated organelle. Together with αII-spectrin, βII-spectrin comprises the spectrin backbone that cross-links the SO filaments. We further investigated how these two subunits are expressed in the developing inner ear using western blot approaches, immunohistochemistry, confocal and electron microscopy. Temporal expression patterns of αII-spectrin and βII-spectrin completely mirror each other and suggest that these two directly interact to form the heterotetrameric spectrin molecule of the SO. The earliest earliest postnatal (P0) tissue studied showed no αII-βII-spectrin immunoreactivity, attesting to the fact that this organelle in the rat is clearly absent at birth. A diffuse spectrin signal is acquired between P0-P1, gradually increasing in intensity and becoming more focused: labeling the cuticular plate (P1-

P2), and then the striated organelle (P2-P3). Around P5-P6, the SO attains its adult like morphology. This time-line indicates that SO formation closely coincides with the onset of terminal mitoses of hair cells, cuticular plate maturation, and the acquisition type I hair cell-characteristic ionic conductances.

2.2. Introduction

2.2.1. General Introduction

In the biological realm, an organelle, by definition, must have function. In other words it must have a purpose for being, otherwise the organism would neither allocate nor marshal resources to invest in consistently fashioning any such structure. Along the same lines of reasoning, an inability to assign 'function' to an organelle may due to either a faulty designation of the 'organelle' status, or insufficient data to make the determination.

One common and consistent characteristic of biological entities are they must be living. Each organelle experiences some beginning and an end to their life, meaning there is a temporal start and end point to its existence and function. Furthermore, assuming there is no redundancy, if an organelle performs one unique function within a cell, its absence (immaturity and senescence) would deprive the cell of the particular activity it confers, just as its addition should impart a gain of function to a new cell that previously did not have the activity. In inner ear developmental studies, correlating temporal coincidences between observed structural maturation of a cell and the subsequent acquisition of a specific function has been an important line of inquiry to pursue when one wants to glean function (Romand et al., 1987). This approach has its limitations and by no means provides a direct cause-and-effect relationship on its own, but can be an instructive first step, and in combination with other lines of evidence can bolster a functional claim. Faced with no functional information on the striated organelle (SO), we took the approach of tracking

its development as a means to not only learn more about its biology, but also to accord us the opportunity of a glimpse of its physiology.

2.2.2. Development of Vestibular and Auditory Function

It is well known that the time of onset of vestibular and auditory function varies between species. At the time of birth, humans and guinea pigs have fully developed and functional inner ears, while the common laboratory mice and rats are deaf and their perception of balance and equilibrium so inadequate that it takes them almost two additional weeks before they are fully working (Kraus and Aulbach-Kraus, 1981). Whereas human semicircular canals are already adult-size, the labyrinth is still immature and continues to increase in size in the rat, up to P22 (Curthoys, 1979). However, it has also been reported that the inner ear developmental processes occurring across these species are sequentially the same (Kraus and Aulbach-Kraus, 1981). Hence the basic organization of the auditory and vestibular apparatus is highly conserved across species, making the rat an excellent model to study structural development.

Central to this organization are the hair cells. These are specialized columnar epithelial cells with microvilli-like actin-core protrusions (called stereocilia) on their apical surfaces that are critical for sensing sound, angular and linear acceleration (DeRosier and Tilney, 1989). Just like neurons, mammalian hair cells, for the most part, are terminally differentiated post-mitotic cells incapable of regeneration, whereas their supporting cells are considered ‘mitotically quiescent’ (Jorgensen and Mathiesen, 1988). Most hair cells and supporting cells are born within a very short period during embryonic developmental. For instance, over 90% of both cell types are born

between E12.5-E14.5 in the mouse cochlea (Ruben, 1967). In the developing rat vestibular system sensory epithelium, the first hair cells to be born are located centrally with newer ones added peripherally (Sans and Chat, 1982). In the mouse cochlea, Ruben (1967) reported that the oldest cells will be found at the apex and the youngest at the base. While these are receptor cells and not themselves neurons, they are in direct contact with bouton and calyceal nerve terminals through which they convey this information to the brain. Interestingly, in some species that exhibit late onset of hearing, it is the hair cells that have been implicated in the rate limiting step; the entire vestibulocochlear neuronal network is fully formed first and ready to transmit, but has to wait for its hair cells to mature before it is operational (Marty and Thomas, 1963; Tokimoto et al., 1977).

Mature and functional hair cells are polarized. The apical pole, with its stereocilia, detects the sound or gravito-inertial stimulus and acts as the mechanical transducer, whereas the basal pole shapes the receptor potential and propagates the message by facilitating the release of neurotransmitter. To maintain this functional gradient, it is crucial that proteins and organelles localize and assemble at the proper place and at the right time, so as to form the correct connections. In vertebrate auditory and vestibular hair cells, this organization and intricate attention to detail is demonstrated in that a consistently occurring cytoskeletal structure has been observed to localize just below the cuticular plate, where it associates with microtubules, apical mitochondria and stereociliar rootlets, etc. Named the striated organelle (SO), in the cases encountered, it is made up of electron-dense thick (35nm in diameter) and thin (10nm diameter) ‘striations’ cross-linked by yet still thinner fibrils. Remarkably from rat to man, the successive dense bands are always about 130 nm apart and are themselves made up of multiple thinner ones

grouped and running together. Equidistant between any two successive thick dense bands, one encounters the lighter ones.

Named the striated organelle (SO) from its appearance, we now reasonably understand its morphological structure but there is a dearth in information as pertains to its biology (Vranceanu et al., 2012). Three plausible explanations as to how this scenario emerged are proposed. In the first instance, its initial designation as simply some 'laminated cytoplasmic inclusions' that only assembled in diseased ears meant some of the early workers never really looked for function. Second, the requirement for serial electron microscopy imaging to visualize it properly, a technique not readily available to most inner ear laboratories, and the need to capture it in the right orientation, has meant that this fairly common organelle has not been easily apparent to inner ear researchers. Lastly, with the limited amount of data on SO protein composition, it is that much harder to hypothesize what the SO could be doing on the apical pole of hair cells, though its mere location has spawned speculation that it plays a role, either passive or active, in cellular processes occurring on the apical end of hair cells, the typical one cited being mechanotransduction.

It is apparent that the ability to readily visualize it, as stated above, has been one of the main challenges faced in attempting to decipher the secrets of the striated organelle. Indeed, identifying that the αII-spectrin subunit is a biomarker for it was of immense importance in moving this field forward (Demêmes and Scarfone, 1992; Vranceanu et al., 2012). Both groups recognized that this spectrin subunit also intensely labels the cuticular plate, and as such is not a

strict SO biomarker. However its use achieves the criterion of making the elusive SO more visible and easier to interrogate in experimental work.

Knowing that functional spectrin occurs as αβ-heteromeric molecules, we set out to identify the putative β-subunit partner to αII-spectrin. We hypothesized that, as in other spectrin molecules, the bulk of the protein's interaction sites would be present in the β-moiety. This would be instructive in meeting our intended ultimate goal of determining SO function. Assuming that a mature functional striated organelle at least has spectrin incorporated into it, we sought to track the development of the SO through the expression and distribution pattern of its αβ-spectrin protein in rat neonatal inner ear sensory epithelia during the first month of life (P0-P28). This approach serves two purposes: firstly it shores up evidence that the striated organelle is a biological entity by highlighting that its 'birth' follows a distinct developmentally driven timeline; secondly, given that most of the structural and functional developmental milestones of the auditory and vestibular system apparatus are known, how these coincide with the SO development can conceivably inform us of its probable function.

2.3. **E**xperimental Methods

Procedures involving the handling and use of the study animals were done in accordance with guidelines and protocols approved by the Institutional Animal Care and Use Committee (IACUC) at the University of Illinois at Chicago.

2.3.1. Antibodies:

Primary antibodies: Rabbit anti-human βII-spectrin (Dr. Jon Morrow, Yale Medical School), mouse anti-βII spectrin (BD Biosciences, San Jose, CA), mouse anti-αII spectrin/fodrin and goat anti-calretinin (Chemicon, Temecula, CA).

2.3.2. Animal Model:

Long-Evans rats (*Rattus norvegicus*) were used in these studies.

2.3.3. Tissue Processing:

Rats of various ages ranging from the day of birth (post-natal day 0) to 4 weeks of life (P28) were utilized in the development studies. Because the animals are housed in the university animal facility, pinpointing the exact time of birth was not possible. However expectant female rats were checked 3 times per day (9am, 1pm, and 5pm), meaning that once a rat had given birth, it was almost certain that the observation was made within, at most, the first 16 hours of life (e.g., 5pm-9am). One pup was processed within one hour after birth, and the exact time point designated as P0. For later time points within the same litter, subsequent animals were processed at the same exact time of day. What follows is the processing protocol employed: Animals were anesthetized with Nembutal (80 mg/kg), then perfused trans-cardially with 10-100 ml physiological saline containing heparin (2000 IU), followed by 2 ml/g body weight of an aldehyde fixative (for confocal microscopy: 4% paraformaldehyde, 1% acrolein, 1% picric acid in 0.1 M phosphate buffer (PB) with 5% sucrose, pH 7.4; for electron microscopy:

2% paraformaldehyde, 3% glutaraldehyde, 1% acrolein in 0.08 M cacodylate buffer with 5% sucrose, pH 7.4). Sensory epithelia were then micro-dissected in PB and cryo-protected overnight by incubation at 4^0C in a solution of 30% sucrose. Background fluorescence was reduced by incubating tissues in a 1% aqueous solution of sodium borohydride (NaBH) for 10 min.

2.3.4. Confocal Microscopy:

Vestibular endorgans and cochleae were embedded in gelatin and frozen sections (40μm) were cut on a freezing sliding AO microtome. Sections were permeabilized in Triton X-100 for 1 hour at room temperature. The actual strength of the Triton X-100 employed varied in accordance with postnatal age: P0-P2: 0.3% Triton in PBS was used; P3-P5: 0.5%; P6-P8: 2%; and >P8: 4%. To minimize non-specific binding, samples were incubated with a blocking solution of 0.5% fish gelatin, 0.5% Triton X-100 and 1% BSA in phosphate-buffered saline (PBS, 0.01M) for 1 hr. Afterwards, samples were incubated for 2.5 days in primary antibodies (1:200) diluted in the blocking solution. After rinsing in PBS, samples were incubated overnight in secondary antibodies (1:200) conjugated to Alexa or TRITC labels directed against the host species of the primary antibodies to reveal specific labeling. For each experiment “no primary antibody” controls, which were meant to show that the observed signals are specific to the given primary antibodies and not due to secondary antibodies and/or detection reagents cross-reactivity with the tissue, were performed. Antibody efficacy was determined by using positive and negative control tissues. We also confirmed expression of each of antibody by performing western blots. All the samples were mounted in Mowiol (Calbiochem, Darmstadt, Germany), and the slides examined

on a Zeiss LSM 510 laser scanning confocal microscope (Carl Zeiss, Oberköchen, Germany). Predominantly Z stack images of the sections were acquired, with individual section thicknesses set between 0.5 – 1.0 μm, depending on overall sample depth being resolved. Occasionally single frame pictures were also taken. Final image processing and labeling was done with Adobe Photoshop C3 (San Jose, CA).

2.3.5. Electron Microscope (EM) Immunogold

The methods described below are similar to those used previously by Lysakowski et al. (2011) and are included here for completeness. Vestibular endorgan tissues were cut into 40μm thick sections using a Vibratome 2000 (Technical Products International, St. Louis, MO). Permeabilization of the sections was effected by incubating them for an hour with 0.5% Triton X-100 in 0.1M PB, followed immediately by a blocking step in 0.5% fish gelatin and 1% BSA in 0.1M PB for another hour. Using the primary antibody of choice at a dilution of 1:50 in blocking solution, the sections were incubated for 72 hrs at 4^0C with gentle shaking on a shaker (Roto Mix 50800, Barnstead/Thermolyne, Dubuque, IA). The secondary antibody tagged with ultra-small (0.8 nm) colloidal gold-labeled F (ab) goat anti-mouse IgG and goat anti-rabbit IgG (Aurion Cat. No. 25413, Electron Microscopy Sciences, Hatfield, PA), diluted to 1:40 also in blocking solution, was incubated with the sections for 24 hrs, after the primary antibody had been sufficiently rinsed off. A 4-8-minute silver enhancement of the gold staining followed using the IntenSEM kit (Amersham Biosciences, Piscataway, NJ). 10-minute serial dehydrations in increasing strength ethanol solutions (i.e., 50%, 70%, 80%, 90%, 100% EtOH) was performed on the sections, followed by 2 X10-minute incubations, and then embedded in Araldite resin (Fluka

Durcupan, Ronkonkoma, NY) freshly poured into a plastic mold. The resin was allowed to harden in an oven at 60°C for 48 hrs. The hardened block was then sectioned with a diamond knife (Diatome, Biel/Bienne, Switzerland). Staining with uranyl acetate and lead citrate enhanced the gold signal and allowed it the processed samples to be examined and photographed with a JEOL 1220X transmission electron microscope.

2.4. Results

2.4.1. αII-spectrin and βII-spectrin label the cuticular plate and striated organelle

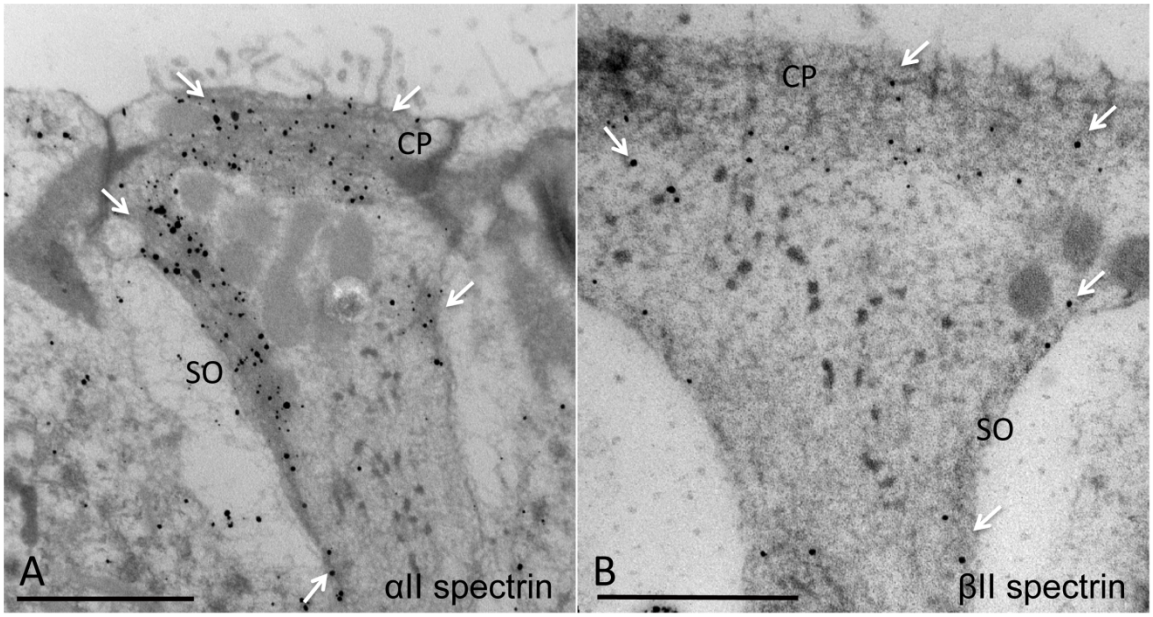

Figure 2.1. Immuno-electron micrographs from the apical portions of two adult type I hair cells showing that αII-spectrin and βII-spectrin subunits both localize to the cuticular plate and striated organelle. Scale bar: 2μm.

The determination that βII-spectrin is the αII-spectrin partner in cuticular plate and striated organelle of rat tissue was done using immuno-electron microscopy (Fig. 2.1). Of all the five mammalian β-spectrin subunits in the rat sensory epithelium, it was the only one that exhibited a labeling pattern resembling that of αII-spectrin (Fig. 2.1). Unequivocal corroborative evidence for this was obtained using confocal microscopy (Fig. 2.2).

2.4.2. βII-spectrin is a component of the striated organelle

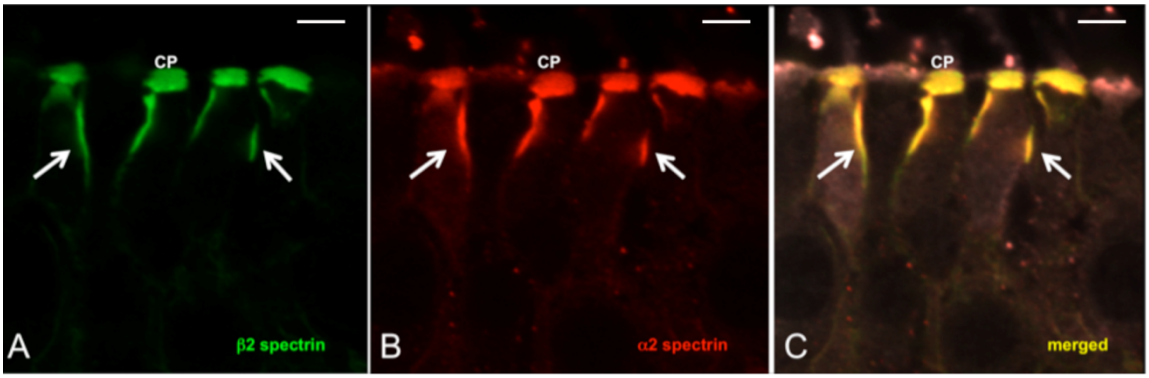

Figure 2.2. Utricula maculae from an adult female rat counterstained for **A**) βII-spectrin and **B**) αII-spectrin. Both subunits exhibit intense cuticular plate (*CP*) as well as striated organelle labeling (*white arrows*), and co-localize completely **(C)**. Scale bar: 5μm.

These two spectrin isoforms, αII-spectrin and βII-spectrin, co-localized in vestibular type I and II hair cells. Hence like the alpha-subunit, βII-spectrin is in the striated organelle. Employing βII-spectrin as bait in co-immunoprecipitation experiments and the then analyzing the eluent with LC-MS, yielded αII-spectrin, suggesting that these two co-purify and likely interact directly in the inner ear.

2.4.3. αII- and βII-spectrin-striated organelle labeling occurs after birth

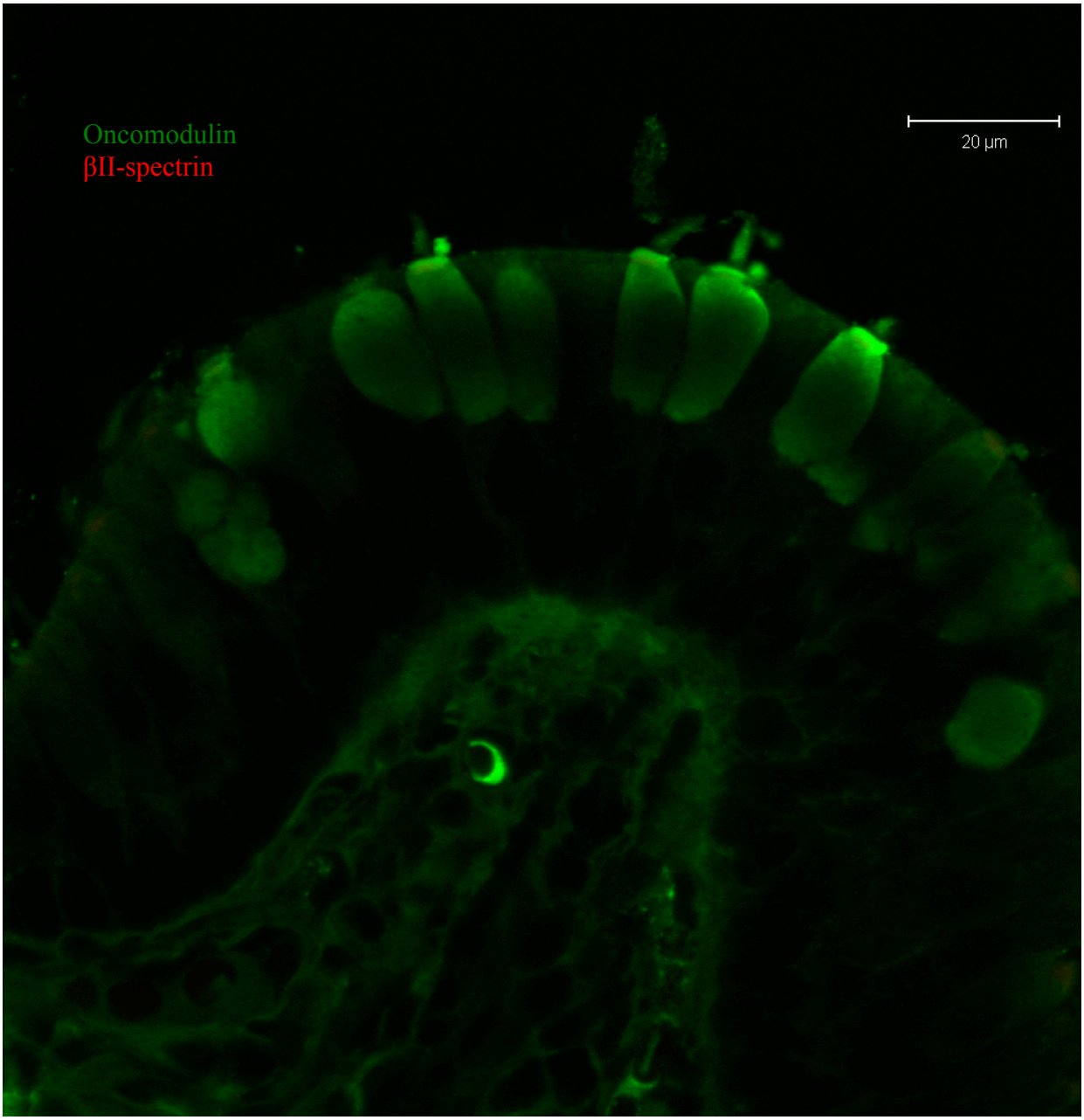

Figure 2.3. Crista ampullaris from P0 rat pup double-labeled for βII-spectrin (red) and oncomodulin (green), a calcium binding protein from the parvalbumin family (Simmons et al., 2010). Only the latter is apparent, with no hint of spectrin, suggesting this epithelium is from a time point before this protein is expressed. This implies that the signal for the hair cell SO spectrin in the rat develops post-natally.

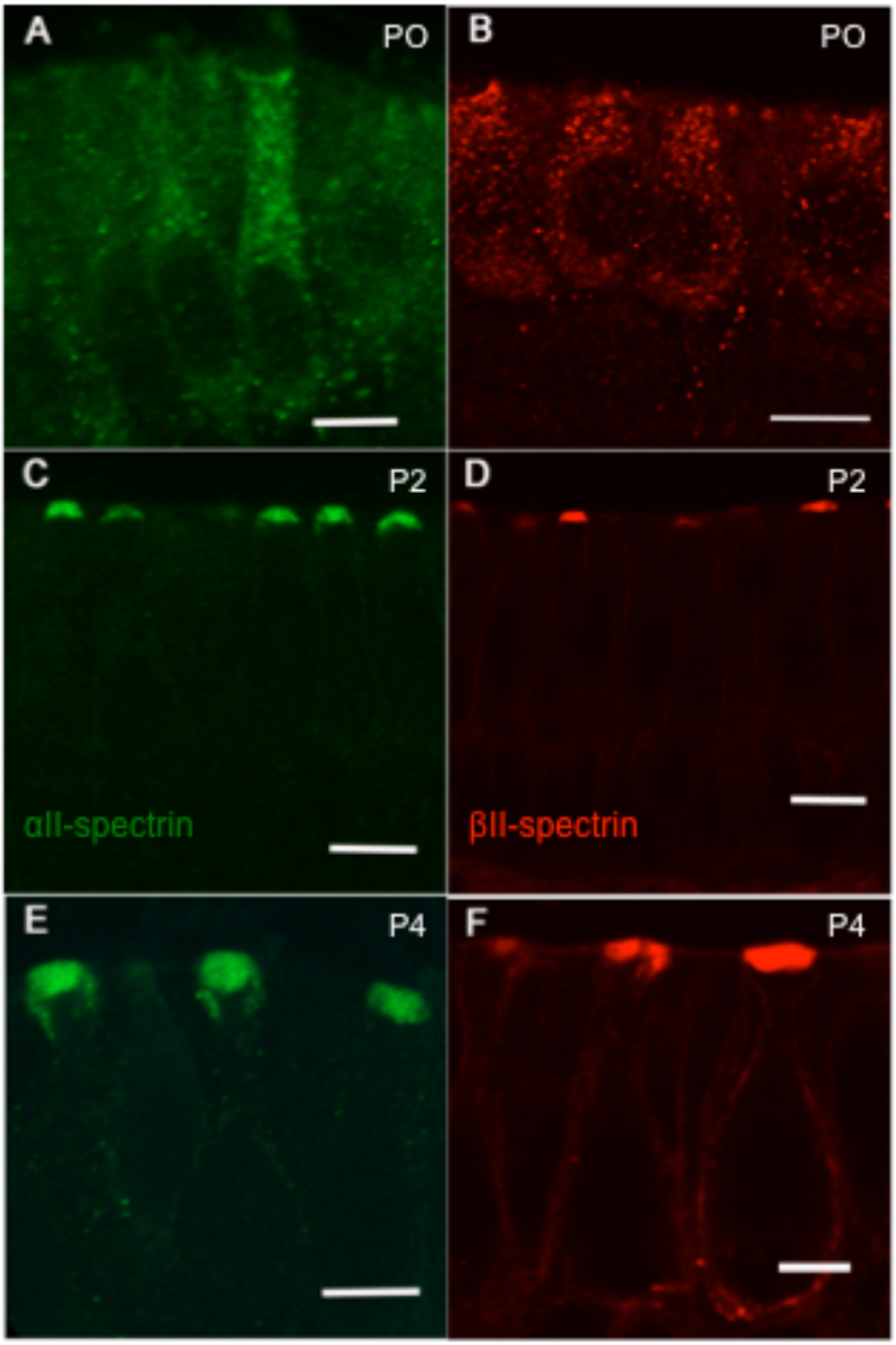

Figure 2.4. Confocal imaging of tracking the expression of the αII-spectrin in the developing crista ampullaris (**A, C, E**) matched against the βII-spectrin signal in utricular macula (**B, D, F**). Development in both the crista and utricle appears well-coordinated, with diffuse labeling at PO, which is likely a trafficking stage, and then the spectrins first appear in the cuticular plate (*P2*), before the SO signal appears (*P4*). Scale bars: 5μm.

Some of the P0 material points to the absence of the SO at birth (Fig. 2.3). In the initial stage of development, as seen in the P0 material, labeling using either antibody is diffuse and in the hair cell soma, with no cuticular plate signal. In the P2 material, cuticular plate plate is now labeled and no cytoplasmic labeling is apparent. P4 extensions from the cuticular, absent in the earlier material are clearly visible, indicating that the striated organelle is now present. However the hair cells are all not at the same stage of development, so the cuticular plate and SO are not universally labeled until P6 (Vranceanu et al., 2012).

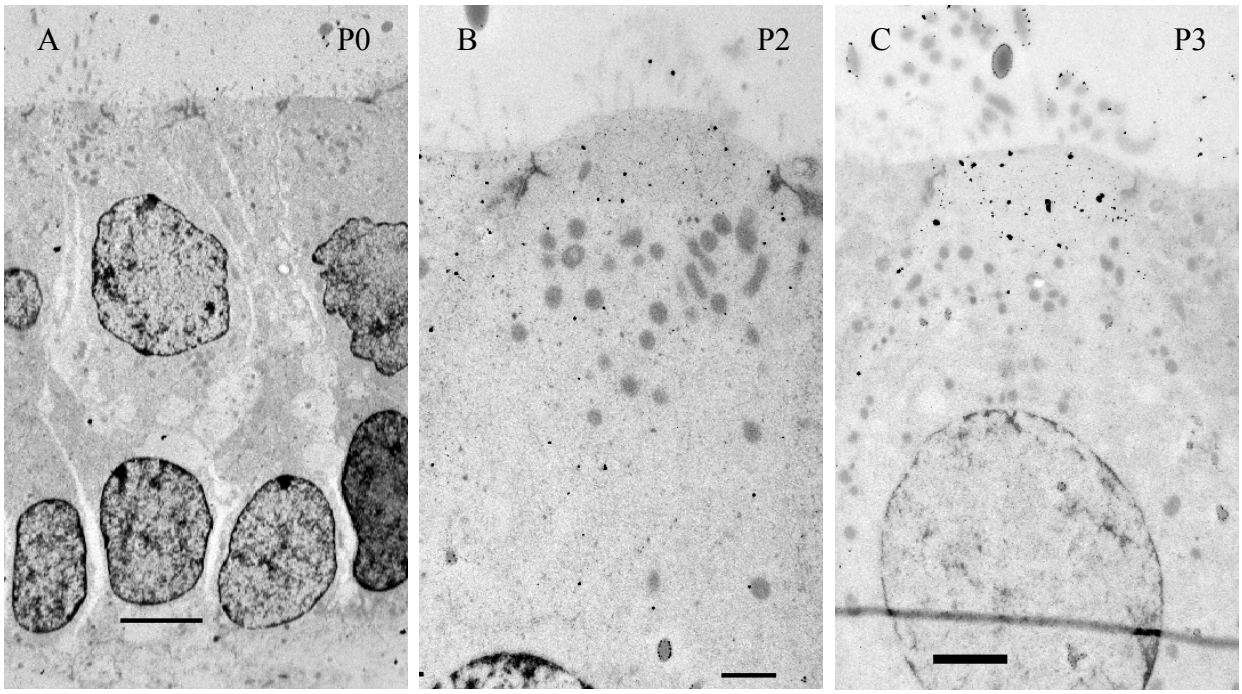

Figure 2.5. EM immunogold at 3 ages: **A)** Postnatal day 0 (P0) showing that there is no immunoreactivity for αII-spectrin, although there is a hint of some surface staining. Cuticular plate is not well defined. **B)** At this P2 stage, there is widespread cytoplasmic, but less focused immunogold labeling. The cuticular plate has become distinguishable. **C)** In this P3 animal, the cytoplasmic labeling is gone and the immunogold labeling is now concentrated in the cuticular plate, and there is a hint of what could indeed be label projecting from the cuticular plate inferiorly and laterally on one side. This is a good example of the advantage that using a biomarker brings, in that even though the SO might not be visible on the image, the immunogold particles show its presence. Scale bars, A=2μm; B=0.5μm; C=1μm.

2.5. Discussion

The first week of postnatal life is a busy time in the life of a hair cell. It is riddled with important developmental milestones that are occurring and have to be strictly followed. Much of the machinery the hair cell harnesses for mechanotransduction is still maturing and non-functional, hair cell terminal mitoses is occurring. It is in this fluid environment that the striated organelle forms.

The first major contribution that this study makes is the recognition that βII-spectrin is the heteromeric partner of αII-spectrin in the striated organelle. Previously, αII-spectrin's presence in the cuticular plate and striated organelle had been well characterized (Demêmes and Scarfone, 1992; Vranceanu et al., 2012), and the evidence that it was likely the thin cross-linking component of the structure was demonstrated (Nishida et al., 1993). Spectrins being obligate $(\alpha\beta)_2$-heteromers (Bennett and Gilligan, 1993) and there being only 5 β-subunits, it immediately became apparent that there was a fairly small pool of potential partners to investigate, so I set out to identify the putative binding partner of αII-spectrin using EM and confocal microscopy.

Once the two SO spectrin proteins had been identified, I tracked them using confocal and electron microscopy imaging, to establish a timeline for the development of the striated organelle. The challenge was always on how to objectively age the animals, as a lot of events are occurring in the inner ear sensory epithelium during the first week of life. The settled upon formula ensured that the oldest postnatal day 0 (P0) animals could have been just under 16 hours

old when processed, and the youngest P0 could have been a few minutes old. In developmental terms this is a huge window, the pups used could have been at very different stages. One approach taken is that at least 3 replicates were done per time point, so as to capture any variability that could have arisen because of imprecise aging. Based on careful analyses of the developmental series it is apparent that while some P0 animals had no spectrin signal at all others had a diffuse cytoplasmic pattern. One possible interpretation of this observation was that these were the youngest animals for that age group, perhaps even as young as a few minutes old. As the youngest P0 animals show no spectrin signal, this is an indication that these spectrin isoforms start expressing postnatally.

On this premise, a timeline emerges that shows the following major highlights: αII-βII-spectrin starts being expressed after birth during the very first day (P0); the nucleus directs that a lot of this protein be made and we see it being trafficked, first to the cuticular plate (P2) and then to the striated organelle (P4). The cuticular plate, with which it is intimately associated, initially appears as a flat disc at birth, forming a fully shaped cuticular plate at P3-5 (Nishida et al., 1998). This same basic timeline fits in perfectly with the onset of expression of αII-spectrin and βII-spectrin in the cuticular plate and SO. Although we see a diffuse pattern in the spectrins, which we speculated could be a trafficking stage, the spectrins are recruited first to the cuticular plate before they can form the SO. There are two possible reasons for this: 1) the cuticular plate is the more important structure so all resources are directed to make sure it completely forms, or 2) once it has completely formed, the cuticular plate requires the presence of the SO to function optimally, so the developmental program next directs its formation. In either scenario, the SO is intricately invested in those development events.

3. IMMUNOLOGICAL IDENTIFICATION OF CANDIDATE PROTEINS COMPRISING THE RAT'S INNER EAR STRIATED ORGANELLE

3.1. Abstract

It has been previously demonstrated by our laboratory and others that the vestibular striated organelle (SO) in rodents is made up of bands of actin filaments, cross-linked with αII- and βII-spectrin subunits. These bands of filaments exhibit a strict adherence to spatial intervals probably due to the large amount of spectrin between them. No other proteins are known for the organelle, thus it has proven difficult to assign structural correlates that we observe to specific proteins so as to generate testable hypotheses. Utilizing co-immunoprecipitation, followed by western blot, mass spectroscopy and confocal microscopy, we set out to investigate the interacting partners of the two SO spectrin isoforms that have been shown to be associated with the cytoskeletal structure. We report that ankyrin G, nebulin, and γ-actin are promising candidate proteins for the striated organelle, with at least two sets of corroborative data in support of that. Zyxin, trioBP, adducin, myosin 9 and 10, and β-actin, have been examined, but not to a level that we can determine their presence or absence from the SO. One approach we used, in which we undertook to use mass spectroscopy, proved too sensitive for the task at hand, generating more data than we could use. It seemed more likely that a biochemical approach, which involves first isolating the striated organelle then performing co-immunoprecipitation experiments, would work best in combination with the imaging approaches attempted here.

3.2. Introduction

The inner ear can be loosely considered as the 'seat' of two of our most ancient senses: hearing and balance. The fact that these are housed in the petrous portion of the temporal bone, the hardest bone in vertebrate animals' bodies, can be argued to serve as evidence of their importance. Unfortunately this secure location makes the primary sensory epithelia inaccessible to all but the most invasive approaches, which is partly the reason why less in known about them than the other senses. This study focuses on the striated organelle, a novel cytoskeletal structure, found within hair cells, the primary sensory cells of the inner ear.

Hair cells are uniquely designed to deal with the rigors of mechanotransduction. They are highly polarized. Their name derives from each cell having, on its apical surface, 100-300 stereocilia, and one kinocilium. The stereocilia have generally been regarded as being anchored in the cuticular plate. This is, however, not strictly accurate as the stereocilia rootlets sometimes pierce the cuticular plate and anchor to the lateral plasma membrane or join a structure that forms the basis of this study, the striated organelle (SO) (Vranceanu et al., 2012).

The SO is still conjecture and its protein composition poorly known. So we set out, using molecular, proteomic and microscopy approaches, to try to find proteins that interact with those in the SO.

3.3. **M**aterial and Methods

Procedures involving the handling and use of the study animals were done in accordance with guidelines and protocols approved by the Institutional Animal Care and Use Committee (IACUC) at the University of Illinois at Chicago.

3.3.1. Antibodies: Primary antibodies:

Rabbit anti-human βII-spectrin (Dr. Jon Morrow, Yale Medical School), mouse anti-βII spectrin (BD Biosciences, San Jose, CA), mouse anti-αII spectrin/fodrin and goat anti-calretinin (Chemicon, Temecula, CA), rabbit anti-nebulin (H300, N-terminal, Santa Cruz, SC-28286), rabbit anti-nebulin (Dr. Carol Gregorio, Univ. of Arizona), rabbit anti-zyxin (Dr. Mary Beckerle, Univ. of Utah), trioBP , β-actin, , mouse anti-ankyrinG2a (clone N106/36, Neuromab, Davis, CA), and rabbit anti-γ-actin (Dr. Karen Friderici, Michigan State Univ.)

3.3.2. Animal Model: Long-Evans rats (*Rattus norvegicus*) were used in these studies.

3.3.3. Tissue Processing:

Rats of various ages ranging from the day of birth (post-natal day 0) to 4 weeks of life (P28) were utilized in the development studies. Because the animals are housed in the university animal facility, pinpointing the exact time of birth was not possible. However expectant female rats were checked on 3 times per day (9am, 1pm, and 5pm), meaning that once it was established

that a rat had given birth, it was almost certain that the observation was made within, at most, the first 16 hours of life, and definitely during the first 24 hours of life. One pup was processed within one hour after that, and the exact time point was designated as P0. For later time points within the same litter, subsequent animals were processed at the same exact time. What follows is the processing protocol employed: Animals were anesthetized with Nembutal (80 mg/kg), then perfused trans-cardially with 10-100 ml physiological saline containing heparin (2000 IU), followed by 2 ml/g body weight of an aldehyde fixative (for confocal microscopy: 4% paraform-aldehyde, 1% acrolein, 1% picric acid in 0.1 M phosphate buffer (PB) with 5% sucrose, pH 7.4; for electron microscopy: 2% paraformaldehyde, 3% glutaraldehyde, 1% acrolein in 0.08 M cacodylate buffer with 5% sucrose, pH 7.4). Sensory epithelia were then micro-dissected in PB and cryoprotected overnight by incubation at 4^0C in a solution of 30% sucrose. Background fluorescence was reduced by incubating tissues in a 1% aqueous solution of sodium borohydride (NaBH) for 10 min.

3.3.4. Confocal Microscopy:

Vestibular endorgans and cochleae were embedded in gelatin and frozen sections (40µm) were cut on a freezing sliding AO microtome. Sections were permeabilized in Triton X-100 for 1 hour at room temperature. The actual strength of the Triton X-100 employed varied in accordance with postnatal age: P0-P2: 0.3% Triton in PBS was used; P3-P5: 0.5%; P6-P8: 2%; >P8: 4%. To minimize non-specific binding, samples were incubated with a blocking solution of 0.5% fish gelatin, 0.5% Triton X-100 and 1% BSA in phosphate-buffered saline (PBS, 0.01M) for 1 hr. Afterwards, samples were incubated for 2 days in primary antibodies (1:200) diluted in the

blocking solution. After rinsing in PBS, samples were incubated overnight in secondary antibodies (1:200) conjugated to Alexa or TRITC labels directed against the primary antibodies to reveal specific labeling. For each experiment "no primary antibody" controls, which revealed a lack of non-specific staining, were performed, in addition to determining antibody efficacy by using positive and negative control tissues. We also confirmed expression of each of antibody by performing western blots. Samples were mounted on slides in Mowiol (Calbiochem, Darmstadt, Germany). Slides were examined on a laser scanning confocal microscope (LSM 510 META, Carl Zeiss, Oberköchen, Germany). Z stacks of optical sections were then acquired on the confocal microscope, with the thickness of the optical sections varying from 0.4 – 1.0 μm. Final image processing and labeling was done with Adobe Photoshop (San Jose, CA).

3.3.5. Electron Microscope (EM) Immunogold:

The methods described below for electron microscopy immunogold are similar to those used previously by Lysakowski et al. (2011) and are included here for completeness. Vestibular endorgans were cut into 40μm thick sections using a Vibratome 2000 (Technical Products International, St. Louis, MO). Permeabilization of the sections was effected by incubating them for an hour with 0.5% Triton X-100 in 0.1M PB, followed immediately by a blocking step in 0.5% fish gelatin and 1% BSA in 0.1M PB for another hour. Using the primary antibody of choice at a dilution of 1:50 in blocking solution, the sections were incubated for 72 hrs at 4^0C with gentle shaking on a shaker (Roto Mix 50800, Barnstead/Thermolyne, Dubuque, IA). The secondary antibody tagged with ultra-small (0.8 nm) colloidal gold-labeled F (ab) goat anti-mouse IgG and goat anti-rabbit IgG (Aurion Cat. No. 25413, Electron Microscopy Sciences, Hatfield, PA),

diluted to 1:40 also in blocking solution, was incubated with the sections for 24 hrs, after the primary antibody had been sufficiently rinsed off. A 4-8-minute silver enhancement of the gold staining followed using the IntenSEM kit (Amersham Biosciences, Piscataway, NJ). Ten minute serial dehydrations in increasing strength ethanol solutions (i.e., 50%, 70%, 80%, 90%, 100% EtOH) were performed on the sections, followed by two 10-minute incubations, and then the sections were embedded in Araldite resin (Fluka Durcupan, Ronkonkoma, NY) freshly poured into a plastic mold. The resin was allowed to harden in an oven at 60°C for 48 hrs. The hardened block was then sectioned with a diamond knife (Diatome, Biel/Bienne, Switzerland). Staining with uranyl acetate and lead citrate enhanced the gold signal and allowed the processed samples to be examined and photographed with a JEOL 1220X transmission electron microscope.

3.3.6. Co-immunoprecipitation:

Co-immunoprecipitation was performed using protein extracts from inner ear tissue and reagents as previously described (Sridharan et al., 2006). The tissue of interest was dissected in ice-cold buffer with clean autoclaved tools as quickly as possible to prevent degradation by proteases. We collected the tissue in immunoprecipitation (IP) buffer (25 mM Tris-HCl pH 7.3, 125 mM NaCI, 1% Triton X-100, 1% mammalian protease inhibitors- Sigma P8340) on ice in flat-bottomed Eppendorf tubes. After standing in ice for 30 min, tissue was then homogenized mechanically with the variable speed Tissue Tearor Homogenizer (model No. 985370, Biospec, Bartlesville, OK) for 3 minutes at the slowest speed while standing on ice. Tissue was then centrifuged for 20 min at 12,000 g at 4°C in a refrigerated Microfuge 22R centrifuge (Beckman Coulter, Danvers, MA), after which the tubes were gently removed from the centrifuge and

returned to ice. The supernatant was aspirated and placed in a fresh tube kept on ice; discarding the pellet. Protein concentrations were assayed using a Nanodrop spectrophotometer with a Pierce 660nm protein assay kit (Product # 22662, Thermoscientific, Rockford IL). Once the protein concentration was determined, we proceeded with the immunoprecipitation while storing any excess protein at -80°C for later use. We pipetted out 250 µL beads (Protein G sepharose, Catalog # P3296, Sigma-Aldrich, St Louis, MO) for later division into 5 centrifuge tubes (50 µL per tube). Beads were washed first and only once with cold PBS, then 4 times with binding buffer (25mM Tris-HCl pH 7.3, 150mM NaCl, 1% Triton X-100 plus 1% protease inhibitor cocktail). The lysates were pre-cleared for 1 hr with protein A-sepharose (50% slurry) control IgG in binding buffer. Following pre-clearing, samples were incubated with antibody-immobilized protein G-sepharose (50% slurry) for 4 hr in IP buffer on a rotator at 4°C. The antibodies used were mouse anti-αII-spectrin or equivalent amounts of control mouse IgG for the control. Supernatants were collected after each reaction to assess reaction efficacy. Following washes with IP wash buffer (25mM Tris-HCl pH 7.3, 137mM NaCl, 1% Triton X-100, 1% protease inhibitor cocktail), protein complexes were collected, eluted and subjected to SDS-PAGE analysis. To determine which proteins are co-immunoprecipitated with αII-spectrin, some gels were sent to the UIC Proteomics lab for mass spectrometry analysis while others underwent western blot analyses with appropriate antibodies.

3.3.7. Western Blot:

We autoclaved all the dissection tool kits, Eppendorf tubes, and glassware, and ensured that all the plastic ware was new and sealed 24 hours before the scheduled tissue harvesting. We prepared fresh Radio Immuno Precipitation Assay (RIPA) buffer (50mM Tris-HCl pH 8.0, 150mM NaCl, 1% Triton X-100, 0.5% Sodium deoxycholate, 0.1% Sodium dodecyl sulfate) as homogenization buffer. Just before the dissection, we added the Sigma Protease Inhibitor Cocktail **(**P8340) at a concentration of 1:100 to the RIPA buffer**.** Volumes of buffer to be used were determined in relation to the amount of tissue present, typically for 3 animals we used 150µl of buffer for vestibular endorgan tissue, vestibular ganglia, vibrissae and cochlea, and 300µl for the bulkier brain and retina. We dissected the tissue of interest in cold 0.1M PB, and placed it into RIPA (with protease inhibitors) as quickly as possible to prevent degradation. Harvested tissue was either immediately flash-frozen in liquid nitrogen and then stored at -80°C for later use or kept on ice for immediate homogenization. For freshly dissected tissue or tissue from -80°C freezer, we let it stand in RIPA buffer for at 30 minutes at 4°C or on ice with constant agitation on the rotator to allow the homogenizing buffer to completely infiltrate the tissue. Mechanically homogenized tissue using a multi-speed Tissue Tearor (model # 985370, Bartesville, OK) for 3 to 5 minutes. We centrifuged the resultant homogenate in a refrigerated Microfuge 22R centrifuge (Beckman Coulter, Danvers, MA) at 4°C for 20 minutes at 12,000 g. The supernatant was aspirated and placed it in a fresh tube on ice, and discarded the pellet. Performed the Pierce 660 protein assay on a nanodrop. The Pierce 660nm assay comes with a set of protein standards from 125µg/mL to 2000µg/mL. For tissue with protein concentrations above this upper limit, we diluted it until a concentration reading could be determined, then extrapolated back using the dilution factor used. Once the concentration of each sample was

determined, we proceeded with the western blot experiment after storing some samples at -20°C or -80°C for later use. First we boiled the mixture of sample plus loading buffer at 95-100°C for 10 minutes, then we loaded 20-40µl samples per mini-gel well and ran the gel at a constant 190V for 45 minutes, or until the leading edge of the samples had migrated sufficiently. After the electrophoresis, we transferred migrated proteins onto PVDF the membrane by running at 30V constant overnight at 4°C, or for 6 hrs at room temperature (RT). We blocked the membrane in 5% milk for 1 hr. The membrane was probed with the primary antibody of interest for 2 hrs at RT, and with the requisite HRP secondary for 1 hr after that before developing the signal using a chemiluminescent reagent on an Kodak X-Omat Developer.

3.3.8. Mass Spectrometry method (Co-IP gels)

In all but one instance, the University of Illinois at Chicago Research Resources Center's Mass Spectrometry, Metabolomics and Proteomics Facility performed the liquid chromatography mass spectrometry (LC-MS) analysis of bands cut from gels obtained from co-immunoprecipitation experiments following the protocol of Kinter and Sherman (2000). The presence of protein was first confirmed using Coomasie staining (which is compatible with downstream mass spec). Because our interest was in all the interacting partner proteins, typically the whole gel lane was excised in its entirety, or sometimes it was halved with the resultant two pieces analyzed separately to make the analysis more manageable and to see if that would increase the resolution. A fresh sterile razor blade was used in all case to make the excisions under a sterile hood. Gel pieces to be analyzed were further cut into 1 mm^3 blocks, destained, rinsed, and then dehydrated. A dithiothreitol (DTT) step was incorporated specifically to denature the protein by reducing the disulphide bonds within, followed by iodoacetamide treatment, which, by alkylating those same

reduced sulfide bridges, ensures they do not re-form and that the protein stays in the reduced form. The samples were then subjected to an overnight trypsin digestion at 37 °C in 50 mM ammonium bicarbonate in accordance with the protocol (Kinter and Sherman, 2000). Afterwards, the peptide mixture was extracted from the gel matrix, concentrated, and analyzed Thermo Orbitrap Velos mass spectrometer using a chip-based HPLC nanospray technology (Agilent Chip Cube) (Schilling et al., 2010).

3.3.9. Database Searching

After the analysis, the tandem mass spectra generated were extracted by Readw.exe (v. 4.0.2, Institute for Systems Biology) as mzXML files. These files were converted into the Mascot generic format (mgf) using MzXML2Search and then submitted to a Mascot search engine (v. 2.2.04). Using the SwissProt 57.15 database, searches were carried out under the following conditions: parent ion tolerance of 10 PPM, and a fragment ion mass tolerance of 0.6Da, with carbamodomethylation and oxidation as variable modifications, recognizing up to 2 missed cleavages and incorporating a decoy search. Mascot was set up to search the SwissProt 57.15 database for trypsin digestion peptides using the *Rattus* genome.

3.3.10. Criteria For Protein Identification.

Validation of the tandem MS/MS-based peptide and protein data made was done using Scaffold (version 3.1.4.1, Proteome Software Inc., Portland, OR). Acceptance and rejection criteria for peptide and protein identifications were reached according to the specifications of the Peptide Prophet algorithm (Keller et al., 2002). For a protein to be accepted and identified from a sample, the set criteria were that the software had to have a greater than 95.0% probability of

certainty as to its identity, and must have encountered more than one identifiable peptide from that same protein in the sample. The Protein Prophet algorithm assigned these probabilities (Nesvizhskii et al., 2003). In cases where proteins had no unique peptides, or had peptides that were similar thus precluding tandem LC-MS identification, a generic identification was made to satisfy the principles of parsimony.

3.4. **R**esults

3.4.1. Experimental Design

For each antibody used in immunoprecipitation experiments, the first step was the optimization. Results of such an optimization are shown in Fig 3.1. Once the best concentration had been established we proceeded to do the immunoprecipitations.

As the experimental design western blot shows (Fig 3.2), using precast 10-well gels, only one lane was assigned to the experimental immunoprecipitation while the rest were controls. This panel of controls enables us to identify specific signal as opposed to false positives. Identifying the source of any signal as it arises is paramount. The tissue lysate is the positive tissue control meant to show presence of antigen of interest in the sample before the immunoprecipitation. This should never be negative as long as the IP shows a positive immunoreactivity. There are 3 negative controls, one is a no lysate control with the experimental set up in the IP buffer. A negative result is the desired outcome for this panel so that one can be sure the RIPA is not imparting the signal seen; another control is the no primary antibody IP, which essentially aims to show that the signal emanates from the antibody reaction and not from antigen sticking to

beads; and 3) unconjugated immunoglobulin control which shows the antigen is not sticking to IgG chains. The supernatants/or flow through is collected after the IPs to show how effective the antibody-antigen reaction really was. Where it is complete, no protein of interest remains in the supernatant, but where it is only partial some of the protein remains after reaction.

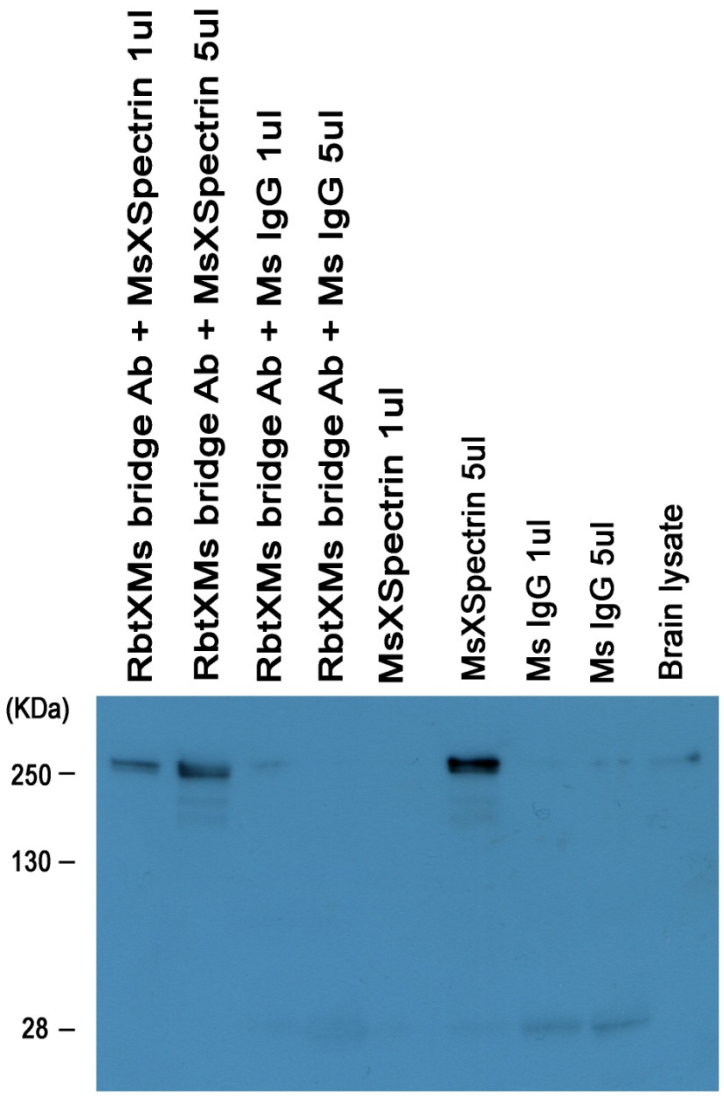

Figure 3.1. Result of optimization study performed to determine optimal antibody to be used for experiment. The two spectrin subunit antibodies for αII-spectrin and βII-spectrin are both of the mouse IgG1 subtype, so we investigated the efficacy of using these antibodies either complexing directly with the sepharose beads, or indirectly via a rabbit anti-mouse IgG1 bridge. The most optimal signal was when using 5μL/600μl of lysate (of a 0.1mg/ml base concentration), meaning throughout our studies we used antibodies of concentration 0.83mg/ml with no bridge.

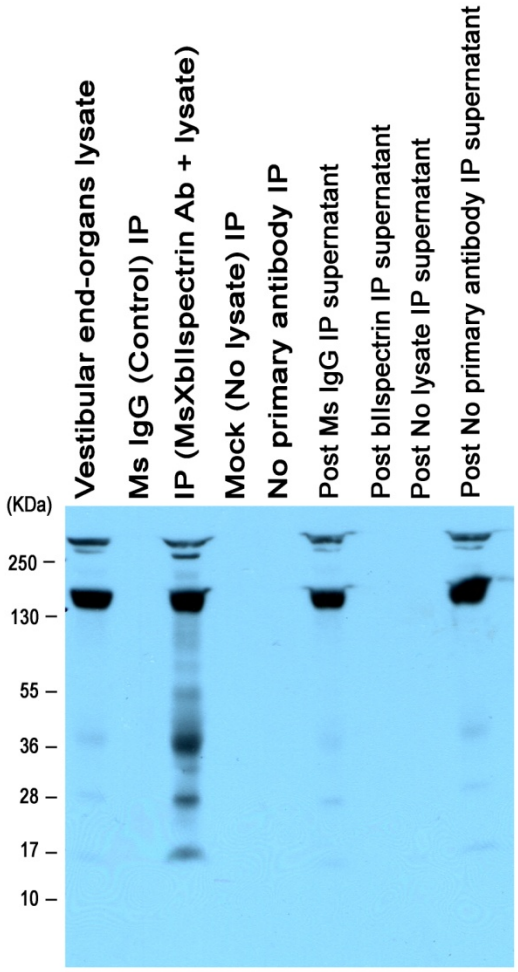

Figure 3.2. Experimental design of the trial immunoprecipitation experiment. While not all results will be presented in this form, this is how each of the co-immunoprecipitation experiments was actually designed.

1. Vestibular endorgan lysate – positive tissue control (tissue lysate) from which the interaction being probed was occurring.
2. Ms IgG control IP – unconjugated antibody from the same background in which the antibody being used as bait was raised → to ensure the IgG was not acting as bait
3. IP – the experiment of interest, with bait antibody affixed to beads and in lysate tissue
4. No primary antibody IP – naked beads incubated with lysate → to ensure that the beads were not the bait
5. Post IgG IP supernatant – supernatant in 2 at the end of IP
6. Post IP (e.g., Ms anti βII spectrin) supernatant – leftover protein not IP'd from col. 3
7. Post No lysate IP supernatant – to show whatever signal is not from the IP buffer
8. Post no primary antibody IP supernatant- supernatant from 4. Should be same as col. 1.

3.4.2. Identification of the β-spectrin partner for αII-spectrin

Of all the spectrin isoforms, αII-spectrin and βII-spectrin, co-localized in vestibular type I and II hair cells. Hence like the alpha-subunit, βII-spectrin is in the striated organelle. Employing βIIspectrin as bait in co-immunoprecipitation experiments and then analyzing the eluent with western blot yielded a positive immunoreactivity for αII-spectrin, suggesting that these two copurify and likely interact directly in the inner ear.

Running the full panel of reaction tubes clearly shows that the positive tissue control does contain αII-spectrin (Fig 3.3). The IP is effective and efficient as it tests positive for the alpha form, and no alpha spectrin signal is detected in the supernatant after reaction. The other positive signals came from the supernatants from the rabbit IgG control and the no primary antibody control. Beads in these two reactions had no specific antibody tethered to sepharose G beads to effect the pull down of proteins, and as such all the proteins just pass through in the fluid after reaction.

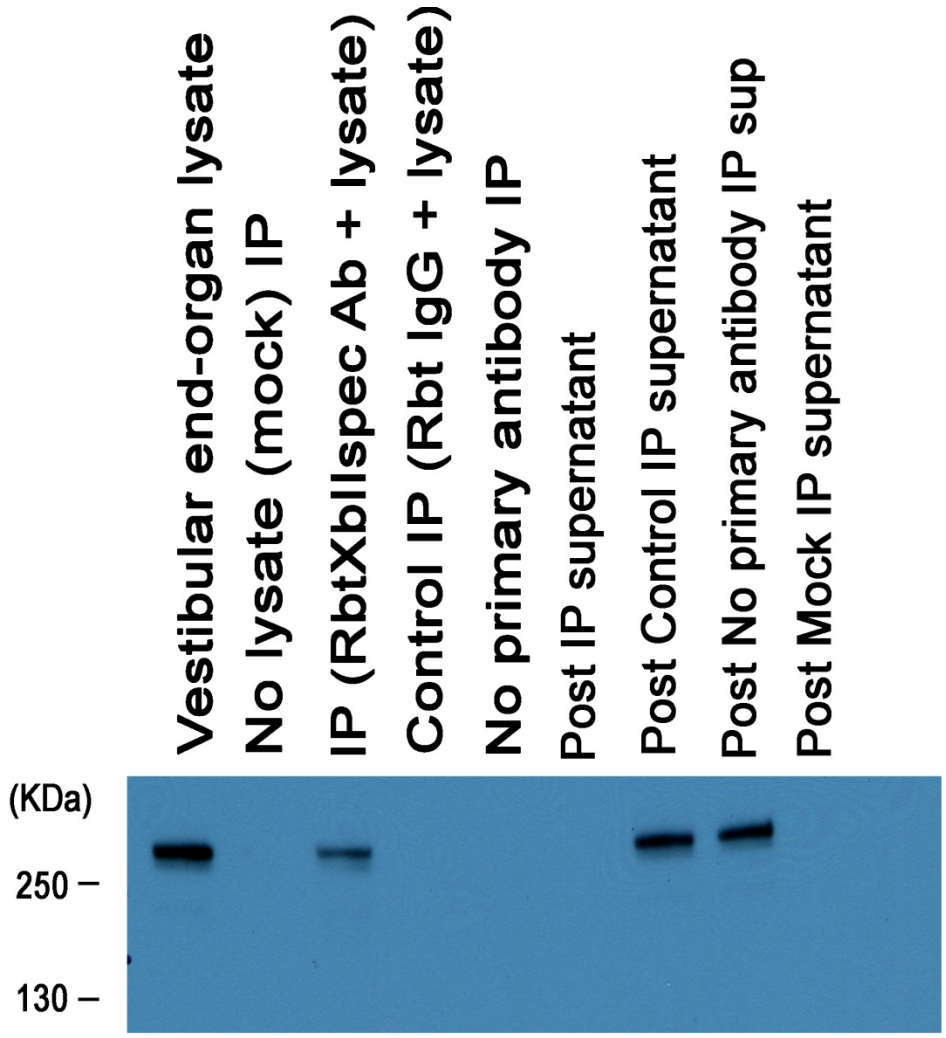

Figure 3.3. Co-immunoprecipitation of the αII-spectrin subunit after employing βII-spectrin as bait. To avoid cross-reactivity, the bait antibody was made in a rabbit background and the probe for the western blot was raised in mouse. This means that the βII-spectrin (bait) co-purifies with αII-spectrin.

3.4.3. Evidence of other SO proteins from confocal microscopy and co-immunoprecipitation

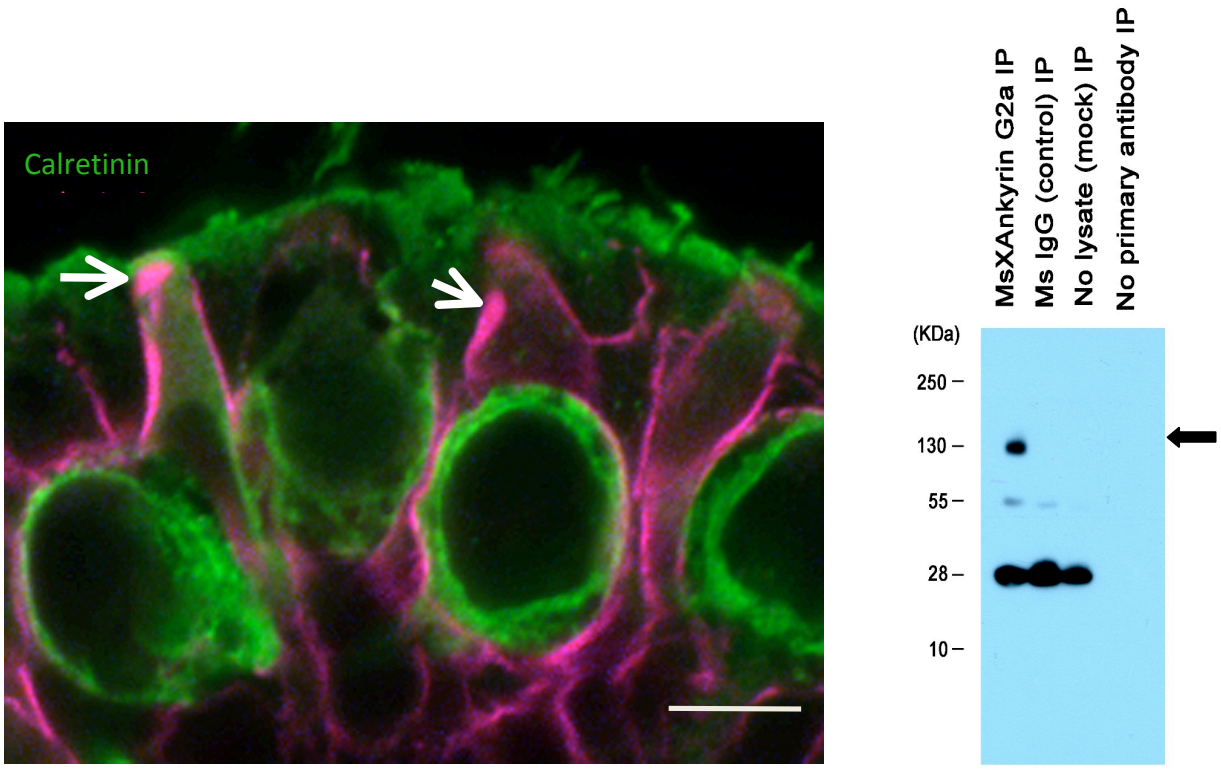

Figure 3.4. **A)** Confocal microscopy image of ankyrin G (*magenta*), counterstained with calretinin (*green*), showing positive immunoreactivity (*white arrows*) in the cuticular plate and striated organelle of type I and II hair cells in the crista ampullaris. As one of the canonical binding partners of β-spectrin subunits, the presence of ankyrin G was expected. **B)** To corroborate the confocal data, a western blot was performed on eluents obtained from an immunoprecipitation experiment in which we probed for the precipitation of βII-spectrin. In the experimental design, the mouse anti-ankyrin antibody was the bait for lane 1, an unconjugated mouse IgG replaced ankyrin as the bait in lane 2; mock IP where the IP buffer replaced the tissue lysate in lane 3; naked beads with no attached antibodies in lane 4. Two bands that show up in lanes 1-3 (viz. in which antibodies were bound to beads) at the 28- and 55-kDa levels are for immunoglobulin light and heavy chains respectively, hence their absence in lane 4, with the βII-spectrin signal apparent only in lane 1 (*black arrow*).

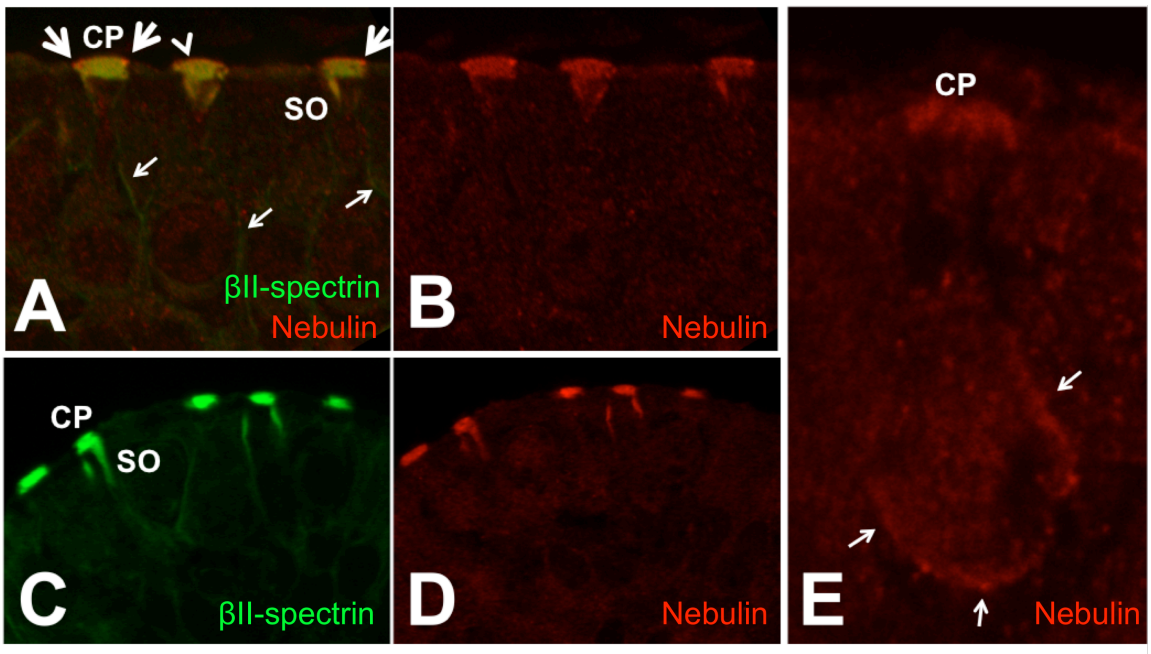

Figure 3.5. **A)** βII-spectrin intensely labels the cuticular plate (*CP*) and striated organelle and also lightly labels the outer surface of calyces surrounding type I hair cells (*thin arrows*). Nebulin antibody also labels these structures, but appears to extend further laterally on the cuticular plate (*thick arrows*). In addition, nebulin appears to label the stereociliar rootlets (*arrowheads*) within the cuticular plate. **B)** Removing the βII-spectrin channel, one can see the rootlets (*arrowheads*) labeled a bit more clearly. **C, D)** In a different experiment, both βII-spectrin and nebulin label the CP and SO. The staining in both channels here is more intense, so the rootlets cannot be observed. **E)** In the vestibular organs, nebulin also labels the basolateral membranes of type I hair cells (*arrowheads*).

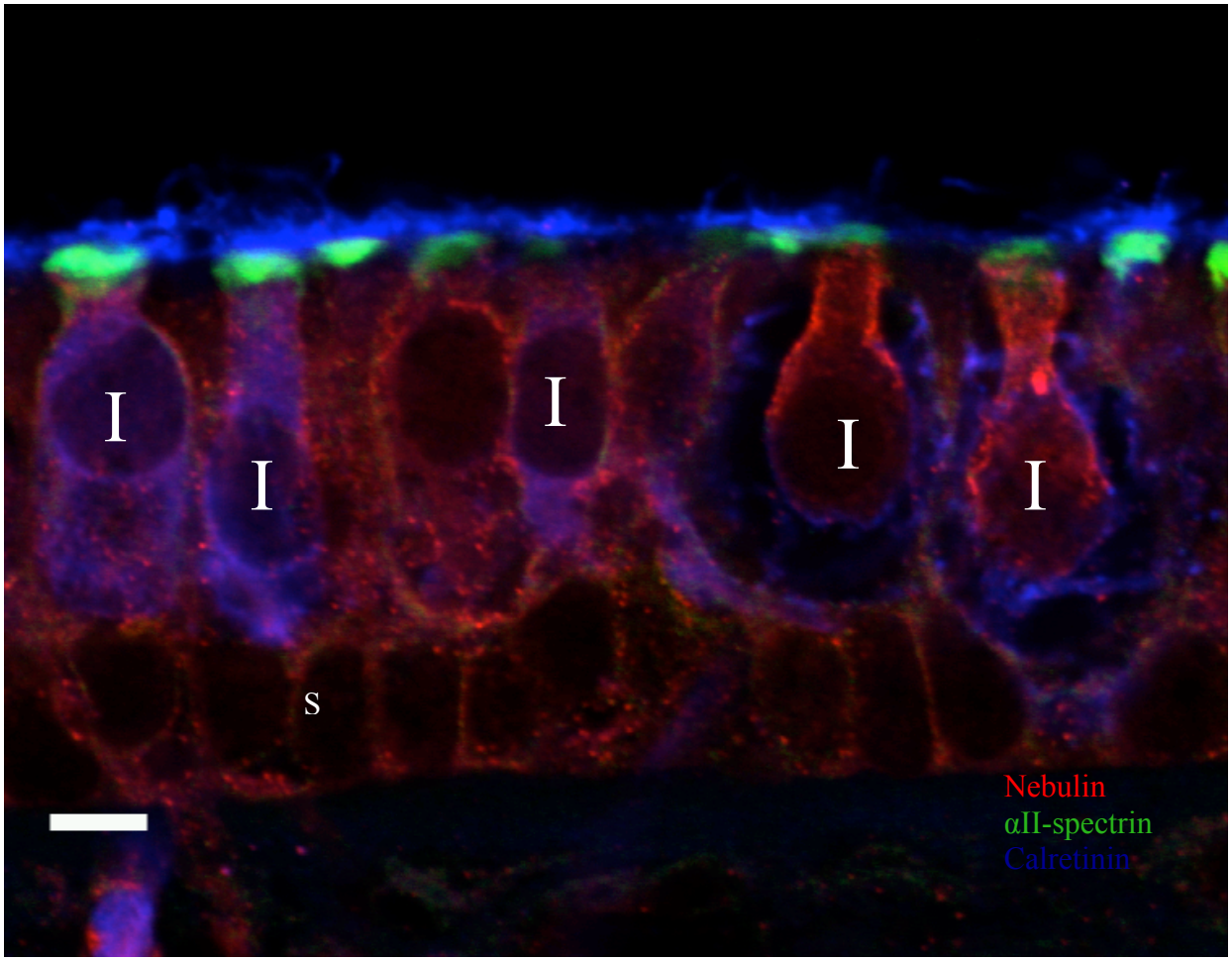

Figure 3.6. Nebulin also labels the lateral membranes of type I hair cells but not type II hair cells. These cells were counterstained with calretinin (a marker for type II hair cells and pure calyx afferents) and αII-spectrin (a marker for cuticular plate and striated organelle). Scale bar =

Nebulin interacts with ankyrin G, γ-actin, αII-spectrin and βII-spectrin subunits. Got a negative result with β-actin, but suspect that this antibody doesn't work as well, so would stay away from mentioning it, and emphasize that γ-actin was probed as its presence had been intimated by mass spec and then localized by immunocytochemistry.

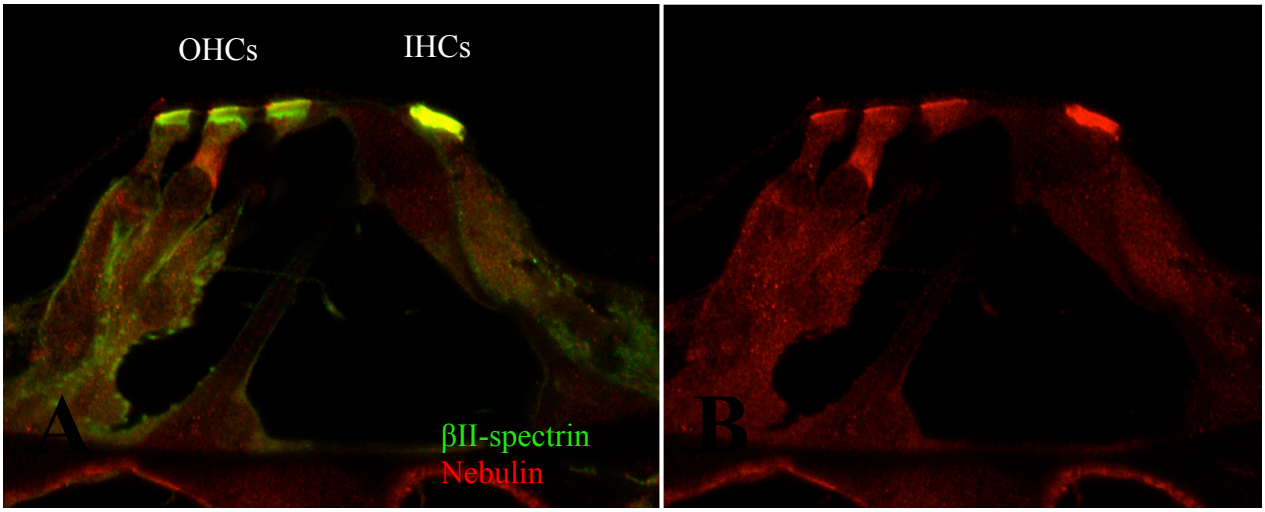

Figure 3.7. Nebulin is found in the cuticular plate of both inner and outer hair cells. In the OHCs a subapical distribution is apparent. This appears to be what other workers have called the infracuticular network, an actin-rich meshwork.

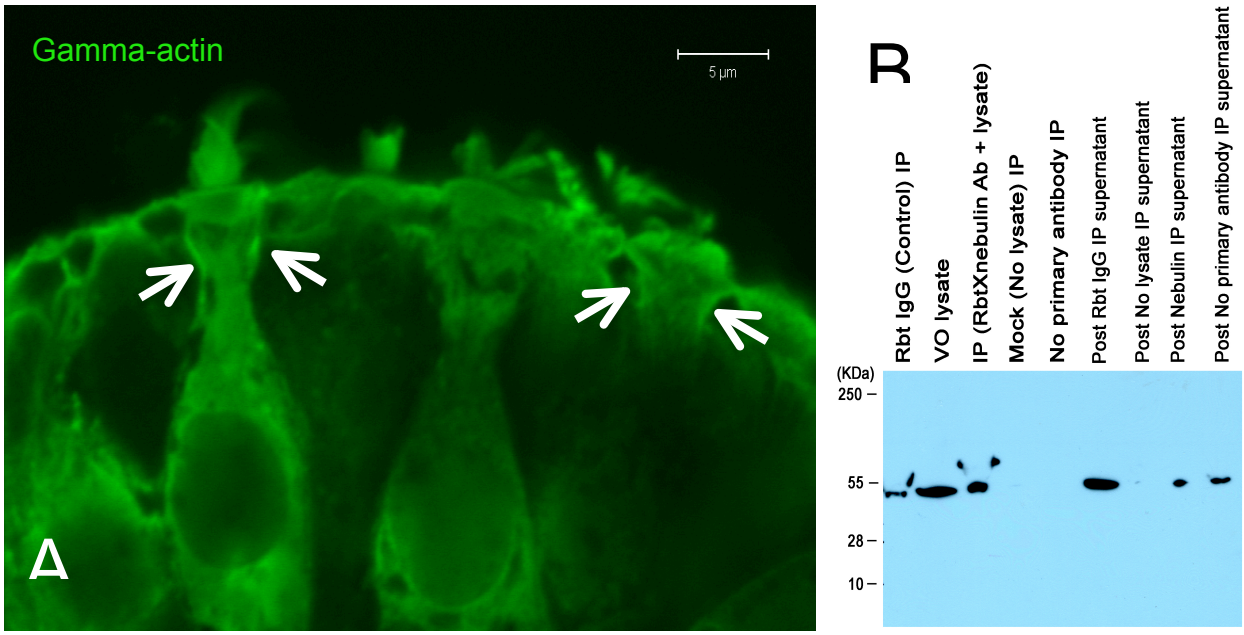

Figure 3.8. A) γ-actin localizes also to the same region where the SO has been found and is likely the actin isoform identified by Slepecky and Chamberlain (1982). **B)** Nebulin actin binding protein (ABP) identified the SO region of the hair cell. When it is used as bait in a co-immunoprecipitation experiment, it co-purifies with γ-actin as shown. This further strengthens the likelihood that they both localize to the SO.

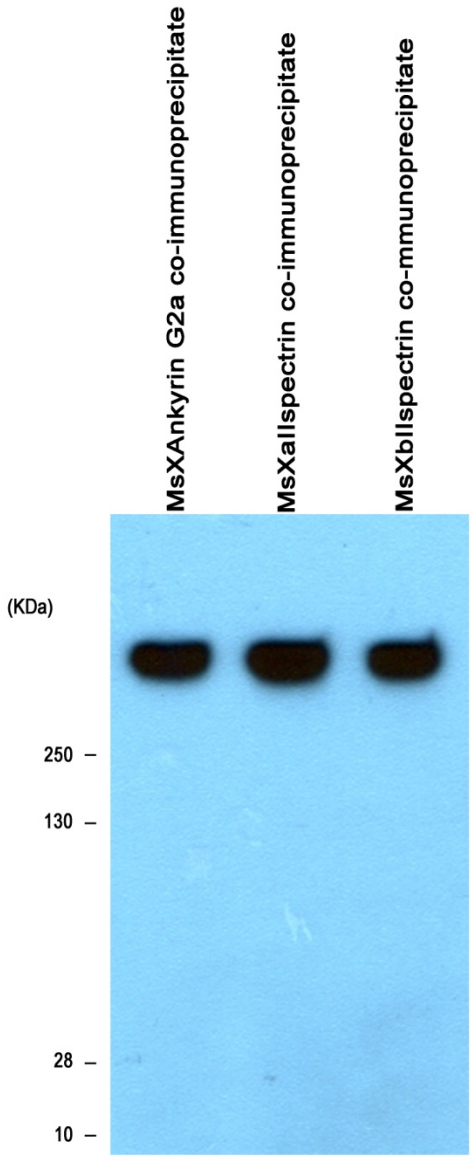

Figure 3.9. Combined western blot from 3 co-immunoprecipitation experiments where only actual IPs were probed for nebulin. The tissue in all cases was of vestibular endorgan origin, reacted with sepharose G beads complexed with mouse anti-ankyrin G, mouse anti-αII-spectrin, and mouse anti-βII-spectrin, respectively. All three had a positive immunoreactions to nebulin.

3.4.5. Other probable proteins

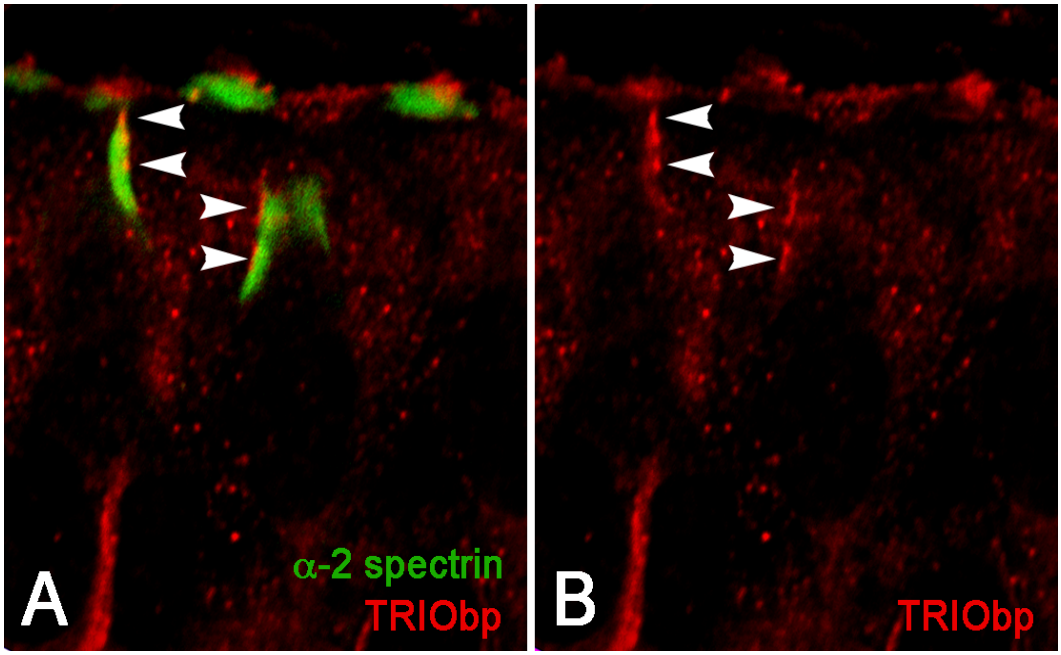

Figure 3.10. A, B: Crista hair cells immunoassayed for α2-spectrin (green) and TRIObp (red), an actin binding protein found in cochlear hair cells (Kitajiri et al., 2009). Staining pattern along the cell walls (white arrowheads) clearly suggests localization of TRIObp in the same area as the SO, as indicated by the α2-spectrin immunolabel.

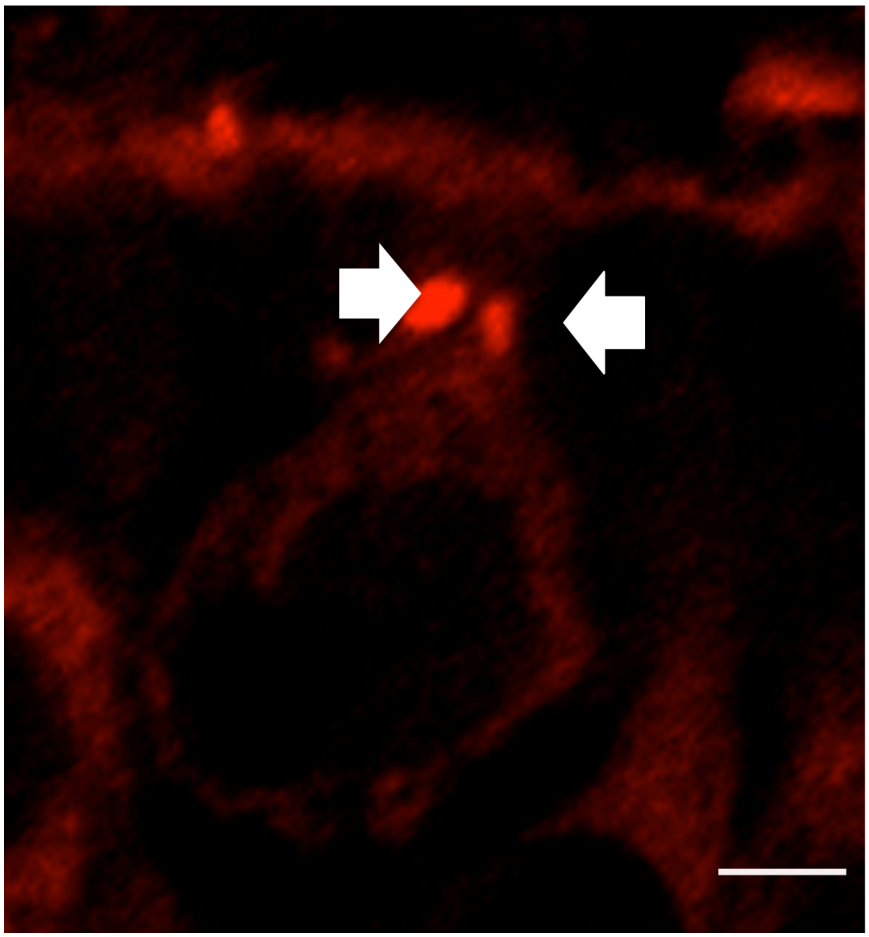

Figure 3.11. Confocal imaging showing focal adhesion protein Zyxin (red) in the same generalized area where the SO occurs. In the cochlea, this protein has been localized to pillar cells together with vasodilator-stimulated phosphoprotein (VASP) where a probable role in actin dynamics has been suggested (Schick et al., 2003)

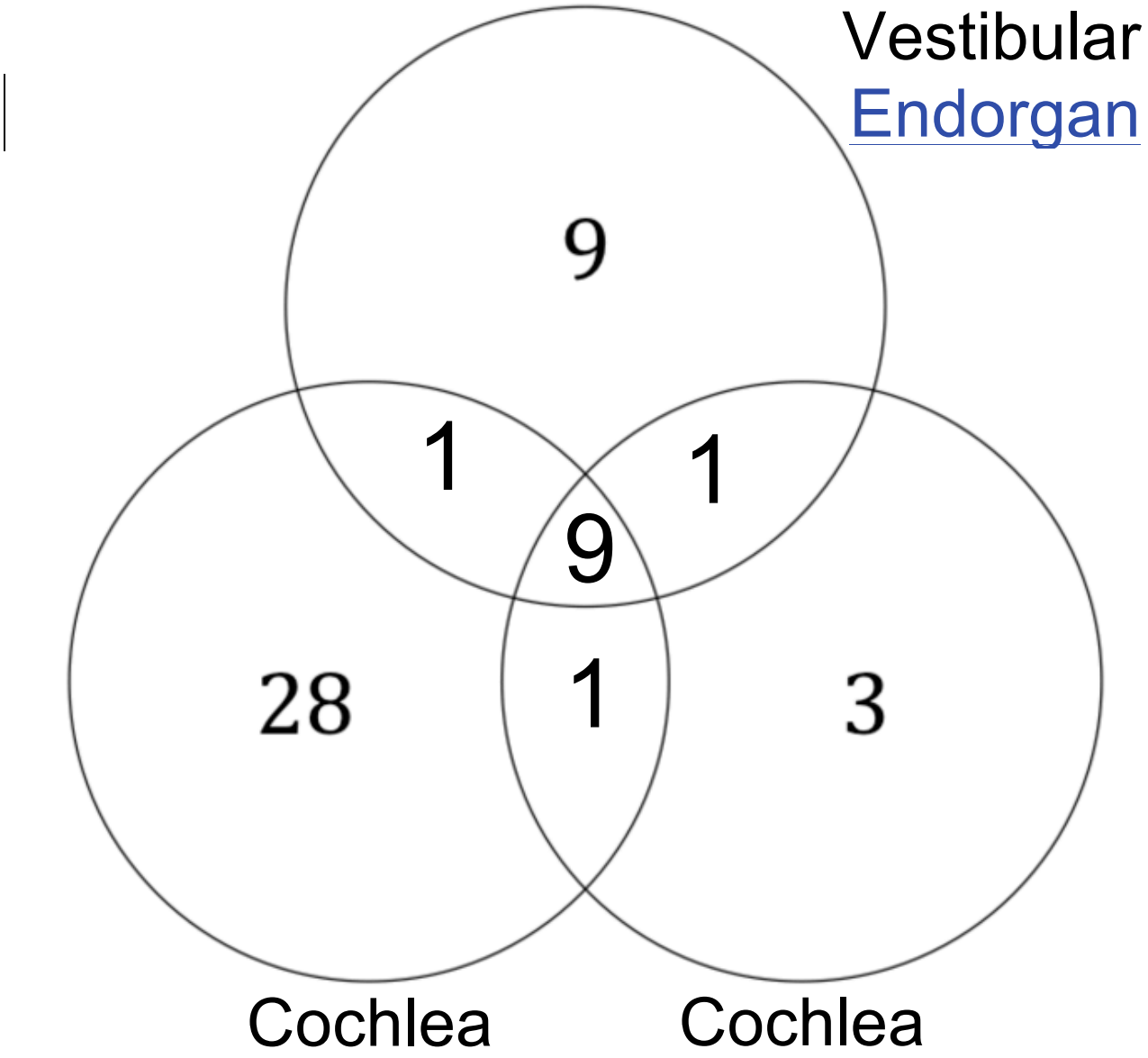

Figure 3.12. Venn diagram of cytoskeletal proteins identified after immunoprecipitating with αII-spectrin as bait in two cochlea samples and one of vestibular endorgans. The vestibular tissue sample and cochlea 2 were from the same experiment and show relatively more proteins in common than the two cochlea samples from different experiments. Nine proteins were found in all three samples, but the majority of these were cytoskeletal keratins.

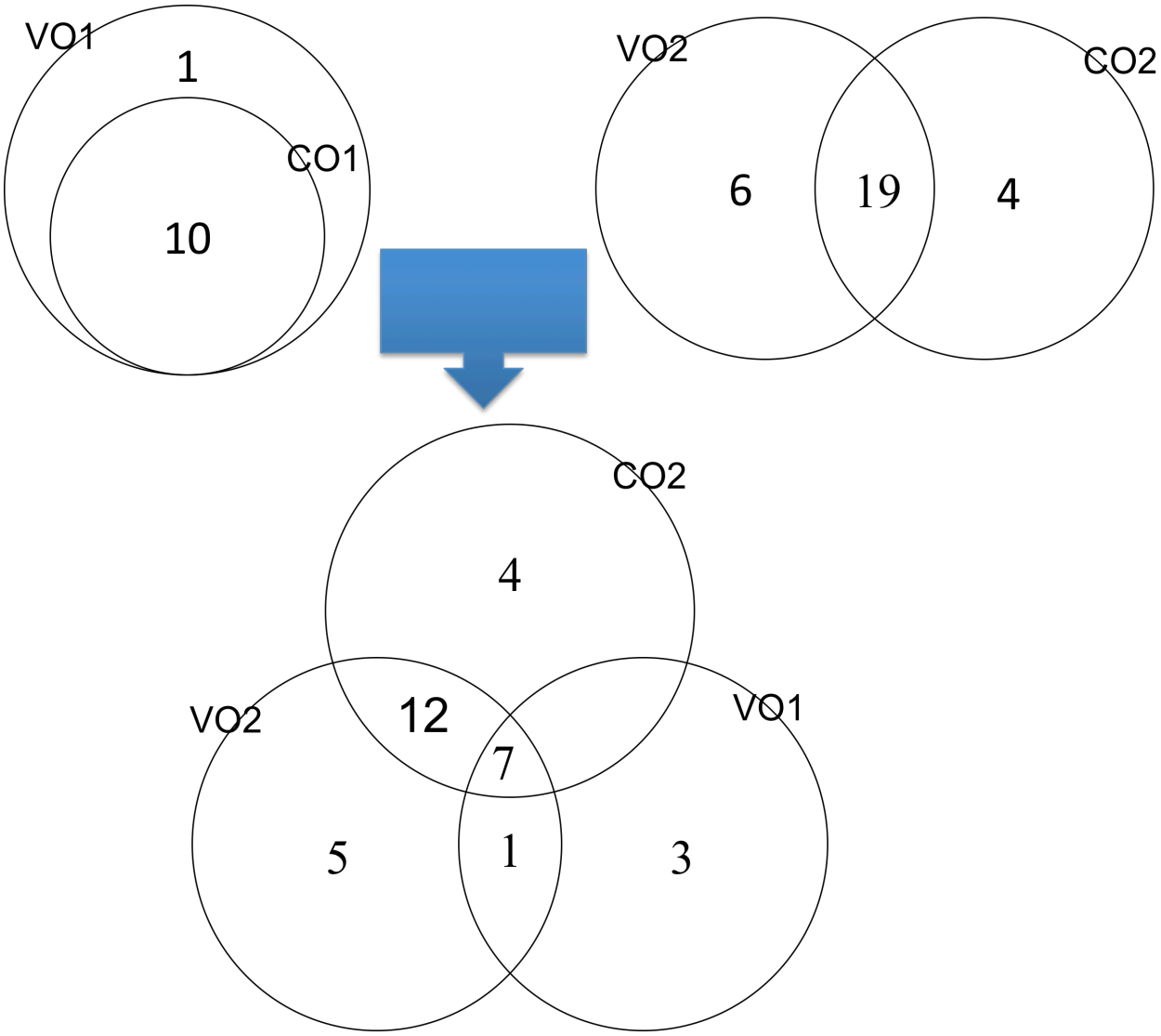

Figure 3.13. Venn diagrams showing summaries of the numbers of common cytoskeletal proteins identified from vestibular end-organ and cochlea tissue after immunoprecipitating with β2-spectrin. Unlike using αII-spectrin, a level of reproducibility was apparent as cochlea and vestibular end organs from same experiment (VO1-CO1 and VO2-CO2, resp.) mostly yielded similar proteins (upper diagrams). It appears the main difference between protein numbers from the two experiments was largely because the second experiment yielded twice as many proteins as the first. Interestingly the 3 unpaired proteins recognized only in VO1 were all cytoskeletal keratins (Krt6A, Krt2, and Krt75), which might have been due to contamination of the sample (lower diagram).

Table 3.1. List of the 7 common proteins identified in all the βII-spectrin co-immunoprecipitation assays of cochlear and vestibular tissue.

Identified Proteins
Spectrin alpha chain, brain (αII-spectrin) (Sptan2) 285 kDa
Spectrin beta chain, brain 2 (βIII-spectrin) (Sptbn2) 271kDa
Myosin -10 (Myh10) 229kDa
Myosin-9 (Myh9) 226kDa
Sodium/potassium-transporting ATPase subunit alpha-2 (Atp1a2) 112kDa
Sodium/potassium-transporting ATPase subunit alpha-3 (Atp1a3) 112kDa
Actin, cytoplasmic 1 (Actb) 42kDa

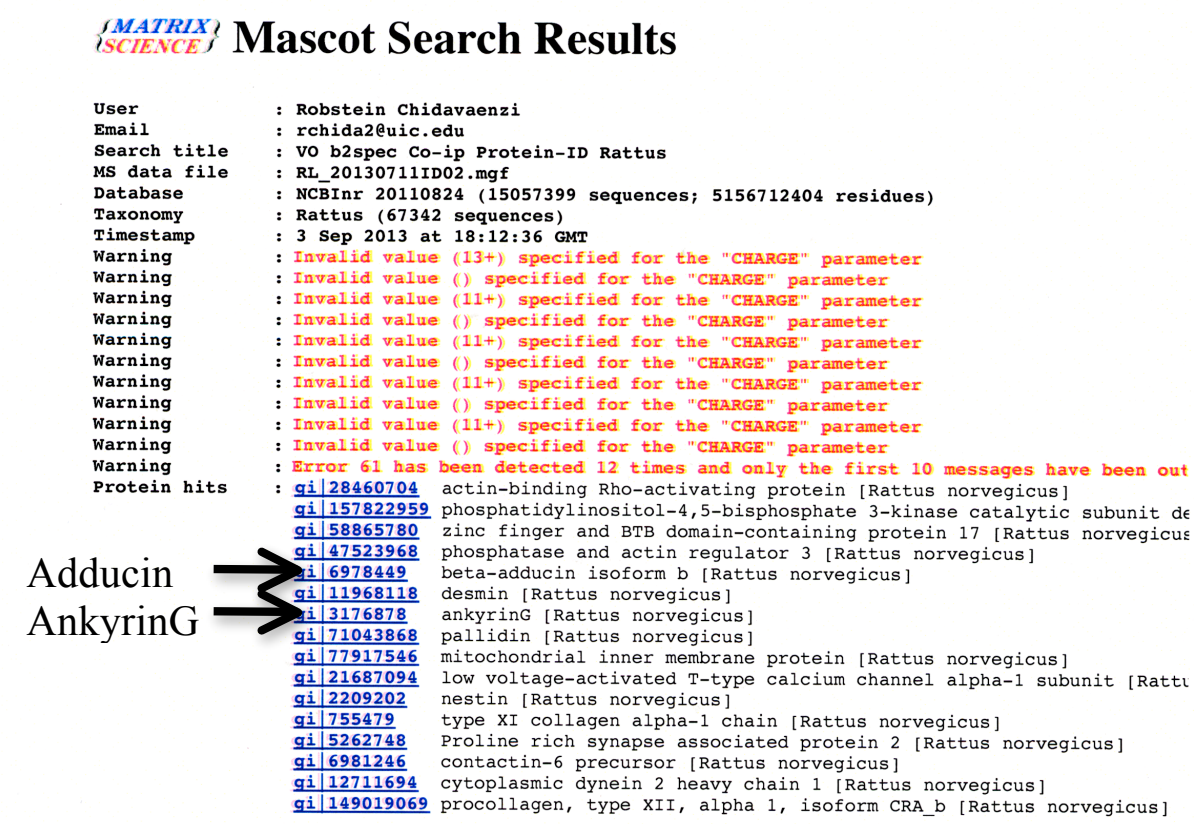

Figure 3.14. Vestibular endorgan tissue immunoprecipitated with βII-spectrin showed that this spectrin subunit co-purifies with its canonical partners, adducin and ankyrin G. This is the only occasion when we saw these proteins in the , but we lost all the other proteins we had been getting, like the αII-spectrin. This only happened after using a ThermoFisher proprietary IP buffer.

3.5. Discussion

The striated organelle seems to be a structure that is assembled using cytoskeletal and dynamic players, viz., αII-spectrin and βII-spectrin, γ-actin, ankyrin G and nebulin among others. Given these have themselves been described and implicated in diverse roles in cellular environments, this cocktail of proteins, unfortunatelt does not advance our cause to discover function.

Developmentally, we have no information for nebulin as our data was contaminated by the rogue goat anti-oncomodulin antibody that turned out to be rabbit and totally masked anything in the rabbit channel. The only known information is from Anthony Peng's thesis (MIT, 2009) where he first saw the presence of nebulin in cochlear HCs at P6.

This relatively late appearance would suggest that nebulin is not needed in HCs during development when all the apical machinery is coming together. It is likely, although we have no direct evidence of this, that when actin accumulates to certain levels, governed by stereocilia, SO, etc., its proper packaging (and hence organization) becomes crucial when the HC starts expressing nebulin in those actin rich domains. Hence it is possible that you would require actin concentrations to reach certain thresholds before the recruitment of nebulin occurs. Also the fact that congenital nebulin anomalies (nemaline myopathy) occur in skeletal muscle where actin assembly and organization occurs very early in embryonic development might indirectly support this hypothesis.

Mass spectroscopy is ideally suited for working with inner ear sensory epithelia in that, given there is so little starting material to work with, the analysis does not require large quantities of tissue to yield results. The caveat is that in separating the different tissue types (i.e., organs and hair cell types) in the tiny confined inner ear spaces poses a new challenge of how to consistently harvest uncontaminated homogenous tissue samples. Thus from the most part the samples apart from being already heterogenous, having both types of hair cells and supporting cells, will likely also have differing amounts of accompanying stroma and might on occasion be contaminated by extraneous debris (viz, blood, brain tissue, skin, etc) which stick to the tissue during the microdissection. This could then account for the difficulties I encountered in attempting to reproduce the mass spectrometry data. It would seem the smaller the tissue samples the higher the odds of getting contamination. Hence it is virtually impossible to ensure that each time one retains the same amount of canals attached to crista, that no debris or the same type and amount of debris in the dissection dish sticks to the tissue, or how much spiral ganglia remains attached to the cochlea, etc. This creates a level of variability in what is ultimately analyzed that the sensitivity of the mass spectrometry method only serves to magnify further.

The great lesson from chemistry is that ‘chemicals react’. When one changes the composition of a chemical in any manner or form one inadvertently changes its basic properties, how it reacts therefrom and with what it reacts. This alterable reactivity is both a major weakness and great strength in determining protein binding partners using immunoprecipitation. Using different IP reagents it was thus possible to resolve the different proteins that could be part of the organelle. Therefore as I pulled down different striated organelle proteins, as defined by αII-spectrin association, and these are βII-spectrin, nebulin, ankyrin G, and γ-actin. Although the resolution from confocal and electron microscopy is not by itself sufficient to show direct interaction, taken together with co-immunoprecipiation data strongly suggest an association of these proteins.

It is apparent that in order to extend our knowledge of the striated organelle, a complete biochemical characterization of this organelle is required. This study, if nothing else, highlighted the challenges of such an undertaking, particularly the extreme difficulties inherent in obtaining pure homogenous tissue samples for any such analysis. A major limitation of the study in this chapter is that the methods we employed treated the whole vestibular and auditory sensory epithelia, respectively, as if it were the striated organelle. The most direct way of determining constituent proteins would be to isolate the SO, and then biochemically identify its constituent proteins. This would be no trivial task.

4. EXPRESSION AND LOCALIZATION OF THE DIFFERENT SPECTRIN SUBUNITS IN THE INNER EAR SENSORY EPITHELIUM

4.1. Abstract

Mammals possess two α-spectrin subunits (αI and αII), and five β-spectrin subunits (i.e., four conventional forms, βI to βIV, and an unconventional heavy subunit, βV). Utilizing western blots, co-immunoprecipitation, mass spectroscopy, immunohistochemistry, confocal and electron microscopy, we present evidence that all these subunits are present in the rat inner ear. They exhibit distinct and consistent distribution patterns in the peripheral sensory epithelium. Most noticeably, in the vestibular system, αII-spectrin and βII-spectrin subunits completely co-localize and show intense labeling in the cuticular plate and striated organelle, and relatively weaker labeling of the outer calyx membrane surrounding type I hair cells, as well as type II hair cell and supporting cell lateral membranes. On the other hand, βI- and βIII-spectrins are mutually exclusive, with the former localizing to the lateral membranes of both type I and II vestibular hair cells (VHCs), and the latter restricted to supporting cell membranes. The nodal marker βIV-spectrin and the heavy βV-spectrin subunit are both expressed in the general neck region of the hair cell, with the former localized to calyceal membranes the latter appearing at the same locale in type I and II hair cells proper. In what is likely a non-erythroid form, αI-spectrin immunofluorescence is detected in the subcuticular necklace ring, from whence it projects downward through the hair cell neck and continues inferiorly to line the basolateral membrane of the type I hair cell. In the auditory system, αI-, αII- and βI-spectrin subunits label the lateral membranes of both inner (IHCs) and outer hair cells (OHCs); βII-spectrin is confined to the lateral membranes of the IHCs; and βIII-, and βV-spectrin label the lateral membranes of the inner pillar cells. In addition to the lateral membrane labeling, αII-, βII-, and βV-spectrin also

label the cuticular plates of both cochlear hair cell types. In the case of βII-spectrin, intense immunoreactivity is found in the cuticular plate of IHCs, but the signal is appreciably weaker in the OHCs; it also labels the outer spiral fibers between the Deiter cells in the OHC-region. Our confocal data suggest that spectrins are playing much more than a purely structural role.

4.2. Introduction

4.2.1. Spectrins in General

At a very basic level, the story of spectrins is largely one of how they mediate cellular shape and structure. This is hardly surprising given that the first member of this family of proteins identified was the erythroid isoform αI-spectrin. Together with the βI-spectrin subunit, αI forms heterotetramic molecules that make a cytoskeleton mesh underneath the plasma membrane, which confers and preserves the biconcave shape of red blood cells. Without the spectrin network, erythrocytes lose their characteristic shape, are more fragile, less flexible, and result in a severe form of human anemia (Tse and Lux, 1999). Owing to their 'structural' nature, spectrins are quite ubiquitously distributed in not only metazoan, but also in invertebrate species (Bennett and Gilligan, 1993).

Functional spectrin molecules are heterotetramers that are assembled by strict alpha-beta isomer pairings (Bennett and Gilligan, 1993). By this definition, the unit will have the two interacting αβ-subunits lined up in an antiparallel fashion to form a dimer, which in turn associates with a similar dimer in a head-to-head orientation, resulting in the tetramer. Mammals possess five β- and two α-spectrin subunits. αI-βI-spectrin subunits are classically considered "erythroid" forms, while the rest are designated as "non-erythroid". This is in contrast to *Drosophila* epithelia where only a single α- and two β-subunits are recognized (Pesacreta et al., 1989). β_H-spectrin (H for heavy) is found only in epithelial cells whereas the other two, α-spectrin and β-

spectrin are widespread, especially during development (Hulsmeier et al., 2007). The two β-forms exhibit differential distribution patterns; more precisely an apico-basal polarization gradient with heavy β_H-subunit occurring at the apical end and the canonical β-spectrin localized to the basal membrane (Dubreuil et al., 1997).

Additionally, from the *Drosophila* work we also learn that spectrin genes can be either essential or non-essential (Mazock et al., 2010). Flies lacking α-spectrin and β-spectrin genes die before the larval stages, while those without the β_H-spectrin gene only show reduced viability, with some surviving and showing relatively mild phenotypes (Dubreuil et al., 2000; Zarnescu and Thomas, 1999). Taken together, the polarization data and the differential effects on mortality suggest that spectrins likely have other functions apart from merely structural. In both vertebrates and invertebrates, it is now recognized that spectrins also play important roles in protein sorting, signal transduction pathway regulation, DNA repair, axonal pathfinding, stabilization of axon initial segments and nodes of Ranvier, synapse organization, and general neuronal development (Dubreuil et al., 2000; Featherstone et al., 2001; Hulsmeier et al., 2007; Stankewich et al., 2010, 2011).

From a numerical perspective, it is most likely that these diversified functions must largely be attributable to the beta spectrins. There are more β-subunits, hence they are more likely to proffer those interactions not inherent in the common α-spectrin units. In fact, it has been reported that beta subunits contain most of the cell signaling and protein-protein interaction sites (Hu et al., 1995). So when one considers simple cells, like erythrocytes, with one pair of αβ-

subunits, compared to complex non-erythrocytic cells with the entire complement of spectrin subunits, it follows that the latter cells would have more spectrin-mediated roles. Inner ear cells present such a scenario (Legendre et al., 2008).

4.2.2. Spectrins in the Inner Ear

Spectrin association with actin has driven a number of inner ear workers to look closely at spectrin subunits mainly in the organ of Corti, and occasionally in the vestibular system. In the ear, we know that spectrin forms a structural support for hair cells. Identified as fodrin, it has been reported in the cuticular plates, lateral walls of supporting cells, inner hair cells and outer hair cells, cortical lattice, synaptic region, and in a 'cytoplasmic spiraling structure' that extended from the cuticular plate to the nucleus of outer hair cells in the upper turns of the cochlea (Attanasio et al., 1994; Drenckhahn et al., 1991; Mahendrasingam et al., 1998; Nishida et al., 1993; Raphael et al., 1994; Slepecky and Ulfendahl, 1992; Ylikoski et al., 1990, 1992). Interestingly, the signal from lateral wall staining in OHC appeared greatest in middle and basal turns than in apex (Attanasio et al., 1994). The significance of this observation is still not clear.

In a comprehensive study that motivated our own work, Legendre et al. (2008) painstakingly studied the occurrence and distribution of spectrin subunits in the mouse auditory system using RT-PCR, confocal and electron microscopy. They found, with the exception of (erythroid) αI-spectrin, which they did not look at, that all other spectrin forms occurred in the auditory system. As expected, their distribution patterns differed from each other: αII- and βII-spectrin were the

most widely distributed, being found in HCs, supporting cells and fibroblasts; βV-spectrin was only found in HCs (particularly in OHCs); βIII-spectrin was located in cochlear ganglion cell bodies; βIV-spectrin was present at nodes of Ranvier; and βI-spectrin was absent from the sensory epithelia, and only seen in supporting cells.

Staining for fodrin in the vestibular system yielded intense immunoreactivity in the cuticular plate of both type I and type II VHCs, as well as, for the first time, an infracuticular cytoskeletal structure identified as the striated organelle (SO) (Demêmes and Scarfone, 1992).

Although it was fairly clear in these studies that 'non-erythroid spectrin' (or fodrin) referred to the αII-spectrin subunit, and 'spectrin' to αI-spectrin, the identity of the β-subunit was not clear. For instance, fodrin was recognized as having an α-subunit of molecular weight 240 kDa while its β-subunit had a molecular weight of 220 kDa (Mahendrasingam et al., 1998). So while fodrin was localized to the cortical lattice, we now know that αII-spectrin (the alpha form of fodrin) occurs there with βV-spectrin (the heavy unconventional spectrin with a molecular weight in excess of 400 kDa) (Legendre et al., 2008; Nishida et al., 1993). Additionally, the molecular weight of β-fodrin is well within the ballpark range of all the conventional beta-spectrin subunits.

Spectrins have also been implicated in inner ear diseases. Its been reported that a mutation in the βIV-spectrin (in quivering mice) causes a form of deafness in which the brainstem auditory

nuclei are compromised (Parkinson et al., 2001), although the cochlea is morphologically normal. βV-spectrin has also recently been implicated in Usher syndrome type 1B, which results in severe blindness and deafness (Papal et al., 2013).

Using predominantly imaging techniques, we set out to map the expression patterns of spectrin isoforms in the inner ear, and employed co-immunoprecipitation to examine interactions between some of them.

4.3. Materials and Methods

4.3.1. Animal models:

Adult Long-Evans rats (*Rattus norvegicus*), weighing 200-250 g, were used. Procedures involving animals were approved by the Institutional Animal Care and Use Committee (IACUC) at Univ. of Illinois at Chicago.

4.3.2. Antibodies:

Primary antibodies: mouse anti-αII spectrin/fodrin (Chemicon, Temecula, CA), mouse anti-βII-spectrin (BD Biosciences), rabbit anti-αI-, βI-, βII-, βIII-, and βV-spectrin and mouse anti-βI spectrin antibodies from Dr. Jon Morrow (Yale), and goat anti-calretinin (Chemicon) as a marker of hair cell and afferent type.

4.3.3. Fixation:

Adult female Long-Evans rats were first weighed then anesthetized via intraperitoneal injections of Nembutal using a dosage of 80mg/kg. Once it was established the animals were deeply anesthetized, trans-cardial perfusions were commenced, initially using 100-200 ml physiological saline containing heparin (2000 IU) to flush the circulatory system, followed by 2 ml/g body weight of an aldehyde fixative (for confocal microscopy: 4% paraformaldehyde, 1% acrolein, 1% picric acid in 0.1 M phosphate buffer (PB) with 5% sucrose, pH 7.4; for electron microscopy: 2% paraformaldehyde, 2% glutaraldehyde, 1% acrolein in 0.08 M cacodylate buffer with 5% sucrose, pH 7.4). After opening the calvarium and dissecting out the brain to expose the bony labyrinths, the animals were post-fixed in the same aldehyde fixative used for the perfusion for a period of time twice as long as the perfusion; usually 20 minutes. The animals were then transferred to 0.1M PB and refrigerated until dissection. Cochlear and vestibular sensory epithelia were micro-dissected in 0.1M PB, refrigerated overnight in the cryo-protective 30% sucrose buffer. After a 10-minute Cal-ex (Fisher Scientific) decalcification step for otolith organs only, the tissues were incubated in a 1% aqueous solution of sodium borohydride (NaBH) for 10 min prior to sectioning. NaBH reduces background fluorescence.

4.3.4. Confocal Microscopy:

Cochleae were decalcified in 0.1M EDTA in phosphate buffer (Madden and Henson, 1997) in a DFR-10 Pelco Biowave microwave processor (Ted Pella Inc., Redding, CA) at power level 6 for 48 hours. Vestibular endorgans and decalcified cochleae were embedded in gelatin and frozen sections (40μm) were cut on a freezing sliding AO microtome. After permeabilization with

4% Triton X-100 in PBS for 1 hr, non-specific binding was prevented with a blocking solution of 0.5% fish gelatin, 0.5% Triton X-100 and 1% BSA in phosphate-buffered saline (PBS, 0.01M) for 1 hr. Samples were incubated for 2 days in primary antibodies (1:200) diluted in the blocking solution. Specific labeling was revealed in tissue incubated overnight with secondary anti-bodies (1:200) conjugated to Alexa or TRITC labels and diluted in the blocking solution. Samples were mounted on slides in Mowiol (Calbiochem, Darmstadt, Germany) and examined on a laser scanning confocal microscope (LSM 510 META, Carl Zeiss, Oberköchen, Germany). Stacks of confocal transverse sections were acquired. Figures were assembled in Adobe Photoshop CS3 (Adobe Systems Inc., San Jose, CA).

4.3.5. Electron Microscope (EM) Immunogold:

The methods described below for electron microscopy immunogold are similar to those used previously by Lysakowski et al. (2011) and are included here for completeness. Using a Vibratome 2000 (Technical Products International, St. Louis, MO), vestibular epithelia were sectioned into 40 μm thick slices. The sections were then incubated in 0.5% Triton X-100 for 1hr at room temperature in order to permeabilize them. After rinsing, to avoid unspecific binding, the sections placed in a blocking buffer of 0.5% fish gelatin and 1% BSA diluted in 0.1M PB for 1 hr. The primary antibody incubation followed for 72 hrs. An antibody dilution of 1:50 was used. After rinsing, the tissue was incubated in gold conjugated secondary antibody for 24 hrs. The antibody was used at a dilution of 1:40. After rinsing in PBS and fixing the sections, they were then incubated in Intense M silver enhancement solution (Habersham Biosciences, Piscataway, NJ) for 4-8 min. Sections were postfixed with 1% osmium tetraoxide (OsO_4) diluted in 0.1M PB

for 1 hr; and then dehydrated for 10 min each in a graded series of ethanols of progressively increasing strength (i.e., 50%, 70%, 95%, 2 X 100%) and 2 X 10 min in propylene oxide. Treated sections were embedded in Araldite resin (Fluka Durcupan, Ronkonkoma, NY) poured into plastic molds and baked at 60°C for 48 hrs. Ultrathin sections of tissue were cut from the Araldite blocks using a diamond knife (Diatome, Biel/Bienne, Switzerland), and free floating sections counterstained for 15 min with uranyl acetate followed by 5 min with lead citrate. Grid mounted sections were examined and photographed with a JEOL 1220X transmission electron microscope (JEOL, Peabody, MA).

4.3.6. Co-immuno-precipitation:

Co-immunoprecipitation was performed using protein extracts from inner ear tissue and reagents as previously described (Sridharan et al., 2006). The tissue of interest was dissected in ice-cold buffer with clean autoclaved tools as quickly as possible to prevent degradation by proteases. We collected the tissue in immunoprecipitation (IP) buffer (25 mM Tris-HCl pH 7.3, 125 mM NaCI, 1% Triton X-100, 1% mammalian protease inhibitors- Sigma P8340) on ice in round-bottom Eppendorf tubes. After standing in ice for 30 min, tissue was then homogenized mechanically with the variable speed Tissue Tearor Homogenizer (model No. 985370, Biospec, Bartlesville, OK) for 3 minutes at the slowest speed while standing on ice. Tissue was then centrifuged for 20 min at 12,000 g at 4°C in a refrigerated Microfuge 22R centrifuge (Beckman Coulter, Danvers, MA), after which the tubes were gently removed from the centrifuge and returned to ice. The supernatant was aspirated and placed in a fresh tube kept on ice; discarding the pellet. Protein concentrations were assayed using a Nanodrop spectrophotometer with a

Pierce 660nm protein assay kit (Product # 22662, ThermoScientific, Rockford IL). Once the protein concentration was determined, we proceeded with the immunoprecipitation while storing any excess protein at -80°C for later use. We pipetted out 250 µL beads (Protein G sepharose, Catalog # P3296, Sigma-Aldrich, St Louis, MO) for later division into 5 centrifuge tubes (50 µL per tube). Beads were washed first and only once with cold PBS, then 4 times with Binding buffer (25mM Tris-HCl pH 7.3, 150mM NaCl, 1% Triton X-100 plus 1% protease inhibitor cocktail). The lysates were pre-cleared for 1 hr with protein A-sepharose (50% slurry) control IgG in Binding buffer. Following pre-clearing, samples were incubated with antibody-immobilized protein G-sepharose (50% slurry) for 4 hr in IP buffer on a rotator at 4°C. The antibodies used were mouse anti-αII-spectrin or equivalent amounts of control mouse IgG for the control. Supernatants were collected after each reaction to assess reaction efficacy. Following washes with IP wash buffer (25mM Tris-HCl pH 7.3, 137mM NaCl, 1% Triton X-100, 1% protease inhibitor cocktail), protein complexes were collected, eluted and subjected to SDS-PAGE analysis. To determine which proteins are co-immunoprecipitated with our bait (eg. αII-spectrin), some gels were sent to the UIC Proteomics lab for mass spectrometry analysis while others underwent western blot analyses with appropriate antibodies. Mass spec gels first underwent Coomassie staining (as it is compatible with downstream analysis method) to show presence of protein and bands of interest were cut out and sent for analysis.

4.3.7. Western Blot of Co-immunoprecipitation Eluents

Gels earmarked for western blots from the co-immunoprecipitations were immediately placed in a transfer chamber and their proteins blotted onto PVDF membrane overnight at 30V constant.

These blots did not undergo Coomassie staining as this is not compatible with downstream transfer of proteins onto membrane, thus where protein visualization was required, a Ponceau S stain was used instead.

4.3.8. Straight Western Blot

Radio Immuno Precipitation Assay (RIPA) buffer (50mM Tris-HCl pH 8.0, 150mM NaCl, 1% Triton X-100, 0.5% Sodium deoxycholate, 0.1% Sodium dodecyl sulfate) was used as homogenization buffer for straight western blots not designed to show protein-protein interactions (e.g., Fig. 4.1 results). 1% wet volume of the Sigma Protease Inhibitor Cocktail **(**P8340) was added to the RIPA buffer just before the dissection. 3 adult animals were used in a single experiment, and cochlear material and vestibular endorgans we collected in 150μL of buffer, while bulk tissue like retina, brain were collected in at least 300μL. All the instruments used were autoclaved prior to the experiment. Dissected out tissue of interest and placed it in RIPA with inhibitor. Stood on ice for 30 minutes before mechanically homogenizing the tissue using a multi-speed Tissue Tearor tip for 3 to 5 minutes. Centrifuged the homogenate in a refrigerated Microfuge 22R centifuge (Beckman Coulter) at 4°C for 20 minutes at 12,000 g. Collected the supernatant and placed it in a fresh labeled tube kept on ice. This is the extracted protein sample to be used for analyses. Discarded the pellet. Determined the total protein concentration obtained for each sample using the Pierce 660nm assay on a nanodrop. Used the determined concentrations to calculate exact amounts of tissue to be loaded from each tissue type so that normalized total protein amounts are loaded across the board. Before loading onto gels, the tissue was mixed 1:1 with 2X Biorad Laemmli buffer (containing 5% 2-β-mercaptoethanol)

and boiled at 95-100°C for 10 minutes. After boiling the sample, now containing Laemmli loading buffer, was allowed to stand at room temperature for 3 minutes, then centrifuged for 30 seconds. Sample was then loaded using a pre-determined order on BioRad 4-20% precast gels. Also loaded was a prestained ladder, and all free lanes were loaded with loading buffer so that the leading edge migrates at the same rate. We ran the electrophoresis at about 200V constant for 50 minutes, and then the transfer at 30 V overnight at 4°C.

4.4. Results

I studied the occurrence and distribution patterns of spectrin subunits in both vestibular endorgans and cochleae of adult Long Evans rats. All indications were that most of the subunits would be present (Legendre et al., 2008). βV-spectrin has been extensively studied in the cochlea, hence was deliberately omitted from my cochlea analysis, but I focused on its distribution pattern in the vestibular system where no data were available. Similarly αII- and the conventional β-spectrins were scrutinized, owing to general ambiguity arising from the earlier αβ fodrin work which was done at a time when the different β spectrin isoforms were still unrecognized and the main distinction made being fodrin represented the nonerythroid spectrin forms.

4.4.1. Vestibular system

4.4.1.1. *All spectrin subunits are present*

To determine spectrin presence in our tissue we performed western blots on vestibular endorgan tissue that had been freshly dissected from 3 adult female Long Evans rats. Signals were obtained for all but one of the subunits (Fig. 4.1). This one exception, βIV-spectrin has fairly limited distribution compared to the others (Fig. 4.5), being present mainly in nodes of Ranvier. Although we did not investigate further, we speculate that the βIV spectrin subunit may have been present in quantities below the threshold of detection.

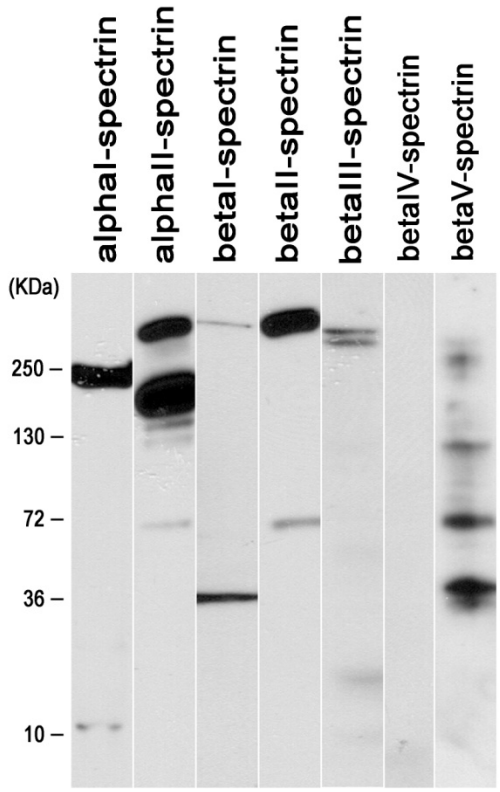

Figure 4.1. Western blot of adult female rat vestibular endorgan tissue showing the presence of all mammalian spectrin subunits (αI-, αII-, βI-, βII-, βIII-, and βV-), except βIV-spectrin, which was not detected. We present evidence of its presence elsewhere, however, and suggest that lack of detection in the western could be simply due to relatively low abundance.

4.4.1.2. *αI-spectrin and αII-spectrin are mutually exclusive*

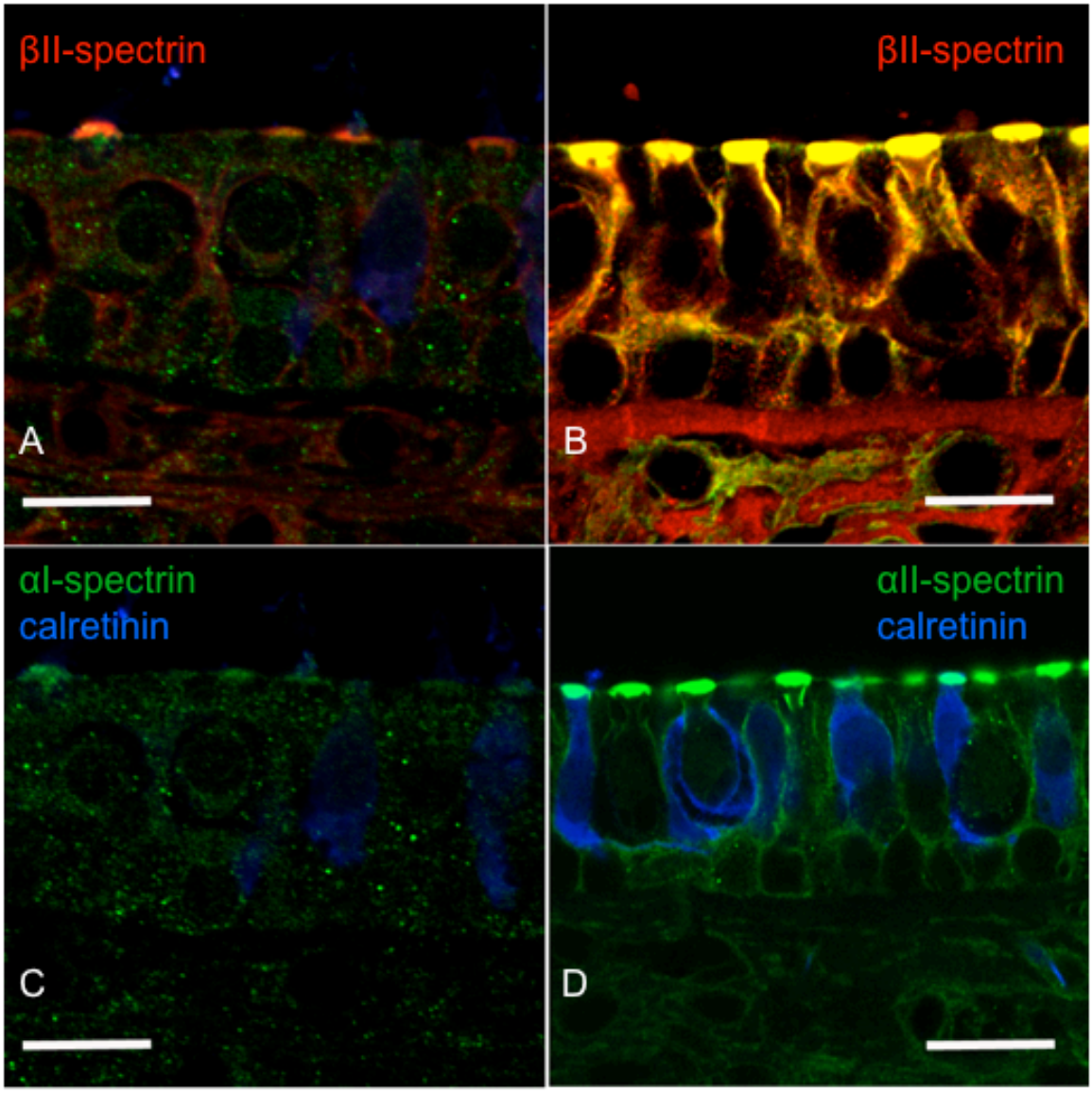

Figure 4.2. Confocal microscopy images of **A)** αI-spectrin and **B)** αII-spectrin counterstained with βII-spectrin in the utricular maculae of adult rat. It is clear that while βII-spectrin completely co-localizes with αII-spectrin, there is no overlap with αI-spectrin. This suggests that the two α-subunits do not coincide. **C)** Counterstaining αI-spectrin with calretinin shows that former only stains type I hair cell lateral membranes and not the type IIs. **D)** Conversely αII-spectrin is in the lateral membranes of type II hair cells (*II*, blue, calretinin label), supporting cells, and outer surface of the calyx surrounding type I hair cells (*I*) but not on the type I hair cell membrane inside the calyx (blue, calretinin label). Scale bars: 10μm.

It is well established that spectrins exist predominantly as strict αβ-heterotetramers (Morrow and Marchesi, 1981). It followed that the various α- and β-isoforms would be distributed in a manner reflecting this. We report mutual exclusivity in the distribution patterns of αI- and αII-spectrin (Fig. 4.2). While not by itself a requirement for adherence to a strict αβ-heterotetrameric form, it clearly supports the assertion that at least αI-spectrin and αII-spectrin are spatially separated in the vestibular system and do not directly interact with each other, and barring homodimerization, they are likely interacting with the resident β-subunits.

4.4.1.3. βI-spectrin and βIII-spectrin are mutually exclusive

Another pair that seems to exhibit mutual exclusivity in their distribution patterns is βI-spectrin and βIII-spectrin. We picked up on this distribution pattern because it has previously been reported as a form of complementarity in the brain (Stankewich et al., 2010). βI-spectrin localizes to the lateral membranes of type I hair cells. It is the only β-subunit found there, where it likely pairs with αI- spectrin, the one alpha subunit there. Immunoreactivity for βI-spectrin is also exhibited on the lateral membranes of type II hair cells (αII- and not αI- occurs here); and on the outer surface of the calyx surrounding type I hair cells with αII and βII-spectrin isoforms (Fig. 4.3A), C)

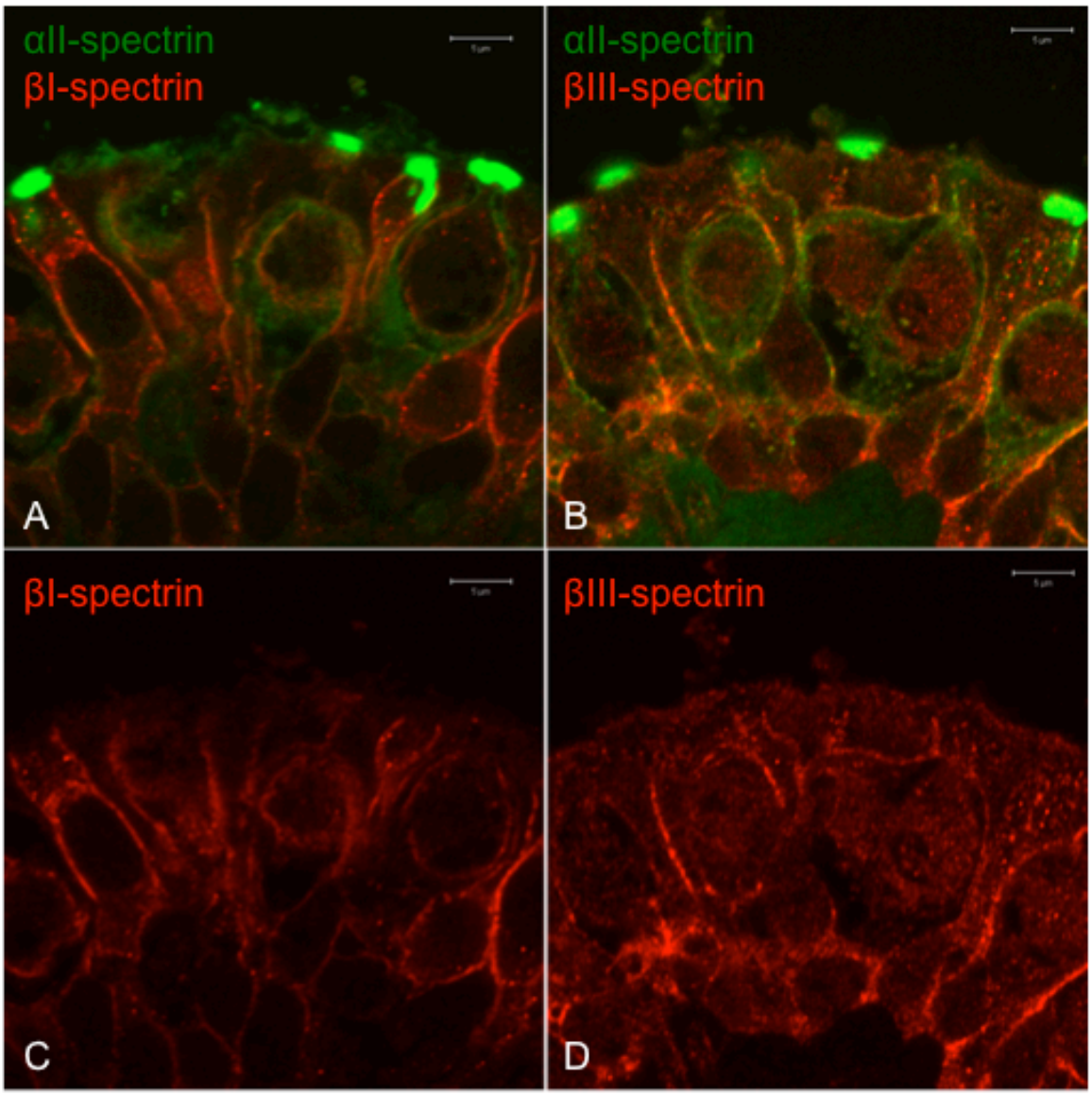

Figure 4.3. A,C) βI-spectrin labels the lateral membranes of type I and II hair cells as well as the outer surface of the calyx membrane; on the other hand βIII-spectrin **(B,D)** labels in turn the supporting cells' lateral membranes, as evidenced particularly by label in the region of the supporting cell nuclei (*SC*).

4.4.1.4. αII-spectrin and βII-spectrin completely co-localize

One direct interaction relationship well represented in the vestibular epithelium is that between αII- and βII-spectrins. They occur in the same locations throughout. Both label the cuticular plate, the striated organelle below, then the outer surface of the calyx, and the lateral membranes of type II hair cells and lateral membranes of supporting cells. The only place from whence they are absent is the lateral membranes of type I hair cells below the calyx (Fig. 4.4).

Additionally, in co-immunoprecipitation experiments using βII-spectrin as bait, this subunit co-purified with the αII-spectrin subunit. This is clearly evidenced by the presence of αII-spectrin in the mass spectroscopy results after just such a pull-down experiment. This association between these two subunits is not just limited to the vestibular endorgan (VO) tissue, as it is also apparent in cerebellum (CB), and cochlea (CO) as well.

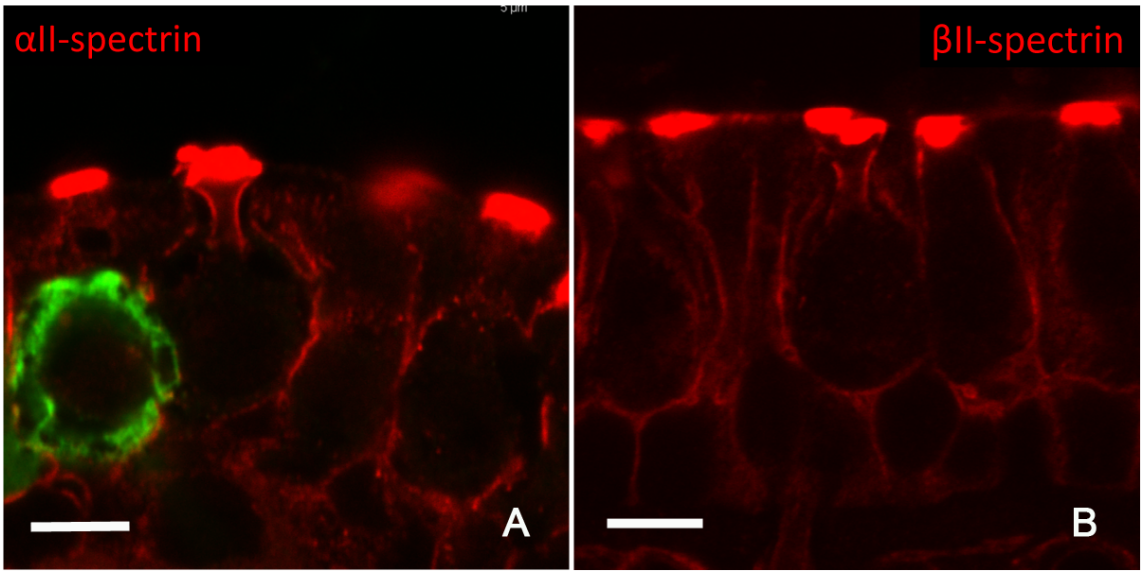

Figure 4.4. In the vestibular endorgans, **A)** αII-spectrin, shown here in the crista, and **B)** βII-spectrin, exhibiting a similar pattern in the utriculus, completely co-localize, labeling the cuticular plate and striated organelle quite intensely, while weakly labeling the outer surface of the calyx surrounding type I hair cells, lateral membranes of type II hair cells and supporting cells. Both subunits are conspicuously absent from type I hair cell lateral membranes, which (according to data shown in Figs. 4.2 and 4.3) are labeled with αI-spectrin and βI-spectrin, respectively. Scale bars: 5μm.

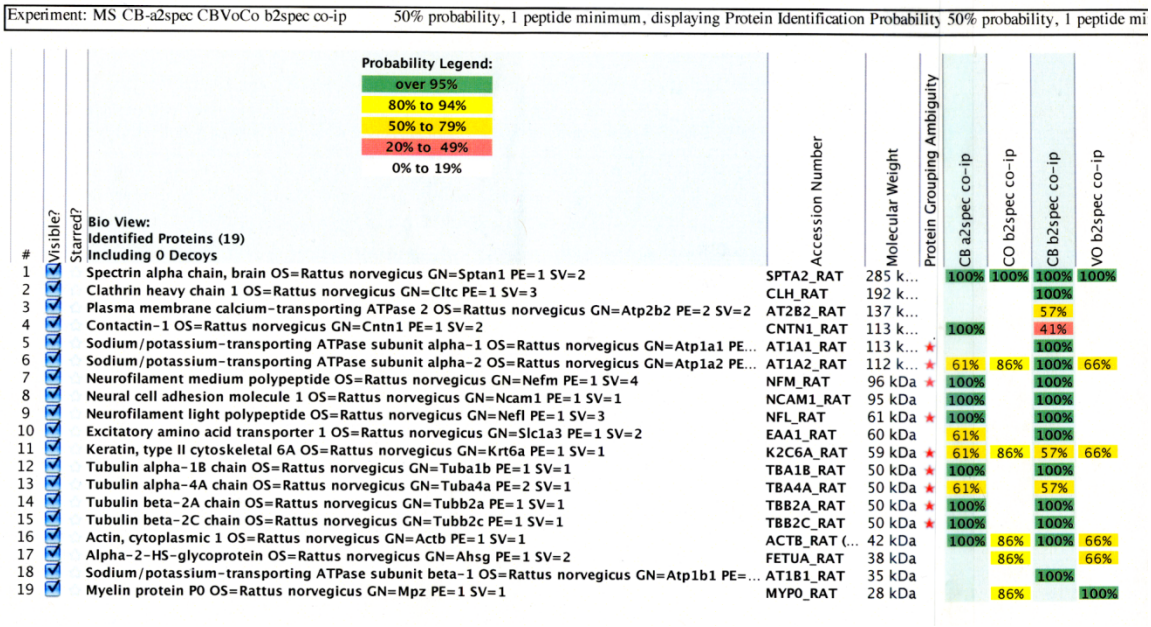

Experiment: MS CB-a2spec CBVoCo b2spec co-ip — 50% probability, 1 peptide minimum, displaying Protein Identification Probability 50% probability, 1 peptide mi

Probability Legend:
over 95%
80% to 94%
50% to 79%
20% to 49%
0% to 19%

Bio View:
Identified Proteins (19)
Including 0 Decoys

#	Visible?	Starred?		Accession Number	Molecular Weight	Protein Grouping Ambiguity	CB a2spec co-ip	CO b2spec co-ip	CB b2spec co-ip	VO b2spec co-ip
1	☑		Spectrin alpha chain, brain OS=Rattus norvegicus GN=Sptan1 PE=1 SV=2	SPTA2_RAT	285 k...		100%	100%	100%	100%
2	☑		Clathrin heavy chain 1 OS=Rattus norvegicus GN=Cltc PE=1 SV=3	CLH_RAT	192 k...				100%	
3	☑		Plasma membrane calcium-transporting ATPase 2 OS=Rattus norvegicus GN=Atp2b2 PE=2 SV=2	AT2B2_RAT	137 k...				57%	
4	☑		Contactin-1 OS=Rattus norvegicus GN=Cntn1 PE=1 SV=2	CNTN1_RAT	113 k...		100%		41%	
5	☑		Sodium/potassium-transporting ATPase subunit alpha-1 OS=Rattus norvegicus GN=Atp1a1 PE...	AT1A1_RAT	113 k...	★			100%	
6	☑		Sodium/potassium-transporting ATPase subunit alpha-2 OS=Rattus norvegicus GN=Atp1a2 PE...	AT1A2_RAT	112 k...	★	61%	86%	100%	66%
7	☑		Neurofilament medium polypeptide OS=Rattus norvegicus GN=Nefm PE=1 SV=4	NFM_RAT	96 kDa	★	100%		100%	
8	☑		Neural cell adhesion molecule 1 OS=Rattus norvegicus GN=Ncam1 PE=1 SV=1	NCAM1_RAT	95 kDa		100%		100%	
9	☑		Neurofilament light polypeptide OS=Rattus norvegicus GN=Nefl PE=1 SV=3	NFL_RAT	61 kDa	★	100%		100%	
10	☑		Excitatory amino acid transporter 1 OS=Rattus norvegicus GN=Slc1a3 PE=1 SV=2	EAA1_RAT	60 kDa		61%		100%	
11	☑		Keratin, type II cytoskeletal 6A OS=Rattus norvegicus GN=Krt6a PE=1 SV=1	K2C6A_RAT	59 kDa	★	61%	86%	57%	66%
12	☑		Tubulin alpha-1B chain OS=Rattus norvegicus GN=Tuba1b PE=1 SV=1	TBA1B_RAT	50 kDa	★	100%		100%	
13	☑		Tubulin alpha-4A chain OS=Rattus norvegicus GN=Tuba4a PE=2 SV=1	TBA4A_RAT	50 kDa	★	61%		57%	
14	☑		Tubulin beta-2A chain OS=Rattus norvegicus GN=Tubb2a PE=1 SV=1	TBB2A_RAT	50 kDa	★	100%		100%	
15	☑		Tubulin beta-2C chain OS=Rattus norvegicus GN=Tubb2c PE=1 SV=1	TBB2C_RAT	50 kDa	★	100%		100%	
16	☑		Actin, cytoplasmic 1 OS=Rattus norvegicus GN=Actb PE=1 SV=1	ACTB_RAT (...	42 kDa		100%	86%	100%	66%
17	☑		Alpha-2-HS-glycoprotein OS=Rattus norvegicus GN=Ahsg PE=1 SV=2	FETUA_RAT	38 kDa			86%		66%
18	☑		Sodium/potassium-transporting ATPase subunit beta-1 OS=Rattus norvegicus GN=Atp1b1 PE=...	AT1B1_RAT	35 kDa				100%	
19	☑		Myelin protein P0 OS=Rattus norvegicus GN=Mpz PE=1 SV=1	MYP0_RAT	28 kDa			86%		100%

Figure 4.5. Mass spectroscopy window results showing that immunoprecipitating with βII-spectrin as bait from cerebellum (*CB*), cochlea (*CO*) and vestibular endorgan tissue (*VO*) yields αII-spectrin (*SPTA2*). This indicates that, in all probability, βII-spectrin and αII-spectrin interact directly.

4.4.1.5. αI-spectrin, βIV-spectrin and βV-spectrin in the hair cell neck region

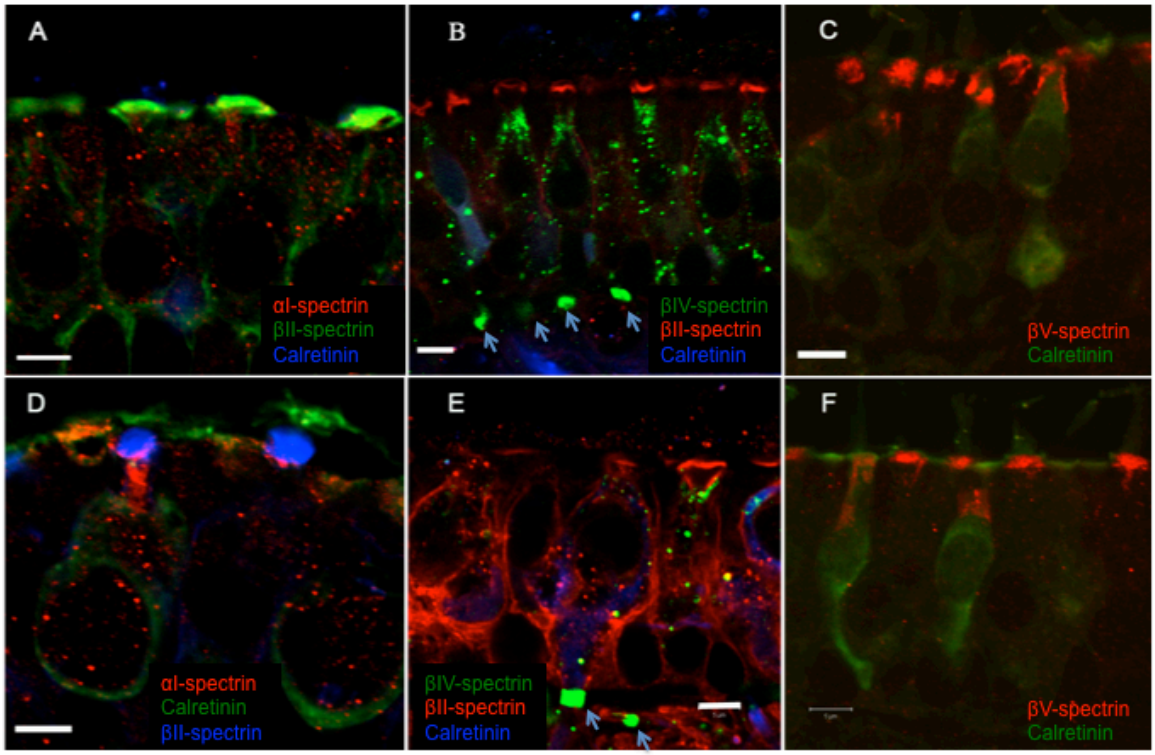

Figure 4.6. A,D) Immunolabeling for αI-spectrin, counterstained with βII-spectrin and calretinin, a marker for type II hair cells and pure calyx afferents, is shown. αI-spectrin is found bordering the cuticular plate (*CP*), in the neck of type I hair cells (*I*), and in the lateral membranes of the type I hair cell underneath the calyx membrane. **B,E)** βIV-spectrin exhibits its characteristic nodal labeling (*blue arrows*) as well as the labeling in the apical neck region of type I hair cells. **E)** The signal is in the calyceal membrane and not the hair cell. **C,F)** βV-spectrin also exhibits apical neck labeling at the same level as that observed for βIV-spectrin. Unlike βIV-spectrin, however, the heavy spectrin signal is in the type I and II hair cell (and not the calyx membrane).

The presence of an erythroid spectrin, αI-, has been revisited and confirmed (Fig. 4.6A,D). Given the distribution pattern for αII-spectrin (Fig. 4.4), however, this is hardly surprising seeing how it is absent underneath the calyx. It is clear that if the spectrins are adhering to a strict αβ-pairing regime then deficiency of one alpha-isoform dictates the expression of the other. Although we identified this subunit using an antibody raised against the erythroid form, without more work it is impossible to say whether this is a 'non-erythroid' form of αI-spectrin or if the 'erythroid αI' is not strictly an erythroid protein.

βIV-spectrin, long accepted as a nodal marker, is shown here to have an additional location away from the heminode (Fig. 4.6B,E). Its location in the calyx membrane is curious and it would be instructive to investigate that further. We did not previously detect βIV-spectrin using western blots, but the fact that we can show that it does label heminodes is itself a good positive control within the experiment.

The unconventional heavy βV-spectrin also localizes to the hair cell neck region (Fig. 4.6 C,F). Even more interesting is that the αI-subunit and βIV-spectrin are within the same general region. So the neck region, where the type I hair cell inexplicably constricts, appears to be a nexus for all these spectrin subunits that seem out of place.

4.4.2. Auditory system

To establish baseline presence, instead of a western blot as in the vestibular system, we relied on RT-PCR data from Legendre et al. (2008) to ascertain that all the seven spectrin isoforms were present. Based on that assumption, we went on to investigate their distribution patterns using immunohistochemistry and confocal microscopy.

4.4.2.1. αI-spectrin is expressed in the sensory epithelium, in both inner and outer hair cells, of the cochlea

In OHCs, the signal is in the hair cell soma, extending from the cuticular plate to just above the nucleus. In IHCs, cuticular plate labeling is apparent, and the soma immunoreactivity does not extend to the nucleus below (see Fig. 4.7A).

4.4.2.2. αII-spectrin is widely expressed

αII-spectrin in the cochlea labels three discernible structures: the cuticular plate of both hair cell types, lateral membranes of both IHCs and outer OHCs, and the outer spiral fibers coursing between the Deiter cells (Fig. 4.7B). We did not detect actual supporting cell labeling. Its distribution map mirrors to a large extent the fodrin expression patterns published. Unlike the vestibular system, cochlear αII-spectrin does not completely co-localize with any β-form. This gives us two essential pieces of information: a) different binding partners could be a sign of spectrins having different functions in the two sensory epithelia, and b) the antibodies used are definitely targeting different subunits.

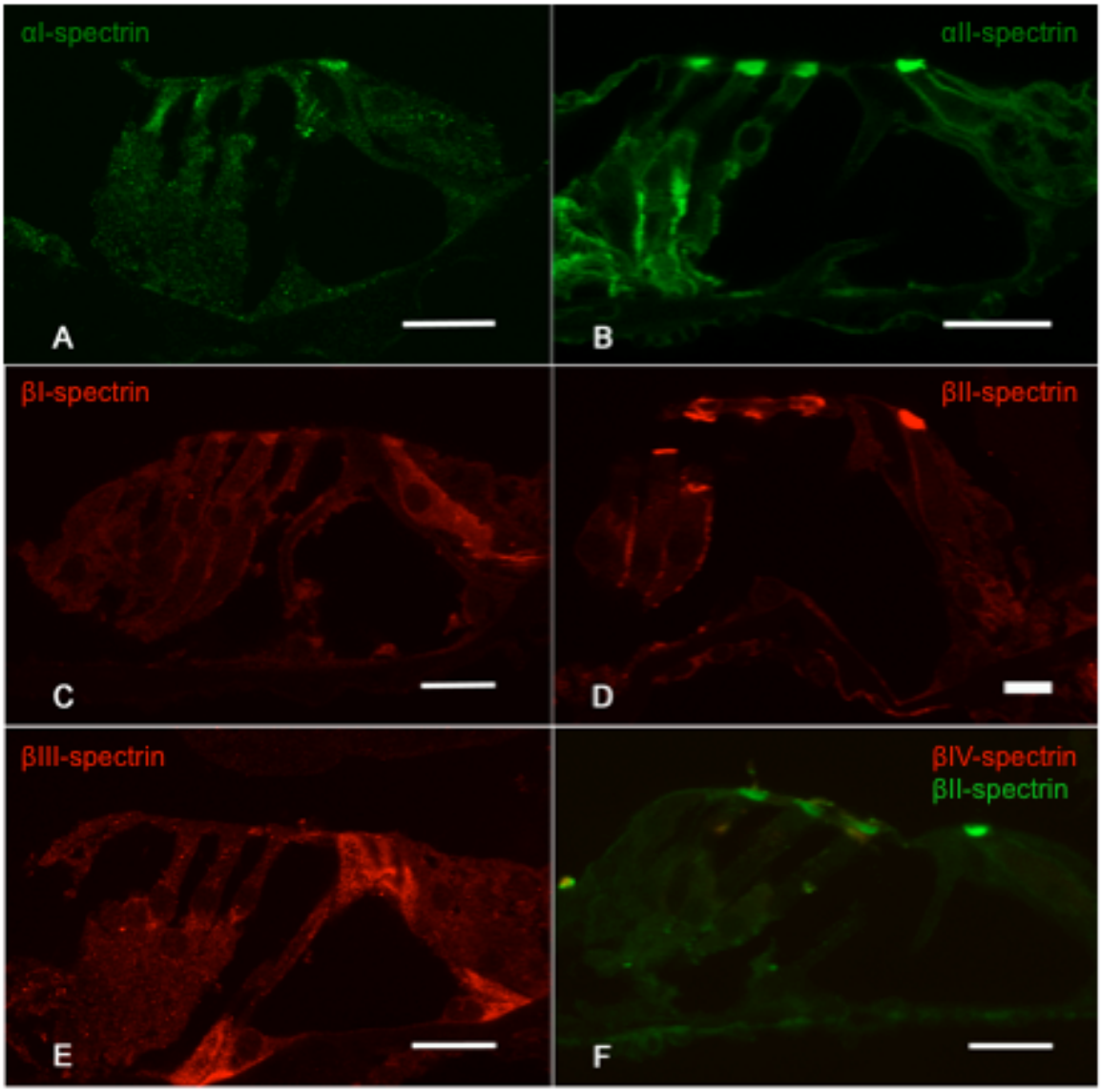

Figure 4.7. Cochlear spectrins. **A)** αI-spectrin is in the hair cell soma of both IHCs and OHCs, possibly representing the "infracuticular network". **B)** αII-spectrin exhibits lateral membrane and cuticular plate labeling of both IHCs and OHCs, and also outer spiral fibers. **C)** βI-spectrin intensely labels the IHCs as well as the lateral membranes of OHCs, plus the outer spiral fibers (*arrows*). **D)** βII-spectrin labels the IHC lateral membrane in addition to IHCs and OHCs cuticular plates. **E)** βIII-spectrin labels pillar cells. **F)** βIV-spectrin is not detected in either IHCs or OHCs. The panel is counterstained with βII-spectrin to bring out contrast so the absence of the red signal for βIV-spectrin is even more apparent. Scale bars: 20μm.

4.4.2.3. βI-spectrin labels the lateral membranes of IHCs and OHCs.

βI-spectrin exhibits an intense immunoreactivity in the IHCs, staining the hair cell soma and lateral membranes, while only the latter are labeled in the OHCs (Fig. 4.7C). Weak outer spiral labeling is also apparent. These results differ from the Legendre et al. (2008) study in that we find hair cell labeling with βI-spectrin.

4.4.2.4. βII-spectrin labels the lateral membranes of IHCs but not OHCs.

βII-spectrin labels the cuticular plates of all hair cell types, the lateral membranes of IHCs but not OHCs, and the outer spiral fibers (Fig. 4.7D). The cuticular plate label for IHCs is more intense than that in OHCs. Why it should be outer spiral fibers and not the lateral membranes of the Deiter cells is uncertain. A probable technical explanation could be that the fibers and Deiter's cells are so closely apposed that the signal we observe 'emanating' from the outer spiral fibers is actually in the Deiter cell membranes.

4.4.2.5. βIII-spectrin labels inner pillar cells

As in the Legendre et al. (2008) study, βIII-spectrin does not label hair cells, but rather supporting cells, in the cochlea. Specifically, it labels the inner pillar cells (Fig. 4.7E). Interestingly, if we again apply our mutual exclusivity rule, having βI-spectrin on the membranes of both OHCs and IHCs automatically excludes βIII-spectrin from occurring in those cells. This conclusion is borne out by the βIII subunit localizing to a subset of supporting cells.

4.4.2.6. βIV-spectrin is not detected in the sensory epithelia.

βIV-spectrin, a nodal marker, is not expressed in hair cells or supporting cells (Fig. 4.7F). We expect that it is located closer to the spiral ganglion neurons where the nodes are. One observation is that βIV does not appear near the hair cells' necks as it does in the vestibular system. It is important to highlight here that even then, it is not actually in the hair cell, but in the calyx membrane. So the calyx seems to give βIV-spectrin an added role to play in the vestibular sensory epithelium.

4.5. Discussion

Although spectrin subunits share a great deal of homology, they are also fairly unique in their interactions (Nestor et al., 2011). In *Drosophila* epithelial cells, the two β isoforms show a polarization in how they segregate out in the cells (Dubreuil et al., 1997). That they are for the most part, spatially separated and in different domains within the hair cells points to the very real possibility that they are occupying different niches.

This data represents the distribution patterns of all seven spectrin subunits within the rat inner ear sensory epithelium. A summary of how the α-subunits segregate out and the possible β-subunit pairings are suggested (Table 4.1). In the vestibular system, αII-spectrin is widely distributed except on the lateral membranes of type I hair cells beneath the calyx membrane, where αI-spectrin occurs with βI-spectrin.

Table 4.1: Summary of the α-spectrin subunit distribution patterns in the inner ear

Spectrin subunit	*Vestibular system expression*	*Auditory system expression*
αI-specrtrin	Lateral membrane of type I HC (βI); Infracuticular network/apical neck (βIV&V)	Infracuticular network IHC and OHC (βI) Cuticular plate-IHC (βI&II)
αII-spectrin	Cuticular plate (βII), Striated organelle (βII), Type II HC lateral membrane (βI&II), Outer calyx surface (βI&II), SC lateral membranes (βII&III)	Cuticular plate- IHC (βII) Cuticular plate-OHCs (βI&II) Lateral membrane - IHC (βI&II) Lateral membrane - OHC (βI&V) Outer spiral fibers (βI&II)

IHC-inner hair cell
OHC-outer hair cell
βx- β-spectrin isoform, x=subunit identity

Similarly in the cochlea αI-spectrin distribution is limited to those regions where βI-spectrin also occurs. However, unlike in the vestibular system other spectrin subunits are found there as well.

The αI-αII-mutual exclusivity is not unexpected, but the basis of the βI-βIII mutually exclusive distribution pattern relationship is unclear. In future work it would be interesting to actually determine the physiological basis of the distribution patterns and how it ties in with hair cell function.

One observation in the spectrins' distribution patterns is how βII-spectrin, besides being in the SO and cuticular plates of all hair cell types, localizes to the lateral membranes of only one hair cell type in both the vestibular and auditory systems. In VHCs it is present in type II HCs' lateral membranes and absent from those of type Is; whereas in the cochlea it is only in IHC lateral membranes and not those of OHCs. One feature of hair cells not fully understood is how they exhibit different shapes and it seems plausible that an underlying spectrin network could be instrumental in this. The shape a HC itself takes does not appear attributable to βII-spectrin alone as vestibular type II hair cells are cylindrically shaped, while cochlear inner hair cells bulge out into goblet forms, and these two are the two types having this isoform. The presence of αI-spectrin and βI-spectrin in hair cells lateral membranes seems to be a better indicator of hair cells' amphora-shapes, and points to their likely involvement in 'shaping' hair cells. The goblet-shape is most pronounced in VHC type I cells where these are only αI- and βI-spectrin isoforms on the hair cell lateral membrane beneath the calyx, and is not so pronounced in IHCs where other spectrin isoforms are found (*viz*. αII- and βII-spectrin).

5. CONCLUDING REMARKS

A lot of work has gone into clarifying the structure of the striated organelle. In most of these studies, besides focusing its morphological dimensions, researchers have documented its widespread occurrence in the animal kingdom. From a point when it was initially considered a disease artefact, the striated organelle has grown in stature and is now generally accepted as the normal apical architecture of vestibular type I and II hair cells, and auditory inner hair cells. In this thesis we have attempted to look at the structure from a different perspective, making the case that it is indeed an organelle.

While αII-spectrin has been well documented as part of the striated organelle (Demêmes and Scaforne, 1992; Vranceanu et al., 2012) we propose that βII-spectrin is its putative partner in the organelle. We document that these two subunits in all probability directly interact as they co-purify in immunoprecipitation experiments, completely co-localize in confocal experiments, and developmentally are starting to be expressed at the same time and manner. They are expressed in all hair types where a striated organelle is known to occur, i.e., vestibular type I and II hair cells, and in cochlear inner hair cells. It is intriguing that the only hair cell type in which these two do not completely coincide is the electromotile outer hair cells, where no striated organelles have been reported.

αII,-βII-spectrin expression is postnatal in nature. The spectrins are trafficked immediately after birth, and are recruited first in the cuticular plate and then the striated organelle. Because of the ubiquitous nature of spectrins in general and these two particular subunits in particular, no functional information can be gleaned from their localizing to the SO. An attempt in this work was undertaken to identify more protein constituents. The approach selected was two-fold, in the

first instance, isolate the spectrin and then investigate other proteins that they interact with. Isolating the spectrins and ensuring they keep their native associations was challenging and we never truly achieved this satisfactorily. When the protocol preserved canonical partner-binding like ankyrinG and adducin, the spectrins had very little other interactions with other proteins, and vice versa. Ultimately it was not clear which of the interactions observed represented native interactions.

An interesting new protein partner, nebulin, was revealed. The largest actin bundling protein at 600-900 kDa, it brings in a new measure of actin regulation to the hair cell.

All the mammalian spectrin isoforms have residence within the hair cell epithelia, including αI-spectrin. It however only appears to interact with βI-spectrin, leaving αII-spectrin to do the bulk of the work as it pair with the remaining β-isoforms.

This work makes a novel contribution to inner ear hair cell architecture.

REFERENCES

Agrawal Y, Carey JP, Della Santina CC, Schubert MC, Minor LB. 2009. Disorders of balance and vestibular function in US adults. *Arch Intern Med*, **169:** 938-944.

Albuquerque AAS, Rossato M, Apparecido de Oliveira JA, Hyppolito MA. 2009. Understanding the anatomy of ears from guinea pigs and rats and its use in basic otologic research. *Braz J Otorhinolaryngol*, **75:** 43-49.

Attanasio G, Spongr VP, Henderson D. 1994. Localization of F-actin and fodrin along the organ of Corti in the chinchilla. *Hear Res*, **81:** 199-207.

Bennett V, Gilligan MD. 1993. The spectrin-based membrane skeleton and micron-scale organization of the plasma membrane. *Ann Rev Cell Bio*, **9:** 27-66

Bignone PA, Baines AJ. 2003. Spectrin alpha II and beta II isoforms interact with high affinity at the tetramerization site. *Biochem J*, **374:** 613-624.

Bottino D, Mogilner A, Roberts T, Stewart M, Oster G. 2002. How nematode sperm crawl. *J Cell Sci,* **115(Pt 2):** 367-384.

Curthoys IS. 1979. The vestibulo-ocular reflex in newborn rats. *Acta Otolaryngol*, **87:** 484-489.

Dallos P, Hallworth R, Evans BN. 1993. Theory of electricity driven shape changes of cochlear outer hair cells. *J Neurophysiol*, **70:** 299-323.

Das A, Base C, Manna D, Cho W, Dubreuil RR. 2008. Unexpected complexity in the mechanisms that target assembly of the spectrin cytoskeleton. *J Biol Chem*, **283:** 12643-12653.

DeMatteis MA, Morrow JS. 2000. Spectrin tethers and mesh in the biosynthetic pathway. *J Cell Sci,* **113:** 2331-2343

Demêmes D, Scarfone E. 1992. Fodrin immunocytochemical localization in the striated organelles of the rat vestibular hair cells. *Hear Res*, **61:** 155-160.

DeRosier DJ, Tilney LG. 1989. The structure of the cuticular plate, an in vivo actin gel. *J Cell Biol*, **109:** 2853-2867.

DeRosier DJ, Tilney LG. 2000. F-actin bundles are derivatives of microvilli: what does this tell us about how bundles might form? *J Cell Biol*, **148:** 1-6.

Drenckhahn D, Engel K, Hofer D, Merte C, Tilney L, Tilney M. 1991. Three different actin filament assemblies occur in every hair cell: each contains a specific actin crosslinking protein. *J Cell Biol*, **112:** 641-651.

Dubreuil RR, Maddux PB, Grushko TA, MacVicar GR. 1997. Segregation of two spectrin isoforms: polarized membrane skeleton assembly. *Mol Biol Cell*, **8:** 1933-1942.

Dubreuil RR, Wang P, Dahl S, Lee J, Goldstein LS. 2000. Drosophila beta spectrin functions independently of alpha spectrin to polarize the Na,K ATPase in epithelial cells. *J Cell Biol*, **149:** 647-656.

Eiserman WD, Hartel DM, Shisler L, Buhrmann J, White KR, Foust T. 2008. Using otoacoustic emissions to screen for hearing loss in early childhood care settings. *Intl J Pediat Otorhino-laryngol,* **72:** 475-482.

Engstrom H, Bergstrom B, Ades HW. 1972. Macula utriculi and macula sacculi in the squirrel monkey. *Acta Otolaryngol Suppl*, **301:** 75-126.

Engstrom H, Engstrom B. 1978. Structure of the hairs on cochlear sensory cells. *Hear Res*, **1:** 49-66.

Featherstone DE, Davis WS, Dubreuil RR, Broadie K. 2001. Drosophila alpha- and beta-spectrin mutations disrupt presynaptic neurotransmitter release. *J Neurosci,* **21:** 4215-4224.

Flock. A. 1983. Hair cells, receptors with a motor capacity? In: Hearing - Physiological Bases and Psychophysics. Editors: R. Klinke and R. Hartman. New York: Springer-Verlag, pp. 1-6.

Flock A, Bretscher A, Weber K. 1982. Immunohistochemical localization of several cytoskeletal proteins in inner ear sensory and supporting cells. *Hear Res,* **7:** 75-89.

Forge A, Wright T. 2002. The molecular architecture of the inner ear. *Br Med Bull*, **63:** 5-24.

Fowler VM, Adam EJH. 1992. Spectrin redistributes to the cytosol and is phosphorylated during mitosis in cultured cells. *J Cell Biology*, **119:** 1559-1572.

Friedmann I, Cawthorne T, Bird ES. 1965. Broad-banded striated bodies in the sensory epithelium of the human macula and in neurinoma. *Nature*, **207:** 171-174.

Friedmann I, Cawthorne T, McClay T, Bird ES. 1963. Electron microscopic observations of the human membranous labyrinth with particular reference to Meniere's disease. *J Ultrastruct Res*, **49:** 123-138.

Friedmann I, Dadswell JV, Bird ES. 1966. Electron microscope studies of the neuroepithelium of the inner ear in guinea pigs treated with neomycin. *J Pathol Bacteriol*, **92:** 415-422.

Furness DN, Mahendrasingam S, Ohashi M, Fettiplace R, Hackney CM. 2008. The dimensions and composition of stereociliary rootlets in mammalian cochlear hair cells: comparison between high- and low-frequency cells and evidence for a connection to the lateral membrane. *J Neurosci*, **28:** 6342-6353.

Glenney JR, Glenney P, Weber K. 1983. The spectrin related molecule, TW-260/240, cross-links the actin bundles of the microvillus rootlets in the brush borders of the intestinal epithelial cells. *J Cell Biol*, **96:** 1491-1496.

Grazi E, Magri E, Rizzieri L. 1989. The influence of substoichiometric concentrations of myosin subfragment 1 on the state of aggregation of actin under depolymerization conditions. *Eur J Biochem*, **182:** 277-282.

Hilding DA, House WF. 1964. An evaluation of the ultrastructural findings in the utricle in Meniere's disease. *Laryngoscope*, **74:** 1135-1148.

Hilding DA, Sugiura A, Nakai Y. 1967. Deaf white mink: electron microscopic study of the inner ear. *Ann Otol Rhinol Laryngol*, **76:** 647-663.

Hirokawa N. 1978. The ultrastructure of the basilar papilla of the chick. *J Comp Neurol*, **181:** 361-374.

Hirokawa N, Heuser JE. 1981. Quick-freeze, deep etch visualization of the cytoskeleton beneath surface differentiations of intestinal epithelial cells. *J Cell Biol*, **91:** 399-409.

Hirokawa N, Tilney LG, Fujiwara K, Heuser JE. 1982. Organization of actin, myosin, intermediate fiaments in the brush border of intestinal epithelial cells. *J Cell Biol*, **94:** 425-443.

Hoshino T. 1975. An electron microscopic study of the otolithic maculae of the lamprey (*Entosphenus japonicus*). *Acta Otolaryngol*, **80:** 43-53.

Hulsmeier J, Pielage J, Rickert C, Technau GM, Klambt C, Stork T. 2007. Distinct functions of α-Spectrin and β-Spectrin during axonal pathfinding. *Development*, **134:** 713-722.

Hu RJ, Moorthy S, Bennett V. 1995. Expression of functional domains of beta G-spectrin disrupts epithelial morphology in cultured cells. *J Cell Biol*, **128:** 1069-1080.

Jahnke V. 1969. Ultrastructure of the vestibular sensory areas in experimental lathyrism. *Acta Otolaryngol,* **68:** 336-349.

Jorgensen JM. 1982. Microtubules and laminated structures in inner ear hair cells. *Acta Otolaryngol,* **94:** 241-248.

Jorgensen JM, Mathiesen C. 1988. The avian inner ear: continuous production of hair cells in the

vestibular organs but not in the auditory papilla. *Naturewissenschaften*, **75:** 319-320.

Keller A, Nesvizhskii AI, Kolker E, & Aebersold R. 2002. Empirical statistical model to estimate the accuracy of peptide identifications made by MS/MS and database search. Anal Chem, 74: 5383–5392.

Kimura RS. 1966. Hairs of the cochlear sensory cells and their attachment to the tectorial membrane. *Acta Otolaryngol,* **61:** 55-72.

Kinter M, Sherman NE. 2000. *Protein Sequencing and Identification Using Tandem Mass Spectrometry,* Wiley-Interscience: New York, pp. 152–160.

Kobayashi T, Gyo K, Yanagihara N. 1999. Combined rupture of Reissner's membrane and round window: an experimental study in guinea pigs: experimental double-membrane rupture. *Am J Otol,* **20:** 179-182.

Kraus H, K Aulbach-Kraus. 1981. Morphological changes in the cochlea of the mouse after the onset of hearing. *Hear Res,* **4:** 89-102.

Labeit S, Ottenheijm CAC, Granzier H. 2011. Nebulin, a major player in muscle health and disease. *FASEB J,* **25:** 822-829.

Lacas-Gervais S, Guo J, Strenzke N, Scarfone E, Kolpe M, Jahkel M, de Camilli P, Moser T, Rasband MN, Solimena M. 2004. βIV∑1 spectrin stabilizes the nodes of Ranvier and axon initial segments. *J Cell Biol,* **166:** 983-990.

Legendre K, Safieddine S, Kussel-Andermann P, Petit C, El-Amraoui A. 2008. αII-βV spectrin bridges the plasma membrane and cortical lattice in the lateral wall of the auditory outer hair cells. *J Cell Sci,* **121:** 3347-3356.

Li A, Xue J, Peterson EH. 2008. Architecture of the mouse utricle: macular organization and hair bundle heights. *J Neurophysiol,* **99:** 718-733.

Lowenstein O, Osborne MP. 1964. Ultrastructure of the sensory hair-cells in the labyrinth of the amnocoete larva of the lamprey, *Lampetra fluviatilis*. *Nature,* **204:** 197-198.

Lysakowski A, Gaboyard-Niay S, Calin-Jageman I, Chatlani S, Price SD, Eatock RA. 2011. Molecular microdomains in a sensory terminal, the vestibular calyx ending. *J Neurosci,* **31:** 10101-10114.

Machnicka B, Grochowalska R, Boguslawska DM, Sikorski AF, Lecomte MC. 2012. Spectrin-based as an actor in cell signaling. *Cell Mol Life Sci,* **69:** 191-201.

Madden VJ, Henson MM. 1997. Rapid decalcification of temporal bones with preservation of ultrastructure. *Hear Res,* **111:** 76-84.

Mahendrasingam S, Furness DN, Hackney CM. 1998. Ultrastructural localisation of spectrin in sensory and supporting cells of guinea-pig organ of Corti. Hear Res, **126:** 151-160.

Marty R, Thomas J. 1963. Electro-cortical responses to stimulation of the cochlear nerve in the newborn cat. *J Physiol (Paris),* **55:** 165-166. [In French]

Mazock GH, Das A, Base C, Dubreuil RR. 2010. Transgene rescue identifies an essential function for Drosophila β spectrin in the nervous system and a selective requirement for ankyrin-2 binding activity. *Mol Biol Cell*, **21:** 2860-2868.

Mizuno M, Fujimoto T, Ogawa T. 1989. Distribution of F-actin, fodrin, and ankyrin in gastric parietal cells of the rat. *Acta Histochem Cytochem,* **22:** 593-603.

Mogensen MM, Rzadzinska A, Steel KP. 2007. The deaf mouse mutant whirler suggests a role for whirlin in actin filament dynamics and stereocilia development. *Cell Motil Cytoskeleton,* **64:** 496-508.

Morrow JS, Marchesi VT. 1981. Self-assembly of spectrin oligomers in vitro: a basis for a dynamic cytoskeleton. *J Cell Biol*, **88:** 463–468.

Neuhauser HK, Radtke A, von Brevern M, Lezius F, Feldmann M, Lempert T. 2008. Burden of dizziness and vertigo in the community. *Arch Intern Med,* **168:** 2118-2124.

Nishida Y, Fujimoto T, Takagi A, Honjo I, Ogawa K. 1993. Fodrin is a constituent of the cortical lattice in outer hair cells of the guinea pig cochlea: immunocytochemical evidence. *Hear Res,* **65:** 274-280.

Nishida Y, Rivolta MN, Holley MC. 1998. Timed markers for the differentiation of the cuticular plate and stereocilia in hair cells from the mouse inner ear. *J Comp Neurol,* **395:** 18-28.

Nestor MW, Cai X, Stone MR, Block RJ, Thompson SM. 2011. The actin binding domain of βI-spectrin regulates the morphological and functional dynamics of dendritic spines. *PLoS ONE*, **6:** e16197. doi: 10.1371/journal.pone.0016197.

Nesvizhskii AI, Keller A, Kolker E, Aebersold R. 2003. A statistical model for identifying proteins by tandem mass spectrometry. *Anal Chem,* **75:** 4646-4658.

Papal S, Cortese M, Legendre K, Sorusch N, Dragavon J, Sahly I, Shorte S, Wolfrum U, Petit C, El-Amaraoui A. 2013. The giant spectrin βV couples the molecular motors to phototransduction and Usher syndrome type I proteins along their trafficking route. *Hum Mol Genet,* **22:** 3773-3788.

Parkinson NJ, Olsson CL, Hallows JL, McKee-Johnson J, Keogh BP, Noben-Trauth K, Kujawa SG, Tempel BL. 2001. Mutant beta-spectrin 4 causes auditory and motor neuropathies in quivering mice. *Nat Genet,* **29:** 61-65.

Peng AW. 2009. A hair bundle proteomics approach to discovering actin regulatory proteins in inner ear stereocilia. *PhD Dissertation*, MIT.

Pesacreta TC, Byers TJ, Dubreuil RR, Kiehart DP, Branton D. 1989. Drosophila spectrin: the membrane skeleton during embryogenesis. *J Cell Biol,* **108:** 1697-1709.

Philp NJ, Nachmias VT. 1985. Components of the cytoskeleton in the retinal pigmented epithelium in the chick. *J Cell Biol,* **101:** 358-362.

Raphael Y, Athey BD, Wang Y, Lee MK, Altschuler RA. 1994. F-actin, tubulin and spectrin in the organ of Corti: comparative distribution in different cell types and mammalian species. *Hear Res,* **76:** 173-187.

Rodman JS, Mooseker M, Farquhar MG. 1986. Cytoskeletal proteins of the rat kidney proximal tubule brush border. *Eur J Cell Biol,* **42:** 319-327.

Rodriguez ML, Brignoni M, Salas PJ. 1994. A specifically apical sub-membrane intermediate filament cytoskeleton in non-brush-border epithelial cells. *J Cell Sci,* **107:** 3145-3151.

Romand R, Despres G, Giry N. 1987. Factors affecting the onset of inner ear function. *Hear Res,* **28:** 1-7.

Rosenhall U, Engstrom B. 1974. Surface structures of the human vestibular sensory regions. *Acta Otolaryng Suppl,* **319:** 3-18.

Ross MD. 1982. Striated organelles in hair cells of rat inner ear maculus: description and implication for transduction. *Physiologist (Suppl),* **25:** S113-S114.

Ross MD, Bourne C. 1983. Interrelated striated elements in vestibular hair cells of the rat. *Science,* **220:** 622-624.

Ross DS, Holstrum WJ, Gaffney M, Green D, Oyler RF, Gravel JS. 2008. Hearing screening and diagnostic evaluation of children with unilateral and mild bilateral hearing loss. *Trends Amplif,* **12:** 27-34.

Ruben RJ. 1967. Development of the inner ear of the mouse: a radioautographic study of terminal mitoses. *Acta Otolaryngol Suppl,* **220:** 1-44.

Salas PJ, Rodriguez MJ, Viciana AL, Vega-Salas DE, Hauri HP. 1997. The apical submembrane cytoskeleton participates in the organization of the apical pole in epithelial cells. *J Cell Biol,* **137:** 359-375.

Santos-Sacchi J. 1993. Voltage dependent ionic conductances of type I spiral ganglion cells from the guinea pig inner ear. *J Neurosci,* **13:** 3599-3611.

Sans A. 1989. Ultrastructural study of striated organelles in vestibular sensory cells of human fetuses. *Anat Embryol (Berl),* **179:** 457-463.

Sans A, Chat M. 1982. Analysis of temporal and spatial patterns of rat vestibular hair cell differentiation by tritiated thymidine radioautography. *J Comp Neurol,* **206:** 1-8.

Scarfone E, Demêmes D, Perrin D, Aunis D, Sans A. 1988. Alpha-fodrin (brain spectrin) immunocytochemical localization in vestibular hair cells. *Neurosci Lett,* **93:** 13-18.

Scarfone E, Ulfendahl M, Löfstrand P, Flock A. 1991. Light- and electron microscopy of isolated vestibular hair cells from the guinea pig. *Cell Tissue Res,* **266:** 51-58.

Schilling AB, Crot C, Helseth DL, Xu H, Davis RG. 2010. Conversion of an Agilent Chip Cube system for the analysis of proteomics samples using a LTQ-FT Ultra mass spectrometer. *58th ASMS Conference on Mass Spectrometry*, Salt Lake City, UT, Poster # MP612.

Schwartz JH,Tattersall I. 1996. Toward distinguishing *Homo neanderthalensis* from *Homo sapiens,* and vice versa. *Anthropologie (Brno)*, **34***:* 79–88.

Schweizer FE, Savin D, Luu C, Sultemeier DR, Hoffman LF. 2009. Distribution of high-conductance calcium-activated potassium channels in rat vestibular epithelia. *J Comp Neurol* **517:** 134-145.

Shipman P, Walker A, Bichell D. 1985. *The Human Skeleton*. Boston: Harvard Press.

Slepecky N. 1989. An infracuticular network is not required for outer hair cell shortening. *Hear Res,* **38:** 135-140.

Slepecky N, Chamberlain SC. 1982. Distribution and polarity of actin in the sensory hair cells of the chinchilla cochlea. *Cell Tissue Res,* **224:** 15-24.

Slepecky N, Chamberlain SC. 1985. Immunoelectron microscopic and immunofluorescent localization of cytoskeletal and muscle-like contractile proteins in inner ear sensory hair cells. *Hear Res,* **20:** 245-260.

Slepecky N, Hamernick RP, Handerson D. 1981. The consistent occurrence of a striated organelle in the inner hair cells of the normal chinchilla. *Acta Otolaryngol,* **91:** 189-198.

Slepecky N, Hamernick RP, Handerson D. 1980. A reexamination of a hair cell organelle in the cuticular plate region and its possible relation to the active process in the cochlea. *Hear Res,* **2:** 413-421.

Slepecky NB, Henderson CG, Saha S. 1995. Post-translational modifications of tubulin suggest that dynamic microtubules are present in sensory cells and stable microtubules are present in supporting cells of mammalian cochlea. *Hear Res,* **91:** 136-147.

Slepecky NB, Ulfendahl M. 1992. Actin-binding and microtubule-associated proteins in the organ of Corti. *Hear Res*, **57:** 201-215.

Spoendlin H. 1966. The organization of the cochlear receptor. *Adv Oto-Rhino-Laryngol,* **13:** 1-227.

Spoon C, Grant W. 2011. Biomechanics of hair cell kinocilia: experimental measurement of kinocilium shaft stiffness and base rotational stiffness with Euler-Benoulli and Temoshenko beam analysis. *J Exp Biol,* **214:** 862-870.

Sridharan et al., 2006

Stankewich MC, Cianci CD, Stabach PR, Ji L, Nath A, Morrow JS. 2011. Cell organization, growth, and neural and cardiac development require αII-spectrin. *J Cell Sci,* **124:** 3956-3966.

Stankewich MC, Gwynn B, Ardito T, Ji L, Kim J, Robledo RF, Lux SE, Peters LL, Morrow JS. 2010. Targeted deletion βIII spectrin impairs synaptogenesis and generates ataxic and seizure phenotypes. *PNAS,* **107:** 6022-6027.

Tilney LG, DeRosier DJ, Mulroy MJ. 1980. The organization of actin filaments in the stereocilia of cochlear hair cells. *J Cell Biol*, **86:** 244–259.

Tilney MS, Tilney LG, Stephens RE, Merte C, Drenckhahn D, Cotanche DA, Bretscher A. 1989. Preliminary biochemical characterization of the stereocilia and cuticular plate of hair cells of the chick cochlea. *J Cell Biol,* **109:** 1711-1723.

Tokimoto T, Osako S, Matsuura S. 1977. Development of auditory evoked cortical and brain stem responses during early postnatal period in the rat. *Osaka City Med J,* **23:** 141-153.

Tse WT, Lux SE. 1999. Red blood cell membrane disorders. *Br J Haematol,* **104:** 2-13.

Vranceanu F, Perkins G, Terada M, Chidavaenzi RL, Ellisman ME, Lysakowski A. 2012. Striated organelle, a cytoskeletal structure positioned to modulate hair-cell transduction. *PNAS,* **109:** 4473-4478.

Yan X, Jeromin A. 2012. Spectrin breakdown products (SBDPs) as potential biomarkers for neurodegenerative diseases. *Curr Transl Geriatr Exp Gerontol Rep,* **1:** 85-93.

Ylikoski J, Pirvola U, Narvanen O, Virtanen I. 1990. Nonerythroid spectrin (fodrin) is a prominent component of the cochlear hair cells. *Hear Res,* **43:** 199-204.

Ylikoski J, Pirvola U, Lehtonen E. 1992. Distribution of F-actin and fodrin in the hair cells of the guinea pig cochlea as revealed by confocal fluorescence microscopy. *Hear Res,* **60:** 80-88.

Zajic G, Schacht J. 1987. Comparison of isolated outer hair cells from five mammalian species. *Hear Res,* **26:** 249-256.

Zarnescu DC, Thomas GH. 1999. Apical spectrin is essential for epithelial morphogenesis but not apicobasal polarity in Drosophila. *J Cell Biol,* **146:** 1075-1086.

Zheng L, Sekerkova G, Vranich K, Tilney LG, Mugnaini E, Bartles JR. 2000. The deaf jerker mouse has a mutation in the gene encoding the espin actin-bundling proteins of hair cell stereocilia and fails to accumulate espins. *Cell*, **102:** 377-385.

Appendix I: Snapshot of some cytoskeletal and associated proteins identified by liquid chromatography mass spectrometry after immunoprecipitation rat cochlea tissue using αII-spectrin as bait.

Experiment: Mass spec expt 08-15-2011 CO a2spec co-ip 50% probability, 1 peptide minimum, displaying Protein Identification Probabilitco-ip 50% probability, 1 peptide minimu

Probability Legend:
over 95%
80% to 94%
50% to 79%
20% to 49%
0% to 19%

#	Visible?	Starred?	Bio View: Identified Proteins (39)	Accession Number	Molecular Weight	Protein Grouping Ambiguity	Taxonomy	Cochlea lower 150kDa band	Cochlea upper 285kDa band
1	☑		Cadherin-23 OS=Rattus norvegicus GN=Cdh23 PE=2 SV=1	CAD23_RAT	365 kDa		...	55%	72%
2	☑		Spectrin alpha chain, brain OS=Rattus norvegicus GN=Sptan1 PE=1 SV=2	SPTA2_RAT	285 kDa		...	100%	100%
3	☑		Spectrin beta chain, brain 2 OS=Rattus norvegicus GN=Sptbn2 PE=1 SV=2	SPTN2_RAT	271 kDa		...		100%
4	☑		Microtubule-associated protein 1B OS=Rattus norvegicus GN=Map1b PE=1 SV=2	MAP1B_RAT	270 kDa		...		82%
5	☑		Myosin-10 OS=Rattus norvegicus GN=Myh10 PE=1 SV=1	MYH10_RAT	229 kDa		...		100%
6	☑		Myosin-9 OS=Rattus norvegicus GN=Myh9 PE=1 SV=3	MYH9_RAT	226 kDa		...	100%	100%
7	☑		Myosin-Vb OS=Rattus norvegicus GN=Myo5b PE=1 SV=1	MYO5B_RAT	214 kDa		...		74%
8	☑		Plasma membrane calcium-transporting ATPase 2 OS=Rattus norvegicus GN=Atp2b2 PE=2 SV=2	AT2B2_RAT	137 kDa		...	61%	49%
9	☑		Neurofilament heavy polypeptide OS=Rattus norvegicus GN=Nefh PE=1 SV=4	NFH_RAT	115 kDa	★	...	46%	100%
10	☑		Contactin-1 OS=Rattus norvegicus GN=Cntn1 PE=1 SV=2	CNTN1_RAT	113 kDa		...	75%	
11	☑		Sodium/potassium-transporting ATPase subunit alpha-1 OS=Rattus norvegicus GN=Atp1a1 PE=1 SV=1	AT1A1_RAT	113 kDa	★	...	100%	100%
12	☑		Sodium/potassium-transporting ATPase subunit alpha-2 OS=Rattus norvegicus GN=Atp1a2 PE=1 SV=1	AT1A2_RAT	112 kDa	★	...	100%	100%
13	☑		Sodium/potassium-transporting ATPase subunit alpha-3 OS=Rattus norvegicus GN=Atp1a3 PE=1 SV=2	AT1A3_RAT	112 kDa	★	...	100%	100%
14	☑		Ankycorbin OS=Rattus norvegicus GN=Rai14 PE=2 SV=2	RAI14_RAT	109 kDa		...	75%	35%
15	☑		Dynamin-1 OS=Rattus norvegicus GN=Dnm1 PE=1 SV=2	DYN1_RAT	97 kDa		...	100%	64%
16	☑		Neurofilament medium polypeptide OS=Rattus norvegicus GN=Nefm PE=1 SV=4	NFM_RAT	96 kDa	★	...	100%	
17	☑		Vesicle-fusing ATPase OS=Rattus norvegicus GN=Nsf PE=1 SV=1	NSF_RAT	83 kDa		...	75%	82%
18	☑		TRAF3-interacting protein 1 OS=Rattus norvegicus GN=Traf3ip1 PE=2 SV=1	MIPT3_RAT	74 kDa		...	68%	22%
19	☑		Keratin, type II cytoskeletal 2 epidermal OS=Rattus norvegicus GN=Krt2 PE=2 SV=1	K22E_RAT	69 kDa	★	...	100%	100%
20	☑		Serum albumin OS=Rattus norvegicus GN=Alb PE=1 SV=2	ALBU_RAT	69 kDa		...	100%	100%
21	☑		Syntaxin-binding protein 1 OS=Rattus norvegicus GN=Stxbp1 PE=1 SV=1	STXB1_RAT	68 kDa		...	100%	100%
22	☑		Keratin, type II cytoskeletal 1 OS=Rattus norvegicus GN=Krt1 PE=2 SV=1	K2C1_RAT	65 kDa	★	...	100%	100%
23	☑		Keratin, type II cytoskeletal 5 OS=Rattus norvegicus GN=Krt5 PE=1 SV=1	K2C5_RAT	62 kDa	★	...	100%	100%
24	☑		Neurofilament light polypeptide OS=Rattus norvegicus GN=Nefl PE=1 SV=3	NFL_RAT	61 kDa	★	...	100%	100%
25	☑		Keratin, type II cytoskeletal 6A OS=Rattus norvegicus GN=Krt6a PE=1 SV=1	K2C6A_RAT	59 kDa	★	...	75%	82%
26	☑		Keratin, type II cytoskeletal 75 OS=Rattus norvegicus GN=Krt75 PE=2 SV=2	K2C75_RAT	59 kDa	★	...	75%	82%
27	☑		Keratin, type II cytoskeletal 72 OS=Rattus norvegicus GN=Krt72 PE=2 SV=2	K2C72_RAT	57 kDa	★	...	75%	82%
28	☑		Keratin, type I cytoskeletal 10 OS=Rattus norvegicus GN=Krt10 PE=2 SV=1	K1C10_RAT	57 kDa	★	...	100%	100%
29	☑		Keratin, type I cytoskeletal 14 OS=Rattus norvegicus GN=Krt14 PE=2 SV=1	K1C14_RAT	53 kDa	★	...	75%	82%
30	☑		Tubulin alpha-1A chain OS=Rattus norvegicus GN=Tuba1a PE=1 SV=1	TBA1A_RA...	50 kDa	★	...	100%	100%
31	☑		Glial fibrillary acidic protein OS=Rattus norvegicus GN=Gfap PE=1 SV=2	GFAP_RAT	50 kDa	★	...	75%	82%
32	☑		Tubulin alpha-4A chain OS=Rattus norvegicus GN=Tuba4a PE=2 SV=1	TBA4A_RAT	50 kDa	★	...	100%	
33	☑		Tubulin beta-2A chain OS=Rattus norvegicus GN=Tubb2a PE=1 SV=1	TBB2A_RAT	50 kDa	★	...	100%	82%
34	☑		Tubulin beta-2C chain OS=Rattus norvegicus GN=Tubb2c PE=1 SV=1	TBB2C_RAT	50 kDa	★	...	100%	100%
35	☑		Keratin, type I cytoskeletal 17 OS=Rattus norvegicus GN=Krt17 PE=2 SV=1	K1C17_RAT	48 kDa	★	...	100%	100%
36	☑		Actin, cytoplasmic 1 OS=Rattus norvegicus GN=Actb PE=1 SV=1	ACTB_RAT...	42 kDa		...	100%	100%
37	☑		Syntaxin-1B OS=Rattus norvegicus GN=Stx1b PE=1 SV=1	STX1B_RAT	33 kDa		...	100%	82%
38	☑		14-3-3 protein epsilon OS=Rattus norvegicus GN=Ywhae PE=1 SV=1	1433E_RAT	29 kDa	★	...	100%	82%
39	☑		Cofilin-1 OS=Rattus norvegicus GN=Cfl1 PE=1 SV=3	COF1_RAT	19 kDa		...		63%

Appendix II: Mass spec data from an αII-spectrin co-IP from brain, cochlea sample split into two, 2 VO samples, one of which is also split into two showing a snapshot of some of the proteins obtained.

Experiment: Mass spec expt 08-15-2011 CO a2spec co-ip 50% probability, 1 peptide minimum, displaying Protein Identification Probabilitco-ip 50% probability, 1 peptide minim

Probability Legend:
over 95%
80% to 94%
50% to 79%
20% to 49%
0% to 19%

#	Visible?	Starred?	Bio View: Identified Proteins (39)	Accession Number	Molecular Weight	Protein Grouping Ambiguity	Taxonomy	Cochlea lower 150kDa band	Cochlea upper 285kDa band
1	☑		Cadherin-23 OS=Rattus norvegicus GN=Cdh23 PE=2 SV=1	CAD23_RAT	365 kDa		...	55%	72%
2	☑		Spectrin alpha chain, brain OS=Rattus norvegicus GN=Sptan1 PE=1 SV=2	SPTA2_RAT	285 kDa		...	100%	100%
3	☑		Spectrin beta chain, brain 2 OS=Rattus norvegicus GN=Sptbn2 PE=1 SV=2	SPTN2_RAT	271 kDa		...		100%
4	☑		Microtubule-associated protein 1B OS=Rattus norvegicus GN=Map1b PE=1 SV=2	MAP1B_RAT	270 kDa		...		82%
5	☑		Myosin-10 OS=Rattus norvegicus GN=Myh10 PE=1 SV=1	MYH10_RAT	229 kDa		...		100%
6	☑		Myosin-9 OS=Rattus norvegicus GN=Myh9 PE=1 SV=3	MYH9_RAT	226 kDa		...	100%	100%
7	☑		Myosin-Vb OS=Rattus norvegicus GN=Myo5b PE=1 SV=1	MYO5B_RAT	214 kDa		...		74%
8	☑		Plasma membrane calcium-transporting ATPase 2 OS=Rattus norvegicus GN=Atp2b2 PE=2 SV=2	AT2B2_RAT	137 kDa		...	61%	49%
9	☑		Neurofilament heavy polypeptide OS=Rattus norvegicus GN=Nefh PE=1 SV=4	NFH_RAT	115 kDa	★	...	46%	100%
10	☑		Contactin-1 OS=Rattus norvegicus GN=Cntn1 PE=1 SV=2	CNTN1_RAT	113 kDa		...	75%	
11	☑		Sodium/potassium-transporting ATPase subunit alpha-1 OS=Rattus norvegicus GN=Atp1a1 PE=1 SV=1	AT1A1_RAT	113 kDa	★	...	100%	100%
12	☑		Sodium/potassium-transporting ATPase subunit alpha-2 OS=Rattus norvegicus GN=Atp1a2 PE=1 SV=1	AT1A2_RAT	112 kDa	★	...	100%	100%
13	☑		Sodium/potassium-transporting ATPase subunit alpha-3 OS=Rattus norvegicus GN=Atp1a3 PE=1 SV=2	AT1A3_RAT	112 kDa	★	...	100%	100%
14	☑		Ankycorbin OS=Rattus norvegicus GN=Rai14 PE=2 SV=2	RAI14_RAT	109 kDa		...	75%	35%
15	☑		Dynamin-1 OS=Rattus norvegicus GN=Dnm1 PE=1 SV=2	DYN1_RAT	97 kDa		...	100%	64%
16	☑		Neurofilament medium polypeptide OS=Rattus norvegicus GN=Nefm PE=1 SV=4	NFM_RAT	96 kDa	★	...	100%	
17	☑		Vesicle-fusing ATPase OS=Rattus norvegicus GN=Nsf PE=1 SV=1	NSF_RAT	83 kDa		...	75%	82%
18	☑		TRAF3-interacting protein 1 OS=Rattus norvegicus GN=Traf3ip1 PE=2 SV=1	MIPT3_RAT	74 kDa		...	68%	22%
19	☑		Keratin, type II cytoskeletal 2 epidermal OS=Rattus norvegicus GN=Krt2 PE=2 SV=1	K22E_RAT	69 kDa	★	...	100%	100%
20	☑		Serum albumin OS=Rattus norvegicus GN=Alb PE=1 SV=2	ALBU_RAT	69 kDa		...	100%	100%
21	☑		Syntaxin-binding protein 1 OS=Rattus norvegicus GN=Stxbp1 PE=1 SV=1	STXB1_RAT	68 kDa		...	100%	100%
22	☑		Keratin, type II cytoskeletal 1 OS=Rattus norvegicus GN=Krt1 PE=2 SV=1	K2C1_RAT	65 kDa	★	...	100%	100%
23	☑		Keratin, type II cytoskeletal 5 OS=Rattus norvegicus GN=Krt5 PE=1 SV=1	K2C5_RAT	62 kDa	★	...	100%	100%
24	☑		Neurofilament light polypeptide OS=Rattus norvegicus GN=Nefl PE=1 SV=3	NFL_RAT	61 kDa	★	...	100%	100%
25	☑		Keratin, type II cytoskeletal 6A OS=Rattus norvegicus GN=Krt6a PE=1 SV=1	K2C6A_RAT	59 kDa	★	...	75%	82%
26	☑		Keratin, type II cytoskeletal 75 OS=Rattus norvegicus GN=Krt75 PE=2 SV=2	K2C75_RAT	59 kDa	★	...	75%	82%
27	☑		Keratin, type II cytoskeletal 72 OS=Rattus norvegicus GN=Krt72 PE=2 SV=2	K2C72_RAT	57 kDa	★	...	75%	82%
28	☑		Keratin, type I cytoskeletal 10 OS=Rattus norvegicus GN=Krt10 PE=2 SV=1	K1C10_RAT	57 kDa	★	...	100%	100%
29	☑		Keratin, type I cytoskeletal 14 OS=Rattus norvegicus GN=Krt14 PE=2 SV=1	K1C14_RAT	53 kDa	★	...	75%	82%
30	☑		Tubulin alpha-1A chain OS=Rattus norvegicus GN=Tuba1a PE=1 SV=1	TBA1A_RA...	50 kDa	★	...	100%	100%
31	☑		Glial fibrillary acidic protein OS=Rattus norvegicus GN=Gfap PE=1 SV=2	GFAP_RAT	50 kDa	★	...	75%	82%
32	☑		Tubulin alpha-4A chain OS=Rattus norvegicus GN=Tuba4a PE=2 SV=1	TBA4A_RAT	50 kDa	★	...	100%	
33	☑		Tubulin beta-2A chain OS=Rattus norvegicus GN=Tubb2a PE=1 SV=1	TBB2A_RAT	50 kDa	★	...	100%	82%
34	☑		Tubulin beta-2C chain OS=Rattus norvegicus GN=Tubb2c PE=1 SV=1	TBB2C_RAT	50 kDa	★	...	100%	100%
35	☑		Keratin, type I cytoskeletal 17 OS=Rattus norvegicus GN=Krt17 PE=2 SV=1	K1C17_RAT	48 kDa	★	...	100%	100%
36	☑		Actin, cytoplasmic 1 OS=Rattus norvegicus GN=Actb PE=1 SV=1	ACTB_RAT...	42 kDa		...	100%	100%
37	☑		Syntaxin-1B OS=Rattus norvegicus GN=Stx1b PE=1 SV=1	STX1B_RAT	33 kDa		...	100%	82%
38	☑		14-3-3 protein epsilon OS=Rattus norvegicus GN=Ywhae PE=1 SV=1	1433E_RAT	29 kDa	★	...	100%	82%
39	☑		Cofilin-1 OS=Rattus norvegicus GN=Cfl1 PE=1 SV=3	COF1_RAT	19 kDa		...		63%

Appendix III: βII spectrin cochlea co-IP samples analyzed using liquid chromatography tandem mass spectrometry (LC-MS/MS)

Experiment: Mass spec expt 08-15-2011 CO a2spec co-ip 50% probability, 1 peptide minimum, displaying Protein Identification Probabilitco-ip 50% probability, 1 peptide minim

Probability Legend:
over 95%
80% to 94%
50% to 79%
20% to 49%
0% to 19%

#	Visible?	Starred?	Bio View: Identified Proteins (39)	Accession Number	Molecular Weight	Protein Grouping Ambiguity	Taxonomy	Cochlea lower 150kDa band	Cochlea upper 285kDa band
1	☑		Cadherin-23 OS=Rattus norvegicus GN=Cdh23 PE=2 SV=1	CAD23_RAT	365 kDa		...	55%	72%
2	☑		Spectrin alpha chain, brain OS=Rattus norvegicus GN=Sptan1 PE=1 SV=2	SPTA2_RAT	285 kDa		...	100%	100%
3	☑		Spectrin beta chain, brain 2 OS=Rattus norvegicus GN=Sptbn2 PE=1 SV=2	SPTN2_RAT	271 kDa		...		100%
4	☑		Microtubule-associated protein 1B OS=Rattus norvegicus GN=Map1b PE=1 SV=2	MAP1B_RAT	270 kDa		...		82%
5	☑		Myosin-10 OS=Rattus norvegicus GN=Myh10 PE=1 SV=1	MYH10_RAT	229 kDa		...		100%
6	☑		Myosin-9 OS=Rattus norvegicus GN=Myh9 PE=1 SV=3	MYH9_RAT	226 kDa		...	100%	100%
7	☑		Myosin-Vb OS=Rattus norvegicus GN=Myo5b PE=1 SV=1	MYO5B_RAT	214 kDa		...		74%
8	☑		Plasma membrane calcium-transporting ATPase 2 OS=Rattus norvegicus GN=Atp2b2 PE=2 SV=2	AT2B2_RAT	137 kDa		...	61%	49%
9	☑		Neurofilament heavy polypeptide OS=Rattus norvegicus GN=Nefh PE=1 SV=4	NFH_RAT	115 kDa	★	...	46%	100%
10	☑		Contactin-1 OS=Rattus norvegicus GN=Cntn1 PE=1 SV=2	CNTN1_RAT	113 kDa		...	75%	
11	☑		Sodium/potassium-transporting ATPase subunit alpha-1 OS=Rattus norvegicus GN=Atp1a1 PE=1 SV=1	AT1A1_RAT	113 kDa	★	...	100%	100%
12	☑		Sodium/potassium-transporting ATPase subunit alpha-2 OS=Rattus norvegicus GN=Atp1a2 PE=1 SV=1	AT1A2_RAT	112 kDa	★	...	100%	100%
13	☑		Sodium/potassium-transporting ATPase subunit alpha-3 OS=Rattus norvegicus GN=Atp1a3 PE=1 SV=2	AT1A3_RAT	112 kDa	★	...	100%	100%
14	☑		Ankycorbin OS=Rattus norvegicus GN=Rai14 PE=2 SV=2	RAI14_RAT	109 kDa		...	75%	35%
15	☑		Dynamin-1 OS=Rattus norvegicus GN=Dnm1 PE=1 SV=2	DYN1_RAT	97 kDa		...	100%	64%
16	☑		Neurofilament medium polypeptide OS=Rattus norvegicus GN=Nefm PE=1 SV=4	NFM_RAT	96 kDa	★	...	100%	
17	☑		Vesicle-fusing ATPase OS=Rattus norvegicus GN=Nsf PE=1 SV=1	NSF_RAT	83 kDa		...	75%	82%
18	☑		TRAF3-interacting protein 1 OS=Rattus norvegicus GN=Traf3ip1 PE=2 SV=1	MIPT3_RAT	74 kDa		...	68%	22%
19	☑		Keratin, type II cytoskeletal 2 epidermal OS=Rattus norvegicus GN=Krt2 PE=2 SV=1	K22E_RAT	69 kDa	★	...	100%	100%
20	☑		Serum albumin OS=Rattus norvegicus GN=Alb PE=1 SV=2	ALBU_RAT	69 kDa		...	100%	100%
21	☑		Syntaxin-binding protein 1 OS=Rattus norvegicus GN=Stxbp1 PE=1 SV=1	STXB1_RAT	68 kDa		...	100%	100%
22	☑		Keratin, type II cytoskeletal 1 OS=Rattus norvegicus GN=Krt1 PE=2 SV=1	K2C1_RAT	65 kDa	★	...	100%	100%
23	☑		Keratin, type II cytoskeletal 5 OS=Rattus norvegicus GN=Krt5 PE=1 SV=1	K2C5_RAT	62 kDa	★	...	100%	100%
24	☑		Neurofilament light polypeptide OS=Rattus norvegicus GN=Nefl PE=1 SV=3	NFL_RAT	61 kDa	★	...	100%	100%
25	☑		Keratin, type II cytoskeletal 6A OS=Rattus norvegicus GN=Krt6a PE=1 SV=1	K2C6A_RAT	59 kDa	★	...	75%	82%
26	☑		Keratin, type II cytoskeletal 75 OS=Rattus norvegicus GN=Krt75 PE=2 SV=2	K2C75_RAT	59 kDa	★	...	75%	82%
27	☑		Keratin, type II cytoskeletal 72 OS=Rattus norvegicus GN=Krt72 PE=2 SV=2	K2C72_RAT	57 kDa	★	...	75%	82%
28	☑		Keratin, type I cytoskeletal 10 OS=Rattus norvegicus GN=Krt10 PE=2 SV=1	K1C10_RAT	57 kDa	★	...	100%	100%
29	☑		Keratin, type I cytoskeletal 14 OS=Rattus norvegicus GN=Krt14 PE=2 SV=1	K1C14_RAT	53 kDa	★	...	75%	82%
30	☑		Tubulin alpha-1A chain OS=Rattus norvegicus GN=Tuba1a PE=1 SV=1	TBA1A_RA...	50 kDa	★	...	100%	100%
31	☑		Glial fibrillary acidic protein OS=Rattus norvegicus GN=Gfap PE=1 SV=2	GFAP_RAT	50 kDa	★	...	75%	82%
32	☑		Tubulin alpha-4A chain OS=Rattus norvegicus GN=Tuba4a PE=2 SV=1	TBA4A_RAT	50 kDa	★	...	100%	
33	☑		Tubulin beta-2A chain OS=Rattus norvegicus GN=Tubb2a PE=1 SV=1	TBB2A_RAT	50 kDa	★	...	100%	82%
34	☑		Tubulin beta-2C chain OS=Rattus norvegicus GN=Tubb2c PE=1 SV=1	TBB2C_RAT	50 kDa	★	...	100%	100%
35	☑		Keratin, type I cytoskeletal 17 OS=Rattus norvegicus GN=Krt17 PE=2 SV=1	K1C17_RAT	48 kDa	★	...	100%	100%
36	☑		Actin, cytoplasmic 1 OS=Rattus norvegicus GN=Actb PE=1 SV=1	ACTB_RAT...	42 kDa		...	100%	100%
37	☑		Syntaxin-1B OS=Rattus norvegicus GN=Stx1b PE=1 SV=1	STX1B_RAT	33 kDa		...	100%	82%
38	☑		14-3-3 protein epsilon OS=Rattus norvegicus GN=Ywhae PE=1 SV=1	1433E_RAT	29 kDa	★	...	100%	82%
39	☑		Cofilin-1 OS=Rattus norvegicus GN=Cfl1 PE=1 SV=3	COF1_RAT	19 kDa		...		63%

Appendix IV: Snapshot of some of the proteins identified predominantly from βII-spectrin co-IPs of cochlea and vestibular tissue. Included in the analysis was also was αII-spectrin co-IP sample that served as a reference point to compare the protein yields from the two isoforms when applied to the same tissue.

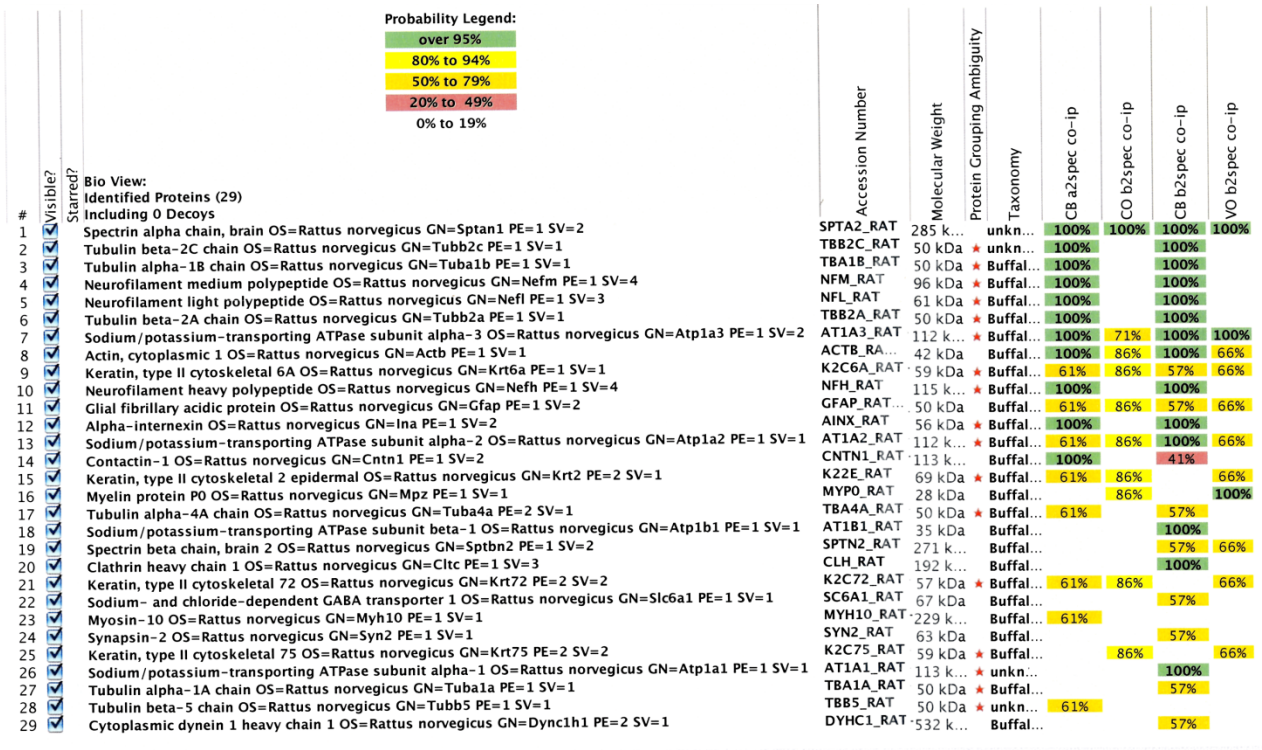

Probability Legend:
over 95%
80% to 94%
50% to 79%
20% to 49%
0% to 19%

Bio View:
Identified Proteins (29)
Including 0 Decoys

#	Visible?	Starred?		Accession Number	Molecular Weight	Protein Grouping Ambiguity	Taxonomy	CB a2spec co-ip	CO b2spec co-ip	CB b2spec co-ip	VO b2spec co-ip
1	☑		Spectrin alpha chain, brain OS=Rattus norvegicus GN=Sptan1 PE=1 SV=2	SPTA2_RAT	285 k...		unkn...	100%	100%	100%	100%
2	☑		Tubulin beta-2C chain OS=Rattus norvegicus GN=Tubb2c PE=1 SV=1	TBB2C_RAT	50 kDa	★	unkn...	100%		100%	
3	☑		Tubulin alpha-1B chain OS=Rattus norvegicus GN=Tuba1b PE=1 SV=1	TBA1B_RAT	50 kDa	★	Buffal...	100%		100%	
4	☑		Neurofilament medium polypeptide OS=Rattus norvegicus GN=Nefm PE=1 SV=4	NFM_RAT	96 kDa	★	Buffal...	100%		100%	
5	☑		Neurofilament light polypeptide OS=Rattus norvegicus GN=Nefl PE=1 SV=3	NFL_RAT	61 kDa	★	Buffal...	100%		100%	
6	☑		Tubulin beta-2A chain OS=Rattus norvegicus GN=Tubb2a PE=1 SV=1	TBB2A_RAT	50 kDa	★	Buffal...	100%		100%	
7	☑		Sodium/potassium-transporting ATPase subunit alpha-3 OS=Rattus norvegicus GN=Atp1a3 PE=1 SV=2	AT1A3_RAT	112 k...	★	Buffal...	100%	71%	100%	100%
8	☑		Actin, cytoplasmic 1 OS=Rattus norvegicus GN=Actb PE=1 SV=1	ACTB_RA...	42 kDa		Buffal...	100%	86%	100%	66%
9	☑		Keratin, type II cytoskeletal 6A OS=Rattus norvegicus GN=Krt6a PE=1 SV=1	K2C6A_RAT	59 kDa	★	Buffal...	61%	86%	57%	66%
10	☑		Neurofilament heavy polypeptide OS=Rattus norvegicus GN=Nefh PE=1 SV=4	NFH_RAT	115 k...	★	Buffal...	100%		100%	
11	☑		Glial fibrillary acidic protein OS=Rattus norvegicus GN=Gfap PE=1 SV=2	GFAP_RAT...	50 kDa		Buffal...	61%	86%	57%	66%
12	☑		Alpha-internexin OS=Rattus norvegicus GN=Ina PE=1 SV=2	AINX_RAT	56 kDa	★	Buffal...	100%		100%	
13	☑		Sodium/potassium-transporting ATPase subunit alpha-2 OS=Rattus norvegicus GN=Atp1a2 PE=1 SV=1	AT1A2_RAT	112 k...	★	Buffal...	61%	86%	100%	66%
14	☑		Contactin-1 OS=Rattus norvegicus GN=Cntn1 PE=1 SV=2	CNTN1_RAT	113 k...		Buffal...	100%		41%	
15	☑		Keratin, type II cytoskeletal 2 epidermal OS=Rattus norvegicus GN=Krt2 PE=2 SV=1	K22E_RAT	69 kDa	★	Buffal...	61%	86%		66%
16	☑		Myelin protein P0 OS=Rattus norvegicus GN=Mpz PE=1 SV=1	MYP0_RAT	28 kDa		Buffal...		86%		100%
17	☑		Tubulin alpha-4A chain OS=Rattus norvegicus GN=Tuba4a PE=2 SV=1	TBA4A_RAT	50 kDa	★	Buffal...	61%		57%	
18	☑		Sodium/potassium-transporting ATPase subunit beta-1 OS=Rattus norvegicus GN=Atp1b1 PE=1 SV=1	AT1B1_RAT	35 kDa		Buffal...			100%	
19	☑		Spectrin beta chain, brain 2 OS=Rattus norvegicus GN=Sptbn2 PE=1 SV=2	SPTN2_RAT	271 k...		Buffal...			57%	66%
20	☑		Clathrin heavy chain 1 OS=Rattus norvegicus GN=Cltc PE=1 SV=3	CLH_RAT	192 k...		Buffal...			100%	
21	☑		Keratin, type II cytoskeletal 72 OS=Rattus norvegicus GN=Krt72 PE=2 SV=2	K2C72_RAT	57 kDa	★	Buffal...	61%	86%		66%
22	☑		Sodium- and chloride-dependent GABA transporter 1 OS=Rattus norvegicus GN=Slc6a1 PE=1 SV=1	SC6A1_RAT	67 kDa		Buffal...			57%	
23	☑		Myosin-10 OS=Rattus norvegicus GN=Myh10 PE=1 SV=1	MYH10_RAT	229 k...		Buffal...	61%			
24	☑		Synapsin-2 OS=Rattus norvegicus GN=Syn2 PE=1 SV=1	SYN2_RAT	63 kDa		Buffal...			57%	
25	☑		Keratin, type II cytoskeletal 75 OS=Rattus norvegicus GN=Krt75 PE=2 SV=2	K2C75_RAT	59 kDa	★	Buffal...		86%		66%
26	☑		Sodium/potassium-transporting ATPase subunit alpha-1 OS=Rattus norvegicus GN=Atp1a1 PE=1 SV=1	AT1A1_RAT	113 k...	★	unkn...			100%	
27	☑		Tubulin alpha-1A chain OS=Rattus norvegicus GN=Tuba1a PE=1 SV=1	TBA1A_RAT	50 kDa	★	Buffal...			57%	
28	☑		Tubulin beta-5 chain OS=Rattus norvegicus GN=Tubb5 PE=1 SV=1	TBB5_RAT	50 kDa	★	unkn...	61%			
29	☑		Cytoplasmic dynein 1 heavy chain 1 OS=Rattus norvegicus GN=Dync1h1 PE=2 SV=1	DYHC1_RAT	532 k...		Buffal...			57%	

VITA

Robstein Lovejoy Chidavaenzi

Institutional address: Dept. of Anatomy & Cell Biology University of Illinois at Chicago (UIC)
808 S Wood St M/C 512 Chicago Il 60612

Tel: 312-996-0585 Fax: 312-413-0354

Education

2014 University of Illinois at Chicago, Chicago, IL

PhD (Anatomy & Cell Biology)
Adviser: Dr. Anna Lysakowski

Project: Development, and protein composition the rodent inner ear striated organelle and the distribution of spectrins in the inner ear

2007 University of Zimbabwe, Harare, Zimbabwe

M.Phil. (Medicine)
Adviser: Dr. Gideon Mawera

Project: The influence of the afferent side-branches on the curvature of the basilar artery and vertebral arteries' size asymmetry in the human vertebrobasilar arterial tree.

1995 University of Zimbabwe, Harare, Zimbabwe

B.Sc. (Biological Sciences) Honors
Adviser: Dr. Adrian Hailey

Project: The basis of diet selection and mixing in the omnivorous African hinged-back tortoise, Kinixys spekii.

Employment 2008-2014 University of Illinois at Chicago, Chicago, IL, USA

Research & Graduate Teaching Assistant (Neuroanatomy)
Department of Anatomy and Cell Biology
University of Illinois at Chicago College of Medicine

2002-2007 University of Zimbabwe, Harare, ZW

Teaching Assistant (Gross Anatomy & Histology)
Anatomy Department
University of Zimbabwe College of Health Sciences

1996-2002 National Museums and Monuments (NMMZ), Bulawayo, ZW

Curator of Herpetology
Natural History Museum of Zimbabwe, Bulawayo

Awards

American Association of Anatomists (AAA) Travel Award, $350 (FYs 2013, 2012, 2011), $250 (2009)

Association of Research in Otolaryngology (ARO) Graduate Student Travel Award, $500 (FYs 2012, 2010)

GH Miller Travel Award, UIC Anatomy Dept, $600 (FY 2013), $400 (FYs 2013, 2012, 2011)

UIC Graduate Student Council Travel Award, $275 (FY 2013), $310 (FYs 2011, 2010), $300 (FYs 2012, 2009)

UIC Graduate College Presenters' Travel Award, $200 (FYs 2012, 2011), (FY 2009) $100

2012 American Association of Anatomists (AAA) Short Term Visiting Scholarship, $1000

2012 Society for Neuroscience (SfN) Graduate Student Travel Award, $1000

2012 Capita Foundation Travel Award towards 2012 Gordon Research Conference, $524.60

2012 Gordon Research Conference- Auditory System Chairman's Award, $800

2009 Biology of the Inner Ear Course (MBL, Woods Hole) Travel Award, $250

2009 Institute of International Education (IIE), FAES Trac24 (NIH) winter course support, $800

2007-2009 Foreign Fulbright Scholarship award funded by US State Department and administered through Institute of International Education

2004-2007 University of Zimbabwe Staff Development Fellowship in Anatomy, under the auspices of the University of Zimbabwe College of Health Sciences

2004, 2005, 2006: Received funding administered and co-sponsored by the International Brain Research Organization (IBRO) in conjunction with the International Society for Neurochemistry, Fogarty International Centre (FIC), and the National Institutes of Health (USA), to attend IBRO African Neuroscience Schools.

2000 Received funding from the Darwin Initiative and the European Commission to a month-long Tropical Biology Association field course in Tanzania

Publications

Cantuti-Castelvetri L, Zhu H, Givogri MI, **Chidavaenzi RL**, Lopez-Rosas A, Bongarzone ER. 2012. Psychosine induces the dephosphorylation of neurofilaments by deregulation of PP1 and PP2A phosphatases. *Neurobiol Dis*, **46(2):** 325-335.

Dalet A, Bonsacquet J, Gaboyard-Niay S, Calin-Jageman I, **Chidavaenzi R**L, Venteo S, Desmadryl G, Goldberg JM, Lysakowski A, & Chabbert C. 2012. Glutamate transporters EAAT4 and EAAT5 are expressed in vestibular hair cells and calyx endings. *PLoS ONE*, **7(9):** e46261. doi:10.1371/journal.pone.0046261

Vranceanu F, Perkins GA, Terada M, **Chidavaenzi RL**, Ellisman MH, Lysakowski A. 2012. Striated organelle, a cytoskeletal structure positioned to modulate hair-cell transduction. *PNAS*, **109(12):** 4473-4478.

Broadley DG, **Chidavaenzi RL**, Rassmussen GSA, Broadley S. 1998. The Herpetology of the Dande Communal Lands, Guruve District, Zimbabwe. *Afr Herp News,* **27:** 3-12.

Hailey A, **Chidavaenzi RL**, Loveridge JP. 1998. Diet mixing in the omnivorous tortoise *Kinixys spekii. Functional Ecology,* **12:** 373-385.

Hailey A, Coulson IM, & **Chidavaenzi RL**. 1997. Fungus eating by the African tortoise *Kinixys spekii. J Tropical Ecology,* **13:** 469-474.

Manuscripts in preparation (5/10/2014)

Chidavaenzi RL, Lysakowski A. Postnatal development of the vestibulocochlear striated organellein the rat inner ear.

Chidavaenzi RL, Lysakowski A. Immunohistochemical identintification of candidate proteins comprising the striated organelle

Chidavaenzi RL, Lysakowski A. Differential distribution patterns of spectrin subunits within the rat's inner ear sensory epithelium.

Chidavaenzi RL, Lysakowski A. A role for nebulin in actin bundling in the rat cuticular plate and striated organelle.

Workshops

2012, Chicago Biomedical Consortium (CBC) Proteomics and Informatics Workshop, UIC College of Pharmacy, Chicago IL. 6-10 August.

2009, Marine Biology Laboratory, Woods Hole, MA, 2nd Biology of the Inner Ear course, 9-30 August.

2009, FAES Trac24 DNA Micro Arrays: Fabrication and Application course, National Institutes of Health, Bethesda, MD. 12-16 January.

2006, 13th IBRO African Neuroscience School on Infections and Toxic Disorders in the Nervous System, Kinshasa, DRC. 1-5 September.

2005, 11th IBRO African Neuroscience School on Behavioral Neuroscience, Nairobi, Kenya. 10-17 December. 2004, 6th IBRO African Neuroscience School on Regeneration and Neurodegeneration, Grahamstown, South Africa. 10-18 September.

2004, participated in the Neurobiology of Epilepsy Workshop organized by the US National Academies, the Society of Neuroscience, the IBRO, and the American Epilepsy Society, at Rhodes University, in Grahamstown, South Africa, 19-20 September.

2003, attended a regional workshop on Ethical Issues in International Health Research, hosted by the Biomedical Research and training institute in collaboration with the University of Zimbabwe College of Health Sciences, in Harare, Zimbabwe, 25-28 August.

Meetings/Symposia Attended

2014, 37th ARO MidWinter Meeting, San Diego, CA. 22-26 February. Podium presentation.
2013, Society for Neuroscience (SfN), San Diego, CA. 09-13 November. Presented poster.
2013, Experimental Biology 2013, Boston, MA. 20-24 April. Attendee.
2013, 35th ARO MidWinter Meeting, Baltimore, MD. 16-20 February. Presented poster.
2012, Society for Neuroscience (SfN), New Orleans, LA. 13-17 October. Presented poster.
2012, Gordon Research Conference – Auditory System, Lewiston, ME. 8-13 July. Presented poster.
2012, Gordon Research Seminar – Auditory System, Lewiston, ME. 7-8 July. Presented poster.
2012, Experimental Biology, San Diego, CA. 21-25 April. Presented poster.
2012, 35th ARO MidWinter Meeting, San Diego, CA. 25-29 February. Presented poster.
2011, Experimental Biology, Washington DC. 9-13 April. Presented poster.
2011, 34th ARO MidWinter Meeting, Baltimore, MD. 19-23 February. Presented poster.
2010, 33rd ARO MidWinter Meeting, Anaheim, CA. 6-10 February. Presented poster.
2009, Experimental Biology, New Orleans, LA. 18-22 April. Presented poster.
2009, Chicago Chapter SfN Annual Meeting 2009, De Paul University. 26 March. Presented poster.
2009, American Association for the Advancement of Science (AAAS) Annual Meeting, Chicago, IL. 12-16 February. Volunteer Session Aide.

Alumni Memberships

Marine Biology Laboratories – Woods Hole, MA – Biology of the Inner Ear 2009

Fulbright Association

International Brain Research Organization (IBRO) (African Regional Committee)

Tropical Biology Association

Graduate Student Memberships

American Anatomical Association

Association for Research in Otolaryngology

Society for Neuroscience

Extracurricular Activities

UIC Graduate Student Council member 2010-2011